


2013-7

Advanced Circularly Polarised Microstrip Patch Antennas

Adam Z. Narbudowicz
Technological University Dublin

Follow this and additional works at: <https://arrow.tudublin.ie/engdoc>

 Part of the [Electrical and Electronics Commons](#)

Recommended Citation

Narbudowicz, A. Z. (2013) *Advanced Circularly Polarised Microstrip Patch Antennas*. Doctoral Thesis. Technological University Dublin. doi:10.21427/D7F31N

This Theses, Ph.D is brought to you for free and open access by the Engineering at ARROW@TU Dublin. It has been accepted for inclusion in Doctoral by an authorized administrator of ARROW@TU Dublin. For more information, please contact arrow.admin@tudublin.ie, aisling.coyne@tudublin.ie, vera.kilshaw@tudublin.ie.



ADVANCED CIRCULARLY POLARISED MICROSTRIP PATCH ANTENNAS

Adam Z. Narbudowicz
Magister Inzynier

Doctor of Philosophy

Supervisors:
Prof. Max J. Ammann
Dr. Xiulong Bao

DUBLIN INSTITUTE OF TECHNOLOGY
SCHOOL OF ELECTRICAL & ELECTRONIC ENGINEERING

July 2013

*Do not follow where the path may lead,
go instead where there is no path
and leave a trail.*

- Ralph Waldo Emerson

ABSTRACT

The thesis describes outcomes of research on advanced circularly polarised antennas. The proposed designs are intended for integration into small mobile devices, therefore low profile and easy manufacturability are key parameters, along with good CP radiation properties. The designs were validated by simulation and measurement, and are also backed by theory and design guidelines.

The primary focus is on the development of planar omnidirectional circularly polarised antennas, which are fabricated using multilayer PCB techniques and thus are lightweight and cost-efficient. Unlike in classical microstrip patch antenna designs, the groundplane of the proposed antenna was substantially reduced. This helps to achieve an omnidirectional circular polarisation pattern and miniaturize the antenna, however at the cost of increased feed circuit complexity. The basic design, its advantages and disadvantages are discussed in Section 3.

In the next step, the omnidirectional circularly polarised antenna was extended with additional, advanced features. A miniaturized version is investigated, which offers a 20% footprint reduction by folding parts of the patch underneath itself. Further miniaturization is possible by increasing the dielectric constant of the substrate.

A method to adjust the omnidirectional circularly polarised antenna performance by trimming four lumped capacitors is also investigated. Manufacturing inaccuracy in large scale production may cause some of the units to radiate outside of the desired frequencies. By integrating four trimmed capacitors into the antenna it can be precisely tuned to the desired band.

Simulated results demonstrate this property by trimming the antenna between GPS L1 band (centre frequency at 1.575 GHz) and Galileo/Beidou-2 E2 band (1.561 GHz).

Furthermore, a dual-band omnidirectional circularly polarised antenna is presented, which employs slots and capacitor loading to steer the current path of the first and second resonant mode. The design offers a small frequency ratio of 1.182.

The methods to obtain a planar omnidirectional circularly polarised antenna have been further advanced to propose a reconfigurable antenna. The beam reconfiguration is capable of rotating its dipole-like radiation pattern around an axis, thus allowing reception or transmission from any spherical angle. The switching method is simple and does not require any semiconductor devices.

Finally, a dual circularly polarised antenna is presented, which achieves dual-polarisation by employing even and odd modes in a coplanar waveguide. This technique allows greater flexibility and size reduction of the feed network, as two signals can be transmitted by a single multi-mode transmission line.

DECLARATION

I certify that this thesis which I now submit for examination for the award of PhD, is entirely my own work and has not been taken from the work of others save and to the extent that such work has been cited and acknowledged within the text of my own work.

This thesis was prepared according to the regulations for postgraduate study by research of the Dublin Institute of Technology and has not been submitted in whole or in part for an award in any other Institute or University.

The work reported on in this thesis conforms to the principles and requirements of the Institute's guidelines for ethics in research.

The Institute has permission to keep, to lend or to copy this thesis in whole or in part, on condition that any such use of the material of the thesis be duly acknowledged.

Signature: _____ Date _____
Adam Z. Narbudowicz

ACKNOWLEDGMENTS

Firstly, I'd like to express my sincere gratitude to my supervisors, Prof. Max Ammann and Dr Xiulong Bao, not only for their research expertise and open-minded attitude, but also for support and encouragement, which very often extended far beyond professional levels.

I'm also grateful to my colleagues from DIT, with whom I had the great pleasure to work and socialize for the last four years: Shynu, Giuseppe, Vit, Matthias, Andreas, Padraig, Antoine, Maria, Oisin, Afshin and Abraham, with special thanks to Domenico.

I also want to thank Prof. Dirk Heberling, Hammam Shaktour and the team of the mechanical workshop at Institute for High Frequency Technology, RWTH Aachen University. Their expertise allowed me to measure the reconfigurable antenna and discussion with them seeded some ideas for future research. I would also like to thank Prof. David Jackson from the University of Houston, Prof. Steven Gao from the University of Kent and Dr Steven Best. Their opinions and suggestions were strongly appreciated at various stages of my PhD work.

Completion of this thesis would not be possible without my former teachers and supervisors: Dr Grzegorz Adamiuk and Dr Juan Pontes from the Karlsruhe Institute of Technology, as well as the team of Department of Microwave and Antenna Engineering led by Prof. Michal Mrozowski at Gdansk University of Technology.

Moving to a new country is always a bit difficult at the beginning, therefore I'd like to acknowledge my *Dublin friends*, who supported me all the time: Joseph, Milan, Lena, Grzegorz, Fabiola, Rali, Anthony, Dee, Michal,

Tomasz and Beata, and members of the Hillwalkers Club. Also, I could not forget about my *old friends*, who despite the huge distance always stayed close: Kaja and Pankrac, Rafal and Agnieszka, Janusz, Olemka *the Witch*, Maciej, Marta, Marysia, Krzysztof Maria, and Dorota and Michal. Special thanks go to Celina, who supported me when I was applying for this PhD project.

Last, although definitely not least important, I'd like to thank to my family, parents Lena and Leszek and grandparents: Celina and Zdzislaw, and Genowefa and Jan. I am garteful for their love, support and all those things that can not be listed on this limited pages. Especially I would like to acknowledge my two grandfathers, Zdzislaw and Jan, who regrettably passed away before the completion of this work.

NOMENCLATURE

BW	impedance bandwidth
c_0	speed of light in vacuum, 299 792 458 m/ s
C	capacity (F)
η_{rad}	radiation efficiency
η_{total}	total efficiency
f	frequency (GHz)
G	gain (dBic)
G_r	realized gain (dBic)
h	substrate thickness
L	inductance (H)
λ_0	wavelength (m)
Q	antenna quality factor
R_{in}	input resistance of antenna (Ω)
S_{nn}	input reflection coefficient at port n
S_{mn}	transmission coefficient between ports n and m
δ_{tan}	loss tangent of a dielectric material
ϵ_r	relative dielectric constant of a dielectric material
ϵ_{eff}	effective relative dielectric constant (i.e. in a microstrip line)
Z_{in}	input impedance of antenna (Ω)
θ, ϕ	angular coordinates in spherical coordinate system (°)
x, y, z	coordinates in a cartesian coordinate sytem (m)

ABBREVIATIONS

AR	Axial Ratio
AUT	Antenna Under Test
CNR	Carrier to Noise Ratio
CP	Circular Polarisation
CPW	Coplanar Waveguide
CRLH	Composite Right-Left Handed
CST	Computer Simulation Technology GmbH
DIT	Dublin Institute of Technology
EMI	Electromagnetic interference
FIT	Finite Integration Technique
FR	Frequency Ratio
GNSS	Global Navigation Satellite System
GPS	Global Positioning System
HDOP	Horizontal Dilution of Precision
IEEE	Institute of Electrical and Electronics Engineers
IFA	Inverted F Antenna
LHCP	Left-Hand Circular Polarisation
MIMO	Multiple Input Multiple Output
OCPA	Omnidirectional Circularly Polarized Antenna
PCB	Printed Circuit Board
RFID	Radio Frequency Identification
RHCP	Right-Hand Circular Polarisation
SMA	SubMiniature Type A
SNR	Signal to Noise Ratio

TL	Transmission Line
TT&C	Telemetry, Tracking & Command
VNA	Vector Network Analyser
VSWR	Voltage Standing Wave Ratio
UWB	Ultra Wide Band
WLAN	Wireless Local Area Network

CONTENTS

Abstract	iii
Declaration	v
Acknowledgments	vi
Nomenclature	viii
Abbreviations	ix
List of Figures	xv
List of Tables	xviii
1. Introduction	1
1.1. Benefits of Circularly Polarised Antennas	1
1.2. Challenges for Circularly Polarised Antennas	3
1.2.1. Omnidirectional Radiation Pattern	3
1.2.2. Pattern Reconfigurability	5
1.2.3. Wideband Radiation	5
1.2.4. Manufacturability and Miniaturization	6
1.3. Methodology	7
1.4. Antenna Parameters	8
1.4.1. Reflection and Transmission Coefficients	9
1.4.2. Radiation Pattern, Directivity, Gain and Realized Gain	10
1.4.3. Axial Ratio	12

1.5. Research Summary	13
2. State of the Art Circularly Polarised Antennas	14
2.1. Microstrip Patch Antennas	14
2.1.1. Single Fed Circularly Polarised Patch	14
2.1.2. Dual and Multiple Feeds	17
2.2. Crossed Dipoles and Slot Antennas	18
2.3. Spiral Antennas	21
2.4. Sequentially Rotated Arrays	23
2.5. Antennas for GNSS Applications	24
3. Omnidirectional Circularly Polarised Antennas	28
3.1. Background	28
3.1.1. Linear Antenna Surrounded by a Polariser	28
3.1.2. Array of Rotated CP Antennas	29
3.1.3. Combination of Horizontal and Vertical Radiators	30
3.1.4. Use of Metamaterials and Zeroth-Order Resonance	31
3.1.5. Back-to-Back Coupled Patches	33
3.2. Use of Omnidirectional CP Antennas for GPS Applications	34
3.3. Feed Technique	36
3.4. Ground Plane Effect	38
3.5. Single Band Implementation	41
4. Advanced Omnidirectional CP Antennas	46
4.1. Motivation	46
4.2. Miniaturization	46
4.3. Fine Tuning of Omnidirectional CP Antenna	51
4.3.1. Principles of Operation	53
4.3.2. Results	56
4.4. Dual Band Enhancement Techniques	56

4.5. Dual Band Omnidirectional CP Antenna	62
4.5.1. Design Process	68
4.5.2. Impedance Match	69
4.5.3. Axial ratio	69
5. Reconfigurable Omnidirectional CP Antenna	73
5.1. Reconfigurable CP Antennas	73
5.2. Antenna Geometry	75
5.3. Principles of Operation	76
5.4. Measurements	78
5.4.1. Configuration $\Delta_{ph} = 0^\circ$	82
5.4.2. Configuration $\Delta_{ph} = 180^\circ$	85
5.4.3. Configuration $\Delta_{ph} = +90^\circ$	88
5.4.4. Configuration $\Delta_{ph} = -90^\circ$	91
5.5. Measurement Improvement	94
6. Dual Circularly Polarised Patch Antenna	95
6.1. Background	95
6.2. Antenna Design	97
6.3. Antenna Measurements	100
6.4. Port-to-Port Isolation	104
7. Conclusions and Future Developments	106
7.1. Conclusions	106
7.2. Impact of the Proposed Solutions	106
7.2.1. Omnidirectionality	107
7.2.2. Reconfigurability	107
7.2.3. Dual Polarisation	108
7.3. Future Work	109
7.3.1. Generalization to Other Polarisation	109
7.3.2. Bandwidth Enhancement	109

7.3.3. Measurement Improvement	110
Bibliography	111
A. List of Publications	124

LIST OF FIGURES

1.1. Poincare sphere	2
1.2. Flow diagram of the methodology used	8
2.1. Geometries of classical CP patches	15
2.2. Crossed dipole antenna	19
2.3. CP aperture antenna fed from CPW	20
2.4. Dipole-like UWB CP antenna	21
2.5. Sequentially rotated geometries	24
2.6. Propagation scenarios for GNSS signals	26
3.1. Background omnidirectional CP antennas	29
3.2. Transmission line models	31
3.3. Bidirectional CP antenna	37
3.4. Parameter study of bidirectional CP antenna	38
3.5. Omnidirectional CP antenna	42
3.6. S_{11} of the omnidirectional CP antenna	44
3.7. AR of the omnidirectional CP antenna	44
3.8. Gains of the omnidirectional CP antenna	45
4.1. Miniaturized multilayered OCPA	47
4.2. Parameter study of the miniaturized OCPA feed	48
4.3. S_{11} of the miniaturized antenna	49
4.4. Realized gain of the miniaturized antenna	50
4.5. Axial ratio of the miniaturized antenna	51
4.6. OCPA with fine frequency tuning capability	52

4.7. Parameter study of frequency tunable antenna	54
4.8. Reflection coefficient of the frequency tunable antenna	55
4.9. Smith chart for frequency tunable antenna	55
4.10. Realized gains of frequency tunable antenna	57
4.11. Depiction of the slot load of a dual-band patch antenna	59
4.12. Dual-band OCPA	60
4.13. Parameter study of capacitors of the dual-band OCPA	61
4.14. Parameter study of slots of the dual-band OCPA	62
4.15. S_{11} of the dual-band omnidirectional CP antenna	64
4.16. AR of the dual-band omnidirectional CP antenna	65
4.17. AR vs. angle and frequency for the dual-band OCPA	65
4.18. Realized gains of dual-band OCPA ($\phi = 0^\circ$ cut, lower frequency)	66
4.19. Realized gains of dual-band OCPA ($\phi = 90^\circ$ cut, lower frequency)	66
4.20. Realized gains of dual-band OCPA ($\phi = 0^\circ$ cut, higher frequency)	67
4.21. Realized gains of dual-band OCPA ($\phi = 90^\circ$ cut, higher frequency)	67
4.22. Parameter study of the protruding stubs of the dual-band OCPA	70
4.23. Parameter study of the slot difference (S_{11}) of the dual-band OCPA	72
4.24. Parameter study of the slot difference (AR) of the dual-band OCPA	72
5.1. Reconfigurable OCPA	75
5.2. Electric field between points C_1 and C_3	79
5.3. Photo of the reconfigurable OCPA	80
5.4. S_{11} of the reconfigurable OCPA	81
5.5. Realized gains of reconfigurable OCPA ($\Delta_{ph} = 0^\circ$, xz -plane)	83

5.6. Realized gains of reconfigurable OCPA ($\Delta_{ph} = 0^\circ$, yz -plane) .	83
5.7. Axial ratio map of reconfigurable OCPA ($\Delta_{ph} = 0^\circ$)	84
5.8. Realized gains of reconfigurable OCPA ($\Delta_{ph} = 0^\circ$, yz -plane) .	84
5.9. Realized gains of reconfigurable OCPA ($\Delta_{ph} = 180^\circ$, yz -plane)	86
5.10. Realized gains of reconfigurable OCPA ($\Delta_{ph} = 180^\circ$, xz -plane)	87
5.11. Axial ratio map of reconfigurable OCPA ($\Delta_{ph} = 180^\circ$)	87
5.12. Realized gains of reconfigurable OCPA ($\Delta_{ph} = 180^\circ$, yz -plane)	88
5.13. Realized gains of reconfigurable OCPA ($\Delta_{ph} = +90^\circ$, γ_{45} plane)	89
5.14. Realized gains of reconfigurable OCPA ($\Delta_{ph} = +90^\circ$, γ_{135} plane)	90
5.15. Axial ratio map of reconfigurable OCPA ($\Delta_{ph} = +90^\circ$)	90
5.16. Realized gains of reconfigurable OCPA ($\Delta_{ph} = +90^\circ$, γ_{45} plane)	91
5.17. Realized gains of reconfigurable OCPA ($\Delta_{ph} = -90^\circ$, γ_{135} plane)	92
5.18. Realized gains of reconfigurable OCPA ($\Delta_{ph} = -90^\circ$, γ_{45} plane)	92
5.19. Axial ratio map of reconfigurable OCPA ($\Delta_{ph} = -90^\circ$)	93
5.20. Realized gains of reconfigurable OCPA ($\Delta_{ph} = -90^\circ$, γ_{135} plane)	93
6.1. Depiction of even and odd transmission line modes	96
6.2. Dual CP antenna	98
6.3. Electric fields in the feed network of dual CP antenna	99
6.4. S_{mn} of the dual CP antenna	100
6.5. AR of the dual CP antenna	101
6.6. Realized gains of dual CP antenns (yz -plane, port 1)	102
6.7. Realized gains of dual CP antenns (yz -plane, port 2)	103
6.8. Realized gains of dual CP antenns (xz -plane, port 1)	103
6.9. Realized gains of dual CP antenns (xz -plane, port 2)	104
6.10. Schematic depiction of the port-to-port isolation mechanism .	105

LIST OF TABLES

3.1. CNR of GPS L1 signals for antennas in various orientation . .	34
4.1. Impact of various capacitors on dual-band OCPA performance	61
5.1. Phase between corresponding quadrature points in reconfig- urable OCPA	77

1. INTRODUCTION

The study of polarisation of radio waves can be dated back to the experiments conducted by Heinrich Hertz between 1886-1889, when he investigated transmission through horizontally or vertically aligned conducting grids ([1], p. 190). Around 1892 the concept of Poincare sphere (Fig. 1.1) was introduced, allowing easy viewing and analysis of all possible polarisations. On the sphere surface, the azimuth angle is double the tilt of the major axis of the polarisation ellipse and the polar angle corresponds to the phase shift between the two orthogonal components.

From a practical point of view, the polarisation can be classified into three categories: linear at the equator of the Poincare sphere (with horizontal and vertical polarisation being in antipodes), two circular polarisations at the poles and elliptical polarisation elsewhere. The elliptical polarisation is a very general term and radio systems are rarely designed to use explicitly this type, although both linear and circular polarisations can be considered as special cases of elliptical polarisation. Linear polarisation is very simple to generate and is used for radio broadcasting, mobile phones and in many classical radio applications. However circular polarisation (CP) exhibits unique properties, which are employed in high performance radio systems.

1.1. Benefits of Circularly Polarised Antennas

To generate circular polarisation, two orthogonal components of electric field are needed. These components need to be equal in amplitude, but shifted in phase by $\pm 90^\circ$ (hence located at the poles of Poincare sphere).

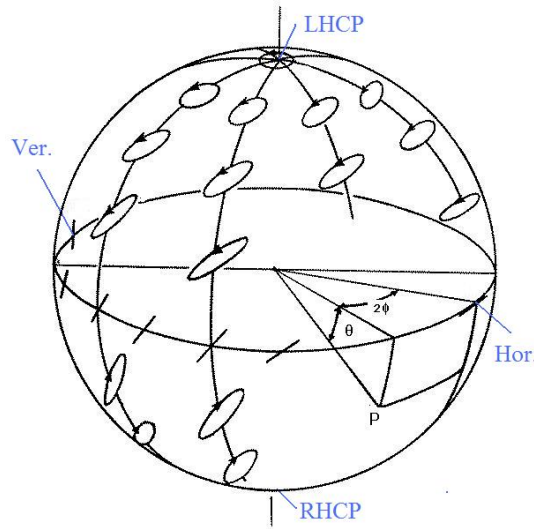


Figure 1.1. The Poincaré sphere depicting all possible polarisations of electromagnetic waves in the far field. Left hand CP is located at the very top of the sphere, whereas right hand CP is at the bottom.

CP antennas are demanding to design, however offer multiple benefits:

- **Immunity to Faraday rotation.** The Faraday effect causes a rotation of the plane of polarisation. This rotation is proportional to the component of the magnetic field in the direction of propagation. This causes a problem in higher parts of Earth's atmosphere, where highly ionized plasma generates strong magnetic fields [2]. However the strength of this field varies, depending on many difficult to predict factors (i.e. time of the day, year, solar activity etc.). For linear polarisation this would cause polarisation mismatch of the signal. Circular polarisation is immune to this effect, as both orthogonal components are equal in magnitude and rotated by the same angle. This is main reason for using CP in almost all Earth-satellite communication systems.
- **Mitigation of multipath propagation.** A circularly polarised wave, after reflection from a conducting, flat surface, becomes counter polarised (that is right hand CP wave becomes left-hand CP and vice

versa). This allows the antenna to filter out reflected signal [3] and is of huge benefit for navigation systems, especially satellite based. It also offers benefits for high data rate communication in indoor environments, as it decreases interference between direct and reflected signal.

- **Polarisation losses due to misalignment.** For linearly polarised communication systems the receiving and transmitting antenna must be aligned to avoid polarisation mismatch. For CP this is not required [4]. It is worth mentioning that if ideal CP signal is received by a linearly polarised antenna the loss is 3 dB, regardless of the orientation of the receiving antenna. This property is especially useful for RFID systems, as it ensures the portable tag will be detected regardless of its orientation [5].

1.2. Challenges for Circularly Polarised Antennas

Given the above advantages, there is a large demand for advanced CP antennas. Despite this, many features available for linearly polarised antennas (i.e. wideband, omnidirectionality) are currently not possible for CP. The aim of this work is to overcome those drawbacks and propose new designs that will benefit the telecommunication market. The challenges are:

1.2.1. Omnidirectional Radiation Pattern

Although the oldest and most simple linearly polarized antennas (i.e. dipoles and monopoles) produce omnidirectional radiation pattern, achieving similar performance with circularly polarized antennas is much more difficult. This is mainly due to the fact, that the CP generation requires two orthogonal components of the electric field, each with equal magnitude and $\pm 90^\circ$

phase shift. However for wider angles it is difficult to maintain the orthogonality of these components. For microstrip patch antennas, which are very convenient due to easy manufacturability, the ground plane attenuates the electric component parallel to it, degrading the axial ratio. So far proposed omnidirectional CP antennas usually either use multiple radiators or complex polarisers. Neither of these solutions are convenient for applications on small portable devices.

Compact and easy to manufacture omnidirectional CP antennas could have many applications. Some examples include:

- Point-to-multipoint communication. Omnidirectional CP antennas could provide all the benefits of circular polarization in systems, where a centrally located node broadcast radio messages to surrounding units.
- In radio frequency identification (RFID) the omnidirectional pattern would minimize the risk of not detecting a tag due to nulls in radiation pattern. The circular polarisation would ensure a tag is detected regardless of its orientation. This is especially valuable in security systems, where RFID is employed to prevent carrying objects outside of a certain area.
- For many remote tracking applications the proper antenna orientation can not be guaranteed at all times. This is because the tracking device (and antenna) is attached to tracked object. If the object is rotated, so will be antenna. Currently all satellite navigation signals are right-hand circularly polarized, therefore omnidirectional CP antenna could overcome this problem.
- Many satellites use spin stabilisation as a simple and low cost way to maintain their orbit. This means the spacecraft rotates constantly. To provide satellite-Earth communication (i.e. for telemetry, tracking and command (TT&C)) an omnidirectional pattern is required and

circular polarisation is employed to mitigate the effect of Faraday rotation in the ionosphere. Currently used state-of-the-art antennas for TT&C on a spinning stabilized satellites are complex, expensive and heavy. Solutions outlined in this thesis could provide less expensive and more lightweight alternatives for them.

1.2.2. Pattern Reconfigurability

There are many CP antennas offering a reconfigurable sense of polarisation, however only a few designs offer pattern reconfigurability. This is because of the difficulty in maintaining orthogonality of the two components for all switched beams.

Classical antenna arrays incorporating simple CP antennas can be employed to steer the CP beam. However to achieve a wide scanning angle, each element should be either omnidirectional or radiate within very large beamwidth (in terms of both power and axial ratio). This refers back to the problem of omnidirectionality in Section 1.2.1. Apart from this, the use of antenna arrays is again not practical in small and low cost devices.

1.2.3. Wideband Radiation

CP antennas require a 90° phase shift between the two components of electric field. This imposes a limitation on the bandwidth of such antennas. There are two most often used methods for generating circular polarisations. One is to use a perturbation element integrated within the radiator, which generates two orthogonal modes. This method is simple to manufacture, however it is also very narrowband, as it uses only a small fraction of the impedance bandwidth.

Alternatively a radiator with multiple inputs can be implemented and the phase shift is generated by external circuitry. This method is more wideband, however it is still limited by phase shifter performance. It was

only recently, that UWB phase shifters were introduced in the literature [6]. Unlike classical solutions they employ capacitive coupling mechanism, which acts as a differentiation the UWB pulse. When the parameters are properly adjusted, the circuit can produce relatively stable phase shift across multiple frequencies. The use of such shifters should help overcome the problem of narrowband CP [7].

An exception to the above categories are spiral antennas (described in more details in Section 2.3), which are considered as frequency independent and therefore offer CP radiation across ultra-wide band (UWB). They are however large in size, require a balun and the phase centre varies with frequency. They also radiate two counter polarised beams towards their front and back. This performance can be suppressed by placing absorber on one side, however this leads to low efficiency as half of the power is wasted. The addition of a reflector would destroy the frequency independent performance, as it should be located at $\lambda_0/4$ distance from antenna.

1.2.4. Manufacturability and Miniaturization

The important factor for the antenna designs is its manufacturability. There is growing commercial pressure on miniaturization of antennas, especially with decreasing size and increased demand for multiple radio systems (GPS, Glonass, WLAN, Bluetooth etc.) in mobile phones [8]. This is in fact very difficult to achieve with CP antennas, as two orthogonal components require more space than only one component for linear polarisation. The classical miniaturization approaches - well used for linearly polarised antenna, such as fractal structures, folding or short-circuiting of the radiator - would decrease polarisation purity. The use of high permittivity material may solve the problem, however at the price of reduced bandwidth.

Another important factor is the cost of antenna manufacture and mounting, which should be kept as low as possible. Currently CP antennas available on the market with good AR performance are expensive. The signif-

icance of this problem may be highlighted by the fact, that many mobile phone manufacturers decided to use linearly polarised inverted-F antennas as GPS receiving antennas, despite the loss of 3 dB of signal due to polarisation mismatch and increased positioning error due to vulnerability to multipath propagation.

1.3. Methodology

The methodology used in this thesis is schematically shown in Fig. 1.2. Based on an idea, the proposed antenna is first designed and simulated in a full wave simulation software CST Microwave Studio [9]. If the simulated antenna achieves the expected performance, it is prototyped. For this purpose, the LPKF Proto Mat C60 milling machine [10] is used to shape the metallisation on the PCB and drill holes for vias. To manufacture multi-layer structures, a press machine LPKF Multipress S [11], available at the National University of Ireland Maynooth, is used to bind the PCB layers together. The manufactured prototype is measured using a Rohde & Schwarz ZVA-24 Vector Network Analyzer [12] for reflection and where applicable, transmission coefficients. The radiation parameters, such as gain, pattern and axial ratio are measured (with exception of Section 5) in a semi anechoic chamber, operated by the DIT Antenna and High Frequency Research Centre. The chamber performs far field measurements using a ZVA-24 VNA and a Schwarzbeck BBHA 9120 D [13] standard gain horn antenna. To suppress reflections Emerson & Cuming Eccosorb VHP-18 pyramidal carbon loaded urethane foam absorber (45 cm long) are located in 5 areas identified to produce strongest reflections. The rotating table allows to perform the measurement in one dimension.

Measurements of reconfigurable antennas, presented in Section 5, were performed at the Institute for High-frequency Technique, RWTH Aachen University in Aachen, Germany. The chamber used is a compact measure-

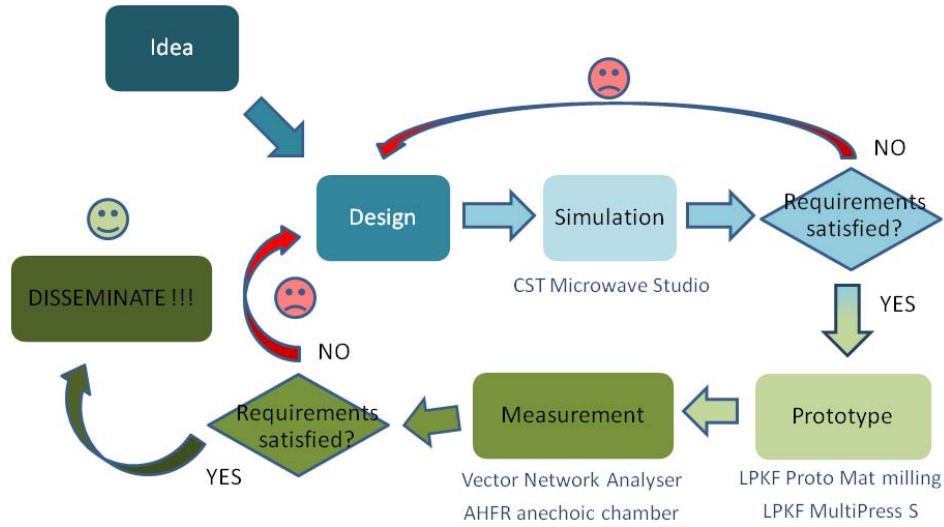


Figure 1.2. Flow diagram of the research methodology used.

ment range with single reflector and a 3-D positioner, able to perform far field measurements in the range of 2 - 75 GHz. The chamber is shielded and fully anechoic [14].

If the measured results do not satisfy the requirements, the design goes back to the design and simulation stage. During this phase it is attempted to identify possible differences between the simulated and measured structure, for instance manufacturing inaccuracies, impact of glue used to bind the PCB layers or current on the outside of the feed cables. The design is modified, to either remove these discrepancies or ensure they won't be influential on antenna performance. Then the modified prototype is manufactured and the process continues until the desired antenna requirements are satisfied by the prototype.

1.4. Antenna Parameters

The antenna performance is evaluated, depending on many different criteria. Of course each antenna is intended for different applications and there-

fore the significance of each parameter varies for different design. However usually the following parameters are measured:

1.4.1. Reflection and Transmission Coefficients

Reflection coefficient in dB, usually referred to as S_{nn} , indicates the amount of power that is reflected at an antenna port n . For single port antennas ($n = 1$), due to the **law of conservation of energy** the power that is not reflected can be either transformed into heat or radiated by the antenna. For most antennas, it is assumed that the losses generated by conductive elements and δ_{tan} of dielectric substrate are negligible and therefore the reflection coefficient S_{11} is a reliable measure to determine the percentage of power that an antenna is radiating; It is assumed, that the antenna is a good radiator at a certain frequency f if S_{11} at this frequency is below -10 dB (for some small commercial or low frequency antennas this limit is relaxed to -6 dB, however such applications are not covered in this thesis). Therefore **impedance bandwidth** can be defined as a frequency range, in which for all frequencies f the requirement $S_{11}(f) < -10$ dB is fulfilled. It needs to be remembered however, that the assumption of a loss-free structure is not true if an antenna incorporates absorbing material, resistors (i.e. in a Wilkinson divider) or uses an additional port terminated by a match. To avoid this problem, antenna reflection coefficient were measured directly at the antenna input and not at the input of feed network.

For multiport antennas the reflection coefficient S_{nn} alone is not sufficient to measure antenna performance, as—in addition to thermal losses and radiation—the power can be transmitted from one port to another. The transmission coefficient expressed in dB, S_{mn} , defines the amount of power that is transmitted from one port to another. Therefore, in this thesis, it is assumed that for a certain frequency f the investigated antenna is a good radiator excited at port n if $S_{nn}(f) < -10$ dB $\wedge \forall_m S_{mn} < -10$ dB. This criteria is also used to define the impedance bandwidth for multiport antennas.

1.4.2. Radiation Pattern, Directivity, Gain and Realized Gain

For antenna design it is very important to determine the directions in which the antenna radiates. This is done through gain, realized gain, directivity and radiation pattern. The **radiation pattern** shows the amount of power radiated in a certain direction as a function of angles θ and ϕ normalized to the maximum value. Although it gives basic information on angular properties of an antenna, it provides no information on the exact power being radiated.

Directivity can be defined as a ratio of radiation intensity in a certain direction (θ, ϕ) to the radiation intensity of an isotropic antenna. Although it was proven by Mathis [15] that due to the properties of a vector field tangential to a sphere such an antenna is impossible to realise, but it is convenient to use as a reference for real antennas. For an isotropic antenna the radiation intensity in a certain direction is defined as:

$$U_{iso}(\theta, \phi) = \frac{P_{rad}}{4\pi} \quad (1.1)$$

where:

P_{rad} is total radiated power

Applying this to define directivity of an antenna under test (AUT), one obtains:

$$D = \frac{U_{AUT}(\theta, \phi)}{U_{iso}(\theta, \phi)} = \frac{4\pi U_{AUT}(\theta, \phi)}{P_{rad}} \quad (1.2)$$

where:

$U_{AUT}(\theta, \phi)$ is radiation intensity of AUT in a certain direction

Since it is very difficult to exactly measure total radiated power, the definitions of gain and realized gain were introduced. Antenna **gain** is defined as a ratio of 4π times the radiation intensity in a certain direction to total

power accepted by the antenna, that is: all power that was not reflected at the input port. This means gain also takes into account the losses generated in the antenna by conducting elements and δ_{tan} in the dielectric. Gain can also be described as a directivity multiplied by **radiation efficiency**, which is defined as a ratio of total radiated power to total accepted power.

The definition of **realized gain** takes into account also mismatch losses, generated at the antenna port and is defined as a ratio of 4π times the radiation intensity in a certain direction to the total power delivered to the antenna. Realized gain can be also be described as directivity multiplied by **total efficiency**, which is the radiation efficiency multiplied by the ratio of accepted power to the power delivered. For a single port antenna this equals $\eta_{total} = \eta_{rad}(1 - |S_{11}|^2)$ when S_{11} is expressed in linear scale. These relations can be summarized as following:

$$G_{realized} = (1 - |S_{11}|^2)G = \eta_{total}D = (1 - |S_{11}|^2)\eta_{rad}D \quad (1.3)$$

where:

$G_{realized}$ is realized gain

G is gain

η_{total} is total efficiency

η_{rad} is radiated efficiency

and S_{11} is expressed in linear scale.

Total and radiation efficiencies provide much better insight into antenna performance than reflection coefficient. However their measurement poses a significant difficulty, as it requires to measure total radiated power (i.e. to measure all power radiated within whole sphere surrounding the antenna). This is impossible to perform with the facilities currently available at DIT. Therefore the efficiencies provided in these thesis are just estimations, obtained from the CST Microwave Studio simulator.

All results presented in this thesis, both measured and simulated,

depict **realized gain**. This convention is especially practical for multiport antennas, where the calculation of accepted power from both reflection and transmission coefficients would add additional complexity. The isotropic antenna, used as a reference antenna for gain calculations, is assumed to be perfectly circularly polarised, with axial ratio of 0 dB. CP gain values in dB which are referenced to this antenna are expressed in **dBic**.

1.4.3. Axial Ratio

Axial ratio (AR) is a parameter that determines the polarisation purity of CP. For perfect circular polarisation, as seen at the poles of Poincare sphere in Fig. 1.1, the tip of electric field vector *draws* a perfect circle in the polarisation plane. However, in practice, this ideal situation is rarely the case and usually the tip *draws* an ellipse. By comparing the ratio of the major axis of such an ellipse to its minor axis one can quantitatively determine *imperfections* of circular polarisation. A perfect circularly polarised wave has an $AR = 1$ (or 0 dB) and linearly polarised wave has $AR = \infty$.

For CP antennas, the axial ratio is related to cross polarisation. The cross polarisation is the ratio between LHCP and RHCP radiation intensity in a certain direction for antennas intended to generate RHCP and the ratio of RHCP to LHCP for antennas intended to generate LHCP. This relation is given by the following equation [16]:

$$AR_{dB} = 20 \log_{10} \left(\frac{1 + 10^{\frac{-|U_{RHCP} - U_{LHCP}|}{20}}}{1 - 10^{\frac{-|U_{RHCP} - U_{LHCP}|}{20}}} \right) \quad (1.4)$$

where U_{RHCP} and U_{LHCP} are radiation intensities in dB for a certain angle of respective RHCP and LHCP signals.

The **axial ratio bandwidth** describes a frequency range, in which the antenna axial ratio is kept below a certain level. For classical unidirectional antennas a frequency is considered to be within this bandwidth if the AR at boresight is below 3 dB. This definition will be applied to antennas described in Sections 2 and 6. However the antennas in Sections 3 - 5 are

omnidirectional CP antennas, for which this understanding of axial ratio bandwidth is of little use. Therefore in these sections a frequency will be considered to be within AR bandwidth, if for **all** angles in certain plane (called the **omnidirectional plane**) the AR is below a certain level. For planar omnidirectional CP antennas the 3 dB AR limit was relaxed to 5.68 dB. This value was chosen, as it provides 10 dB of cross polarisation level. It was assumed that such cross-polarisation level is sufficient for many applications. Where other AR limits were applied, it will be explicitly noted in the text.

1.5. Research Summary

The innovation of this thesis is focused mainly around various omnidirectional CP antennas, which unlike previously available solutions, are planar and easy to manufacture using multilayer PCB technology. Section 2 provides a background for the proposed innovations and briefly discusses state-of-the-art CP antennas. Section 3 introduces and discusses basic techniques to realize planar Omnidirectional CP Antennas (OCPA). A simple OCPA is simulated and measured to confirm the presented theory. Next, in Section 4, this technique is applied to introduce various advanced antenna designs, for instance dual band or folded miniaturized OCPAs. Section 5 further extends this concept and shows, that an OCPA can be easily modified to achieve pattern reconfigurability. This is considered to be of special significance, as such an antenna can receive or transmit signals from any direction around a full sphere (subject to proper steering and mount). Section 6 presents a compact dual-polarised unidirectional CP patch antenna. To achieve dual polarisation, the design employs even and odd transmission line modes. The resultant feed network is compact and unlike dual polarised CP antennas which use switching elements, it can use RHCP and LHCP channels simultaneously. Finally conclusions and potential future developments are discussed in Section 7.

2. STATE OF THE ART CIRCULARLY POLARISED ANTENNAS

2.1. Microstrip Patch Antennas

Microstrip patch antennas are possibly the most commonly used geometries for circular polarisation. They consist of a dielectric printed circuit board (PCB) with a conducting patch (acting as a resonator) printed on one side and groundplane on the other. Unlike some other antennas (for instance crossed dipoles), the introduction of the orthogonal mode does not increase patch dimensions, as even for linearly polarised antennas the width should be of comparable size to the length to control the input resistance. Microstrip patch CP structures can be divided into single feed and multiple feed types; this determines the mechanism of CP generation. These types are discussed below.

2.1.1. Single Fed Circularly Polarised Patch

Use of single feed has an advantage of simplicity and smaller feed network, without the need to incorporate phase shifters and power dividers. On the other hand this implies, that the two orthogonal modes and the phase shift required for CP need to be generated internally by the antenna geometry. There are many methods to achieve this, with the most commonly used shown in Fig. 2.1.

For the almost-square patch technique (Fig. 2.1a) the feed is located on the diagonal of the patch in order to excite two modes. The phase dif-

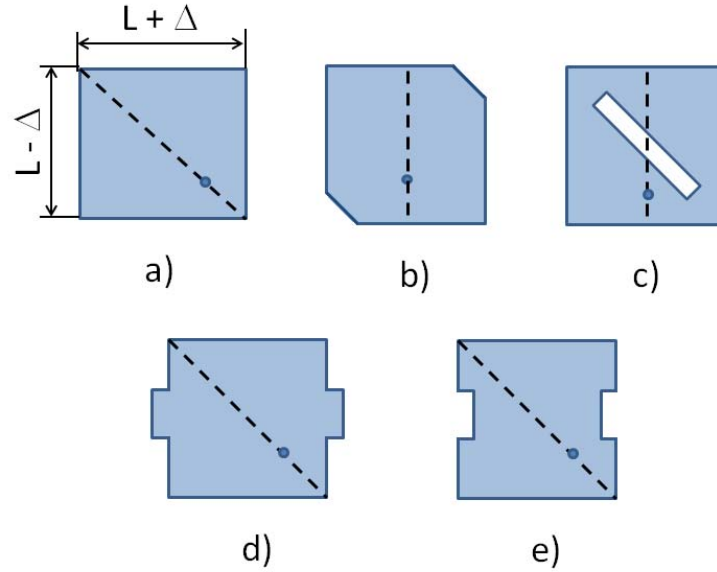


Figure 2.1. Geometries of various CP patches. Dashed line shows the line along which the feed point is located.

ference is achieved by introducing a small difference between the length and width of the patch, making the two modes resonate at slightly different frequencies. Around resonant frequency, the antennas performance switches from capacitive reactance (lower half of the Smith chart) to inductive reactance (upper part of the Smith chart). Therefore in the frequency range between the two resonances, one mode will have positive and the other - negative reactance. By adjusting this values, a 90° phase shift can be obtained. This is made by introducing a small difference Δ between patch length and width (see Fig. 2.1a). The difference should be inversely proportional to antenna quality factor (Q), i.e. lower Q requires greater Δ . This method results in an impedance bandwidth much wider than that of equivalent linearly polarised patch, however the axial-ratio bandwidth is narrow and also inversely proportional to Q [17].

The truncated corner technique (Fig. 2.1.b) employs cutting off two corners on the rectangular patch, located across a diagonal. The feed is lo-

cated at the middle of one of the edges. It therefore directly excites one mode and the other is excited by the irregularity in the square geometry of the patch. The sense of polarisation depends on which two corners are truncated, therefore solutions for polarisation reconfigurability have been proposed by covering and uncovering the truncation, as introduced by Hsu and Chang in [18].

For these antenna types it can be difficult to achieve a good impedance match, when feeding the patch directly from a $50\ \Omega$ microstrip line. For linearly polarised antennas an inset feed can be employed. However the two slots introduced into the patch by this technique will perturb the current for the orthogonal mode and as a consequence degrade circular polarisation. Chen et al. in [19] propose a solution to this problem, where the impact of the inset feed is balanced by additional slots cut along other edges of the patch. This provides good AR performance while feeding the patch directly from a $50\ \Omega$ microstrip line.

Alternatively to the truncated corners, a diagonal slot can be introduced into the patch (Fig. 2.1.c). This acts similarly to the truncated corner, with the narrow slot splitting the energy into two orthogonal modes with appropriate phase shift. It was also demonstrated by Nasimuddin et al. [20] that a set of circular slots can be implemented, as long as there is an asymmetry in the structure to excite two orthogonal modes.

Alternatively, the slot can be located parallel to the edge of the patch and the feed located on the diagonal. In principle this work is similar to the almost-square patch, but the difference in resonant frequency is generated not by the longer patch, but by the fact that the current flows around the slot. This method is also very convenient to introduce polarisation reconfigurability; by introducing a pin diode, MEMS switch or other suitable component the slot can be short circuited or not, switching between the RHCP and LHCP, as in [21].

An interesting method for a patch antenna fed by a coplanar waveguide (CPW) was proposed by Huang and Wong in [22]. In this method the mode

perturbation was made by a 45° inclined slot in a ground plane, protruding on both sides of CPW feed. The patch used is a regular square and both the perturbing and feed structures are located on the groundplane layer. Later Aissat et al. [23] confirmed the same performance for the circular patch.

Last, but not least, a stub protruding from the edge (Fig. 2.1.d) or a section removed from the edge (Fig. 2.1.e), or the combination of both can be used to generate 90° phase shift. Such structures - when properly designed - introduce inductance and capacitance, which generates the phase shift.

2.1.2. Dual and Multiple Feeds

Dual-fed patch antennas require a power divider and a polariser, which increases the antenna complexity and footprint. The advantage is improved axial ratio bandwidth, as this is not dependant on the mode perturbing element. Depending on the bandwidth characteristics of the phase shifter used, the antenna's axial-ratio bandwidth can be as large as the full impedance bandwidth.

A very convenient way to feed these antennas is through a hybrid coupler. This has the additional advantage, that both RHCP and LHCP can be achieved simultaneously, depending which input port of the hybrid coupler is excited. Although classical hybrid couplers require significantly more space than simple phase shifters, recently a miniaturization method was proposed by Ferrero et al. [24]. The method incorporates capacitors to replace two 90° branches. Additionally, by replacing fixed value capacitors with varactors, one can achieve a quad-polarised antenna, with two circular (when varactors are ON) and two linear (when they are OFF) polarisations [25].

Although the use of more than two feeds may seem redundant, it was demonstrated by Sun et al. [26] that such antennas have significantly wider axial ratio bandwidth than dual feed antennas. Also by using four feeds, one can also excite higher modes in the patch as demonstrated by

Huang [27]. For this configuration, the feed points are located at various angles in a circular patch. Three configuration discussed in [27] employ feeds located in 45° (for TM_{21} mode), 30° (for TM_{31}) and 67.5° (for TM_{41}). The phase shift is not proportional to the angle and is either 0° , 90° , 180° and 270° for odd order modes (TM_{11} and TM_{31}), or two 0° and two 90° shifted inputs for even order modes (TM_{21} and TM_{41}). Motivation for this arrangement is to achieve a CP conical beam, where the angle of the beam can be designed in the range of 35° to 70° .

2.2. Crossed Dipoles and Slot Antennas

Crossed dipoles (see Fig. 2.2) and slot antennas are also used to generate circular polarisation, when fed with the appropriate phase shift. Due to a geometric limitation they usually generate opposite-sense (i.e. RHCP and LHCP) polarisation in the front and rear directions. This is accompanied by either nulls or linearly polarised radiation on the sides. This makes this antenna type most suitable for linear-to-circular communication. In such communication, the CP antenna is used (usually as receive antenna) in order to minimize polarisation mismatch with a randomly oriented linearly polarised antenna. As the transmitting antenna is linearly polarised, the sense of CP is of secondary importance. The method is most beneficial for RFID and WLAN applications. An additional advantage for the latter application is the fact, that slot or dipole antennas usually have a wider impedance bandwidth than patch antennas.

The presence of a rearward LHCP beam in a RHCP antenna is an obvious disadvantage for satellite navigation applications. To overcome this issue, a reflector spaced at $\lambda_0/4$ can be implemented to reflect the unwanted LHCP and—as reflected CP signal changes its polarisation—increase RHCP gain. The price for this is increased antenna size and manufacturing complexity.

One of oldest methods to generate CP is to use two dipoles, crossed at an angle of 90° . The dipoles are fed with 90° phase shift. This technique offers

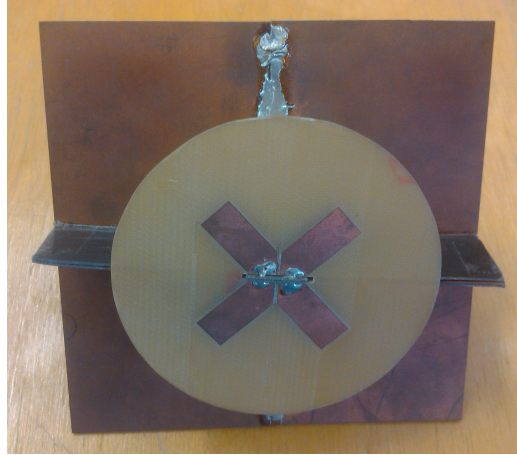


Figure 2.2. Example of a crossed dipole antenna with two separate feeds.

wider bandwidth than patch antennas, as there have been many techniques developed to increase impedance bandwidth of a dipole. The axial ratio bandwidth of crossed dipole antenna is therefore limited by the feed network, i.e. by the frequency range for which a stable 90° phase shift can be produced with equal amplitudes. However, using the wideband and ultra-wideband phase shifters proposed by Abbosh [6], this problem is expected to be solved in the near future. Alternatively, the two dipoles can be tuned to resonate at slightly different frequencies, as demonstrated by Bolster in [28]. This is in principle a similar technique, to the almost square patch and suffers from the same problem of relatively narrow bandwidth. Another disadvantage of the crossed dipole is its complexity and manufacturability. Usually the phase shifter is implemented as an external circuit, located behind the antenna. Baik et al. proposed to integrate the shifter into antenna, by making a $\lambda_0/4$ long arc connection between the arms [29]. This enabled the implementation of a crossed dipole using two metallization layers (single substrate layer) with only one feed. Another development by Lin et al. [30] proposed to generate the phase shift employing parasitic metal strips in conjunction with different arm lengths. The antenna is also realised on a single substrate with dual layer metallisation.

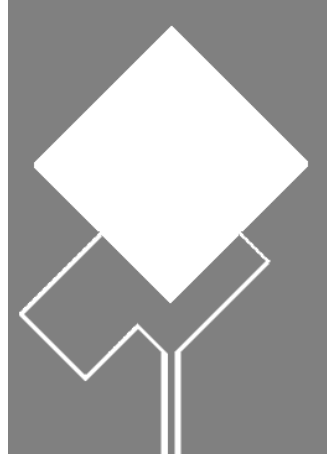


Figure 2.3. Aperture antenna, where CP is generated by two slot lines separated from CPW

Slot or aperture CP antennas can be implemented by introducing a phase perturbation into the slot to generate CP. Many implementations exist with various shapes, with perturbation elements varying from the simple bent stub [31] with AR bandwidth of 17%, to more complex perturbation elements [32] reaching up to 34% of AR bandwidth.

Another possible implementation of a CP aperture antenna uses dual feed with an external phase shifter. Amongst others, an interesting solution was proposed by Soliman et al. [33] to employ two slots of coplanar waveguide (CPW), as seen on 2.3. The slots of CPW are separated from each other at 90° angle, effectively creating a compact power divider with two slot lines as outputs. Next, a 90° phase shift is applied to one of the slots. This solution is compact and offers some interesting functionality, which will be discussed further in Section 6.

Finally, a technique for generating ultra-wideband CP with single dipole-like structure was proposed by Bao and Ammann in [34]. For this technique two arms of a quasi-dipole (with the arms being of unequal length) protrude from a groundplane and are bent at a right angle (see Fig. 2.4). The antenna applies many features to increase both impedance and axial ra-

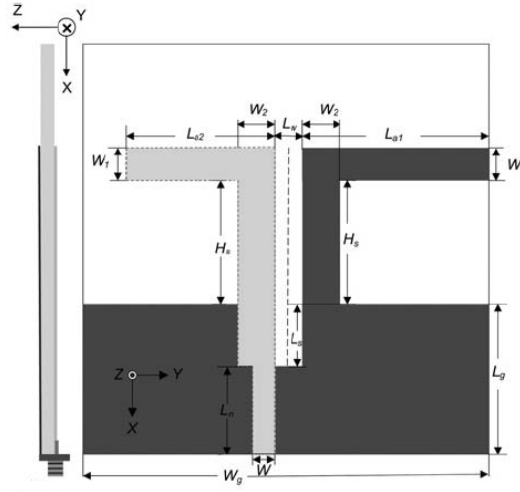


Figure 2.4. Dipole-like CP antenna with 38% AR bandwidth, as presented in [34] (courtesy of X.L. Bao and M.J. Ammann)

tio bandwidth. The most important is a open-ended slot located in the groundplane (L_s as on Fig. 2.4), close to the feed point. By doubling this slot length from 4 to 8 mm the impedance bandwidth was improved by 300 MHz (centre frequency at 2.0 GHz) and AR in the lower part of operating band at 1.9 GHz improved from 3 dB to 1 dB. The length difference between the two arms increased the impedance bandwidth. Also spacing between the dipoles and groundplane was discovered to be a key parameter: with greater spacing the impedance bandwidth shifts downwards and AR bandwidth extends towards lower frequencies. By proper adjustment of all those parameters the antenna achieved an AR bandwidth of 38%. The proposed design is small, compact and easy to manufacture.

2.3. Spiral Antennas

Unique example of circularly polarised antennas dedicated for ultra-wideband (UWB) operation are spiral antennas. The main features of these antennas

can be defined only by angles (not, as with previous types, by lengths and widths) and hence are often called frequency independent antennas [35]. The geometries are spiral shaped, usually with two or four arms, although single arm spirals over a ground plane also exist [36]. The arm lengths need to be significantly longer than a wavelength, limiting the bandwidth for low frequencies. This also implies, that spiral antennae are significantly larger than other CP antennas.

The antenna produces a RHCP beam on one side and a LHCP on the other. The very wide bandwidth prevents the use of reflectors, usually positioned at $\lambda_0/4$ distance and is therefore frequency dependant. To solve this problem, the antenna is sometimes backed by an absorbing material, which however generates additional losses and limits the power handling capability.

The spiral is traditionally fed in the middle through a balun, with the electromagnetic wave propagating outwards. For this configuration there is a risk, that the propagating wave might be reflected from the tip of the arm and propagate backwards, degrading the crosspolar performance. To avoid this, an absorbing material can be placed at the outer perimeter of the spiral [36]. Spiral antennas fed from the outer perimeter are less common, mainly due to much worse axial ratio performance and a tilt of the main beam. However they can be fed without a balun, directly from a CPW, as demonstrated by Muller and Sarabandi in [37].

Despite the ultra-wideband performance, the antenna is significantly larger than most CP antennas and hence difficult to apply for small hand-held devices. Also its property of radiating counter-polarised beams on the opposite sides can be problematic, especially for positioning applications.

2.4. Sequentially Rotated Arrays

A sequentially rotated array allows the realisation of circular polarisation from linear elements, as demonstrated by Huang in [38]. This is done by spacing n identical antennas in the rotational symmetry around a common point (see Fig. 2.5). Each antenna is fed with a phase shift, which is proportional to the orientation of the antenna around the common point. For instance, in the most common configuration with four antennas, the top antenna has 0° , 90° , 180° and 270° phase shifts, as indicated on Fig. 2.5.a. This arrangement would generate LHCP, for RHCP the phase would need to increase counter-clockwise. Another often employed configuration involves three elements, as in [39]. The phase shifts for such configuration are 0° , 120° and 240° , as indicated on Fig. 2.5.b.

To further improve the axial-ratio the single antennas used in the array can be also circularly polarised. Hall in [40] demonstrated a sequentially rotated array based on CP-elements in various configurations. In this case, the sequentially rotated array offers very low AR levels across a wider bandwidth. The most significant improvement for AR bandwidth is seen for 3 and 2 element arrays. Four element arrays offers similar bandwidth when used with CP and linearly polarised elements [40].

The main disadvantage of this method is the dimension of the array. However since the polarisation of a single element does not need to be circular, one can employ electrically small antennas to reduce the size. Bang et al. proposed to use four sequentially rotated inverted-F antennas in a 3D folded configuration to generate CP [41]. The resultant antenna is very compact and can be easily fitted into a tip of an artillery projectile. In another work by Tea et al. [42] four sequentially rotated dual band inverted-F are successfully proposed, with AR levels below 1.5 dB at boresight.

As this antenna type is an array, the designer need to pay attention to the distance between the elements. Similarly to classical arrays, if the distance between antennas is greater than $\lambda_0/2$, the CP beam with good AR



Figure 2.5. Visualisation of sequentially rotated array with three (a) and four (b) elements. The numbers indicate phase shift, at which each element is fed. Generated wave will be RHCP into the page and LHCP out of it.

will become very narrow and randomly polarised sidelobes may occur. If the antennas are too close, some coupling between them might perturb the radiation pattern. Finally, very often this antenna type also radiates RHCP on one side and LHCP on the other. However here - unlike with spiral antennas or crossed dipoles - this problem can be solved by placing a reflector at the $\lambda_0/4$ distance, or by designing elements of the array to radiate only in the forward direction.

2.5. Antennas for GNSS Applications

Global Navigation Satellite Systems (GNSS) demand very specific antenna designs [43]. This is because the system calculates the distance between the satellite vessel and the ground based receiver, based on the time it takes for a radio signal to travel this distance. However, if the radio signal is reflected, the time it takes to reach a receiver will be longer and a positioning error occurs. The use of CP allows the suppression of some of the reflected signals, as RHCP signals reflected from a regular surface be-

comes LHCP (and vice-versa for reflected LHCP signal). This principle is demonstrated in Fig. 2.6 for various scenarios. All operational and planned GNSS satellites (that is American GPS, Russian Glonass, European Galileo and Chinese BeiDou-2) transmit RHCP signals. For a line-of-sight scenario, this signal also arrives at the receiver as RHCP (Fig. 2.6.a). If a signal is reflected once (or odd amount of times) from a regular surface, it changes the sense of polarisation and the signal that reaches the receive antenna is LHCP (Fig. 2.6.b). By using an antenna with good AR, this signal can be filtered out and hence improve positioning accuracy. If the signal is reflected twice (or $2N$ -times, where N is a natural number), it becomes RHCP again and therefore cannot be filtered out by an antenna (Fig. 2.6.c). However, at every reflection part of the power is lost, so these signals usually have very low power levels and therefore are not a significant threat to the positioning accuracy. In Fig. 2.6.d the signal is reflected from an irregular surface, specifically a surface with different reflection properties for horizontally and vertically polarized waves. An example would be a horizontal (or vertical) metallic grid. A RHCP wave reflected from the surface decreases its polarisation purity (axial ratio) and the wave becomes elliptically polarised. The decrease of AR is increased with greater irregularity of the surface.

Good AR is the main mechanism to filter out reflected signals, but not the only one. Usually most of the reflected signals arrive from angles low above horizon. Also, for these directions, many antennas have the worst AR performance. To overcome this issue, high precision GNSS antennas use modified ground planes, EBG structures or choke rings in order to filter out the low angle signals. The performance of these methods was compared by Maqsood et al. in [43]. The main disadvantage is increased antenna dimensions and (especially with the use of choke rings) increased weight and manufacturing complexity. On the other hand, when these antennas are combined with advanced GNSS receivers and positioning techniques, they provide very high accuracy and are therefore often used for geodetic applications.

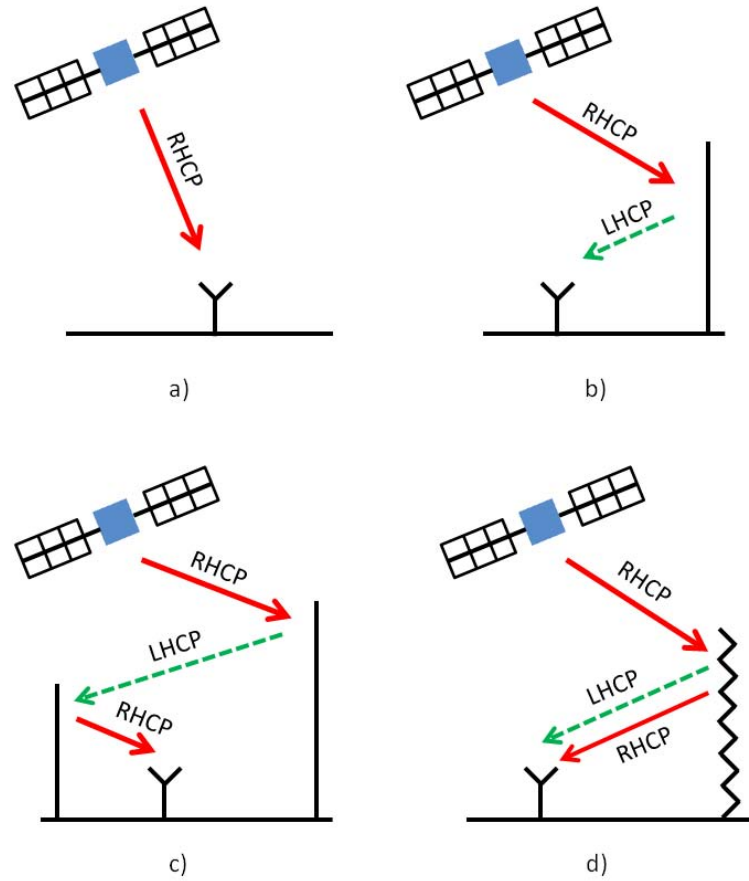


Figure 2.6. Four different scenarios of signal path between satellite and GNSS receiver: a) direct LOS signal, which is RHCP; b) single reflection changes polarisation sense of the signal; c) double reflection changes the polarisation sense twice, therefore resultant signal is again RHCP. However power levels of such signals are usually very low; d) reflection from very irregular surface causes the signal to be randomly polarised

Alternatively, a shorted annual-ring [44] and inverted shorted annual-ring [45] was proposed by Basilio et al. This antenna is designed so that it does not excite surface waves in the antenna substrate. This means a rapid decrease in gain for angles close to the horizon, which cuts-off low-angle signals. The antenna is simpler, smaller and easier to manufacture than choke rings. A combination of inverted shorted annual ring for low frequencies with an embedded classical shorted annual ring for high frequencies can be used to obtain a compact dual band antenna with good low angle rejection properties at both frequencies [44].

3. OMNIDIRECTIONAL CIRCULARLY POLARISED ANTENNAS

3.1. Background

An omnidirectional antenna is an antenna having an essentially non-directional pattern in a given plane of the antenna and a directional pattern in the orthogonal plane [46]. Omnidirectional Circularly Polarised Antennas (OCPA) provide benefits in several applications including Global Navigation Satellite Systems (GNSS), Telemetry, Tracking & Command (TT&C) modules, Wireless Local Area Networks (WLAN) and Radio Frequency Identification (RFID). Linearly polarised omnidirectional antennas are known for more than a century, however the first reported OCPA is dated back to 1955, when Kelleher and Morrow [47] proposed to surround a linear omnidirectional antenna by a polariser. Since then, many new designs were proposed. Examples of these developments are shown on Fig. 3.1.

3.1.1. Linear Antenna Surrounded by a Polariser

The technique introduced by Kelleher and Morrow in 1955 [47] was extended in many works. The antenna consists of an omnidirectional linearly polarised antenna (a dipole [53] or monopole [48]), which is surrounded by a polariser converting the linearly polarised wave into CP. In [53] the polariser consists of narrow metal rods, tilted by 45° with respect to the dipole and separated from it by $0.2 \lambda_0$. In [48] two layers of 45° tilted metallic elements are employed, which are separated by a quarter wavelength. The distance between the antenna and polariser is approximately $3\lambda_0$, which

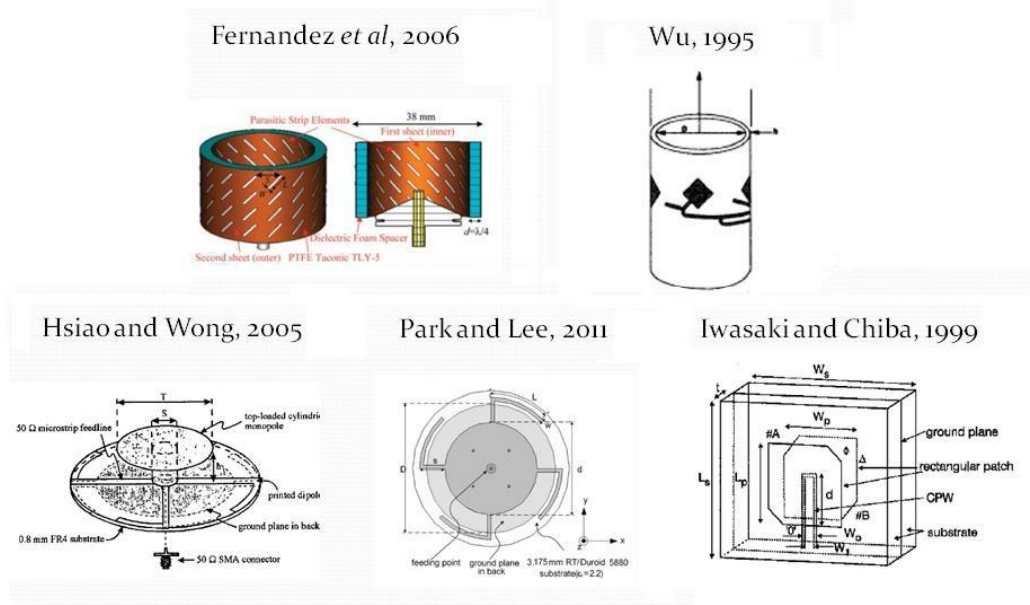


Figure 3.1. Examples of state-of-the-art omnidirectional CP antennas, as in [48–52].

makes this solution efficient only for higher frequencies. In the most recent work [54] the use of dielectric bricks as polariser was proposed. The bricks are also tilted by 45° with respect to the groundplane and symmetrically located around a linearly polarised radiator, forming what is called dielectric bird-nest antenna.

This approach is very complex and difficult to manufacture. The polarisers are not only difficult to manufacture, but require a certain spacing, significantly increasing the antenna's dimensions. It might be considered for higher frequencies, but is very impractical for lower bands, such as GPS or WLAN.

3.1.2. Array of Rotated CP Antennas

Arguably the simplest solution is to use multiple unidirectional CP radiators, wrapped around a common centre. In this configuration each radiator illuminates a small sector of space. As all elements are fed with the same

phase, an omnidirectional pattern is produced from overlapping unidirectional patterns of singular elements. The implementations of this method involve CP patches [49], slots [55] or loops [56] printed on a cylindrical surface. This approach is different from sequentially rotated arrays, where linear elements are used with appropriate phase shifts to provide wide-band unidirectional CP.

A hybrid between this approach and the use of polariser described in Section 3.1.1 was reported by Morrow in [57] where an antenna, providing an omnidirectional radiation pattern with either horizontal, vertical or circular polarisation was proposed. The antenna consists of three dipoles, connected together by a parallel plate line. The switching is done by mechanically rotating the arms of the dipole: by 0° for horizontal, by 45° for circular and by 90° for vertical polarisation. For CP configuration each of the radiating elements, when taken separately, is linearly polarised. It is only the combined field of all three of them (spaced from a common center by $0.2\lambda_0$) that produces circular polarisation. However, the axial ratio in the plane of omnidirectionality is up to 9 dB and there is significant shouldering and dipping visible in the radiation pattern, most likely due to the use of only 3 elements.

The wrapped array is easier to manufacture and smaller than the polariser, however it is still a complex three-dimensional antenna. The number of radiating elements should be kept large (4 to 8 elements in [49, 55, 56], otherwise the decrease in omnidirectional performance is visible.

3.1.3. Combination of Horizontal and Vertical Radiators

Another attempt uses a combination of vertically polarised radiators surrounded by an array of horizontally polarised ones [50]. The spacing between the two is designed to ensure a 90° phase shift. In [50] the vertical radiator is a top loaded cylindrical monopole, which is of lower profile than previous developments (around $0.1\lambda_0$ high). There are four horizon-

tally polarised dipoles located around a common center and feed point. The reported AR is around 1 dB, with a RHCP gain of 0.5 dBic.

3.1.4. Use of Metamaterials and Zeroth-Order Resonance

The low profile solution proposed in Section 3.1.3 can be further decreased by using a meta-material and zeroth-order resonance. Meta-material is an artificially engineered material, which allows to achieve functionality of negative permittivity and permeability (hence sometimes referred to as dual negative material). Normal transmission line is characterized by serial inductance (corresponding to magnetic field around narrow conductor with current flow) and a parallel capacitance (corresponding to electric field between the conductor and groundplane). This is illustrated in Fig. 3.2.a. In dual negative material this properties are reversed, that is the inductance is parallel and the capacitance serial [58], as shown in Fig. 3.2.b. An example of structure introducing such performance is Sievenpiper mushroom [59], where the serial capacitance is realised by slots between segments of transmission line and parallel inductance - by metallic vias connecting the line and the groundplane. However the circuit shown at Fig. 3.2.b can't be fully implemented, as the parallel capacitance and serial inductance originates from the laws of electromagnetism and can't be neglected. Therefore so called Composite Right-Left Handed (CRLH)

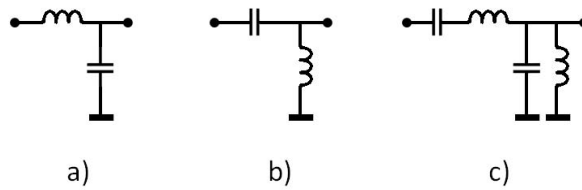


Figure 3.2. Various electrical models of microwave transmission lines: a) standards transmission line; b) idealised metamaterial (left-handed transmission line); c) composite right-left handed transmission line

transmission line was introduced (Fig. 3.2.c), where the dual negative property is achieved within a limited bandwidth.

The zeroth-order resonance occurs in CRLH transmission lines and can be used in antenna designs [60]. Its resonant frequency does not depend on physical dimensions, but solely on the inductances and capacitances introduced to achieve CRLH (as seen on 3.2.c). This resonance is characterized by a quasi-homogeneous electric field distribution in the resonator, i.e. the electric field is not homogeneous within a single CRLH cell, but there is no phase difference between the cells [58]. This performance allows the replacement of the vertically polarised element (a monopole) in [50] by a planar resonator with a CRLH technique. The first attempt in [61] presented a single cell rectangular CRLH patch, surrounded by four stubs generating a horizontally polarised component. The paper presents good simulated results, however no data on measured CP radiation pattern are presented and the S_{11} characteristic shows notable discrepancies between simulation and measurement. Another attempt by Park and Lee [51] was more successful. For this work, four CRLH cells surrounded a coaxial probe feed in the middle. Also four stubs were used as horizontally polarised elements. The measured omnidirectional AR was below 2.5 dB in the whole plane of omnidirectionality. The impedance bandwidth is 10 MHz and LHCP gain is below 0 dBic. This work was later extended by the authors for dual-band operation [62].

The newest development employing CRLH is an OCPA made by Qing et al. [63]. Although it is not planar, it overcomes the difficulty of narrow bandwidth and low gain, as presented in [51, 62]. The antenna consists of a vertically polarised dipole, surrounded by a loop of CRLH transmission line. The antenna has an impedance bandwidth of 300 MHz (from 2.2 to 2.5 GHz) and AR bandwidth of more than 200 MHz (although only half of it overlaps the impedance bandwidth). The reported gain of a four element array is around 4 dBic. The exact details of the antenna are not shown in [63], as at the time of publication the structure was patent-pending.

The main disadvantage of the use of CRLH are manufacturing problems. The value of parallel inductance is determined by the radius of via and thickness of substrates - two parameter, which are difficult to adjust. Available CP designs are complex and their performance is often difficult to adjust to individual need. Also, although zeroth order resonance offer significantly smaller antenna size, it does not overcome the Chu-Harrington limit [64], which binds antenna size with its maximum achievable bandwidth. Due to this reasons zeroth order resonant antennas were not further investigated in this work.

3.1.5. Back-to-Back Coupled Patches

Two back-to-back coupled patches for omnidirectional CP generation were first studied by Iwasaki and Chiba [52]. The antenna comprises two patches, which are located on the opposite side of a common groundplane. If the patches are circularly polarised (in [52] it employs the truncated corner method), then an omnidirectional AR can be achieved. The antenna shows an omnidirectional AR within 4 dB limit, however the radiation pattern variation is up to 6 dB. This decreased performance, both in term of AR and radiated power, occurs for the angles located in the plane of the groundplane.

This approach is compact and realizable with multilayered PCB techniques. The antenna performance is slightly worse than the case of CRLH antennas, however the technique is simpler, more robust and easier to adjust. It is noteworthy, that the antennas described in Section 3.1.4 radiate in the plane of the groundplane, whereas the back-to-back coupled patches radiate in the plane normal to the substrate.

3.2. Use of Omnidirectional CP Antennas for GPS Applications

Traditionally for GPS applications, a CP antenna with a hemi-spherical radiation pattern for sky coverage is required, providing coverage from a large number of satellites. However, this assumes that the antenna is mounted on a fixed platform and the main beam is directed towards the sky. For many scenarios, especially handheld devices or tracking application, this is not the case.

A comparative study was made between three commercially available state-of-the-art unidirectional GPS antennas and an omnidirectional CP prototype antenna (described in Section 3.5). The average Carrier-to-Noise Ratio (CNR) levels for GPS L1 navigation messages were measured using an U – Blox EVK – 5 GPS/Galileo receiver. The experiment was conducted on the roof of the DIT Kevin Street building, which offers good hemispherical sky view without any obstructions. The antennas were studied in three positions: with the main beam directed towards sky (case A), towards ground (case B) and towards horizon (antenna on its side, case C). The results are presented in Table 3.1.

For unidirectional antennas the drop in CNR between case A and case B

Table 3.1. Study of carrier to noise levels in different positions for commercial unidirectional CP antennas and omnidirectional CP prototype antenna.

Antenna	Carrier to noise ratio (dB)		
	Case A	Case B	Case C
50 mm circular patch	39.53	30.43	38.47
25 mm square patch	33.36	24.15	31.15
Active patch antenna	41.81	33.85	39.06
Omnidirectional CP antenna	37.92	36.92	38.42

varies between 8–9 dB. The use of the omnidirectional CP antenna provides a more stable CNR level (± 1.5 dB) across various positions. Each antenna was able to detect 8–9 satellites, regardless of its position. This is most likely due to the on-roof scenario, which offers a good sky view. Although for the unidirectional antennas, the difference between case A and B is significant, the difference between case A and C varies between 1–3 dB. This is again due to on-roof measurement scenario, for which strong signals from low-altitude satellites are received.

For GPS applications, linearly polarised antennas are currently commonly used in small handheld devices, such as mobile phones. In multipath propagation environments (e.g. urban areas) the advantage of CP is lost since the signal is strongly scattered and reflected. It is argued in [65], that for many such configurations no direct signal may be available and the polarisation of the reflected signals may be random. The authors claim, that the benefit of circular polarisation is often lost for such scenarios and it is considered, that the number of observable satellites is a much more important parameter. Due to their small size, mostly inverted-F antennas (IFA) of various types have been implemented in handheld devices, including for GPS applications. Such antennas have the advantage of omnidirectional radiation pattern, covering wide parts of sky and thus providing signals from multiple satellites. In [66] a planar IFA for GPS is designed. The antenna is compared with two CP antennas and one linearly polarised printed IFA in real urban and sub-urban environments in terms of horizontal dilution of precision (HDOP), time-to-first-fix and CNR. It is reported, that the planar IFA proposed in [66] performed similarly to other two CP antennas in term of HDOP (which corresponds to wide sky coverage), but had significantly longer time-to-first-fix. The average CNR was 2 dB worse than those of CP antennas. No data on positioning accuracy was provided.

The use of linearly polarised antennas for GPS offers three advantages, despite strongly decreased performance:

- sky coverage regardless of antenna orientation
- easy and cheap manufacture
- small size

In this work it is however demonstrated, that a CP antenna also provides the first two properties, without giving away the benefit of circular polarisation. Regarding the size, some miniaturization techniques are discussed in Section 4.2, however with the size of inverted-F antenna being usually smaller than a quarter wavelength, this still poses a significant challenge.

3.3. Feed Technique

Among all antennas presented in Sec. 3.1, only two techniques are planar and compatible for manufacturing on printed circuit boards. The back-to-back coupled patch antenna is conceptually simple. It is based on microstrip patch antenna type, which is well understood and has many commercial implementations. Therefore back-to-back coupled patches was chosen for further study. In this chapter, a suitable feed technique is discussed on an example of bidirectional CP antenna. Section 3.4 will discuss how to extend its functionality for fully omnidirectional CP.

Two almost-square patches on opposite sides of groundplane are used to generate CP. This demands that the feed is located on a patch diagonal. From the manufacturing point of view, the most convenient feed is a coplanar waveguide (CPW), which will couple energy simultaneously into both patches through proximity coupling. This is expected to provide equal amplitudes and phase to both radiators. However the CPW consists of slots, which need to be cut in the ground plane. The slot location along the diagonal perturbs the current distribution on the ground plane. To minimize this effect, the feed is only shallowly inserted under the patch, by only 20% of the diagonal length. This may cause some impedance mismatch, as the

input resistance of a patch increases as the feed point moves towards the edge. A quarter wavelength impedance transformer could be used, however this would increase the antenna's dimensions. Instead, the end of the CPW is triangularly tapered to gradually increase its impedance and improve energy coupling to the patches. Fig. 3.3 show the topology of the prototyped bidirectional antenna [67].

The antenna dimensions are $S = 65.3$ mm; $a = 47.8$ mm; $b = 49.4$ mm; $d = 13.7$ mm; $l = 12.0$ mm; $w = 4.8$ mm and $g = 0.9$ mm. It was made using two layers of Taconic RF-35 substrate. Each layer is 1.5 mm thick, with relative permittivity $\epsilon_r = 3.47$ and $\delta_{tan} = 0.0018$. Fig. 3.4 show simulated results of S_{11} of the bidirectional antenna, studying the impact of the feed insertion depth (parameter d on Fig. 3.3). It can be seen, that apart from changing the impedance match also a slight downwards shift in frequency is present with decreased d . This is due to the perturbing effect of the feed,

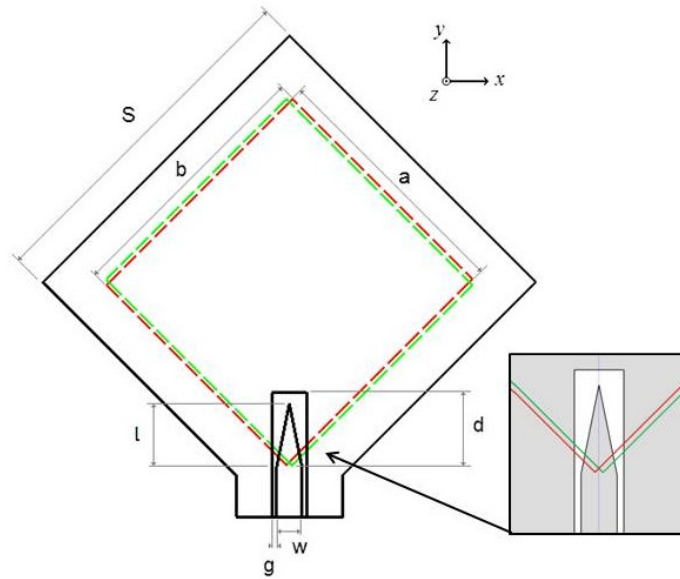


Figure 3.3. Bidirectional CP antenna with enlarged details of the developed feed: black solid line - groundplane; red/green dashed line - top/bottom patch layer.

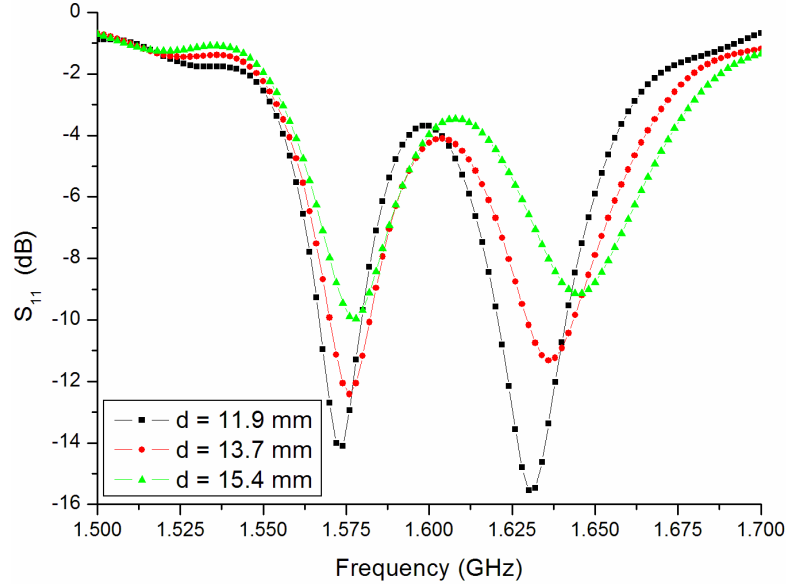


Figure 3.4. Simulated S_{11} for various feed insertion depths.

which involves slots in the groundplane. Although $d = 11.9$ mm offers better impedance match it decreases the AR. Therefore in [67] the value reported as optimal is $d = 13.7$ mm. For 1.575 GHz $S_{11} = -12.8$ dB and axial ratios (AR) on the front and back sides are 2 dB and 2.6 dB.

3.4. Ground Plane Effect

It is commonly accepted for classical CP patch antennas, that the energy cannot be radiated in the plane of the groundplane. This is because CP requires two orthogonal components of the electric field. The groundplane used in most microstrip patch antennas will attenuate the tangential component of the electric field, allowing only normal component to be radiated in the plane of the groundplane. Usually the dimensions of the groundplane are significantly larger than the patch, strengthening this effect. To overcome this problem, in the proposed development the groundplane di-

mension is reduced. This allows the radiation of both orthogonal components in the plane of the groundplane (the condition necessary for omnidirectional CP performance).

This method is able to produce omnidirectional CP, however it has few drawbacks. The electric field is diffracted around the edge of the groundplane, causing interference between both patches. The groundplane size becomes comparable to resonant radiator. As a consequence, there are currents at the edge of the groundplane which contribute to radiation. This imposes that a change in the groundplane shape (for example while integrating it with other electronic devices) may also change antenna performance.

Also the input resistance and operating frequency changes with reduced groundplane. For classical patch antennas, one calculates the resonant length of a rectangular patch as approximately one half of an electrical wavelength, with respect to the effective permittivity. This length is however corrected by subtracting double the thickness of the substrate used, an approximate value, introduced to compensate for edge capacitance of the patch. With the reduced patch dimension, this correction is no longer valid. Part of the electric field couples around the groundplane, changing the edge capacitance and effectively coupling the two patches. This also changes the input impedance. In [68] a study of the effect of the groundplane width on antenna performance is investigated, on the example of a linearly polarised antenna designed for 1.91 GHz. The paper investigates four different groundplane widths (varying from 20 to 70 mm) and four different patch widths (varying from 20 to 47 mm). The patch length is kept constant at 47.3 mm and also the groundplane length is significantly greater at 150 mm. It is demonstrated, that the resonant frequency can vary no more than 40 MHz (2%) depending only on the groundplane width. From a practical point of view, this is of no concern for most linearly polarised antennas. Greater variation is observed for the input impedance. For instance, the decrease of the groundplane width from 25 to 20 mm

(with a patch width constant at 20 mm) results in a decrease of input resistance from 97.8Ω to 73.9Ω . This study does not consider the lengths of the groundplane, which is significantly larger than the patch length. For CP antennas with a single feed, the relation between patch (and also groundplane) length and width should be either unity (eg. for truncated corner technique) or close to unity (for almost-square patch technique). This makes a similar study for CP antennas more complex.

Another drawback is the generation of the currents on the outside of the cable. Classical patch antennas are considered as an unbalanced type of antenna (therefore requiring no balun when fed from coaxial cable). However if the groundplane is of comparable size as the patch, the antenna becomes more symmetric. This means, that part of the current in the coaxial line will flow on the outside of the coaxial cable outer shell, rather than into the antenna. The shell is made of lossy metal, and in an anechoic chamber it is often surrounded by a thin layer of EMI suppressant. This leads to strongly decreased efficiency, especially when compared with simulation results. Another problem is related to the radiation generated by such coaxial line currents. As the cable is usually placed vertically, the field which it generates will be vertically polarised. This degrades the measured axial ratio of the antenna.

The default feed port options in CST Microwave Studio don't allow direct insight into this type of problem. Simple one port antenna simulations assume the energy is either reflected back into the cable, radiated or diffused by lossy material. So far there is no commonly accepted approach for numerical simulations of current propagating down the cable. Liu et al. in [69] discusses simulating small cable section together with antenna. The investigated example consist of small linearly polarized UWB monopole. Its efficiency at low frequencies exhibits strong discrepancy between simulation and measurement. Since the measurement cable was very long, only a 200 mm section was simulated. According to [69] for presented case it was sufficient to eliminate the discrepancy between simulation and mea-

surement. On the other hand, the reported simulation time (on HP Pro 3130 MT business PC) for the antenna only was 10 min, but for the antenna with 200 mm long cable, it increased to approximately 2 hours. This factor 12 increase of simulation time is not acceptable for more complex antenna topologies or for automatic optimisation requiring multiple simulations. Another problem with this technique may occur from additional resonances in the simulated cable section, which is of limited length and can't be increased, due to increased computational complexity. Lowest frequency investigated in [69] is 2 GHz, which in free space corresponds to $\lambda_0 = 150 \text{ mm} - 3/4$ the length of the simulated cable section. Another difficulty arises from the fact, that although for the design and testing phase antennas are fed from a coaxial cable, it is usually not the case for commercial implementations.

In order to avoid the problem of the current on the outside coaxial shell, the antennas were measured with a ferrite bead placed around the feed cable. As ferrite material is characterized by high permittivity and permeability values, it causes a discontinuity, preventing signal propagating further down the cable [70]. Although this is a wideband solution, it becomes less effective for higher frequencies.

3.5. Single Band Implementation

Employing the above mentioned principles, an omnidirectional CP antenna with planar technology was developed [71], as seen on Fig. 3.5. Similarly to [67], the antenna consists of two layers of Taconic RF-35 substrate ($\epsilon_r = 3.47$, $\delta_{tan} = 0.0018$ and height $h = 1.5 \text{ mm}$) and three layers of copper: the patches comprising two outer layers and the groundplane with CPW on the buried layer between. The antenna is fed using an SMA connector, soldered to a 50Ω microstrip line (3.6 mm wide) printed on a single layer of substrate. After 6 mm it transforms to a 50Ω CPW (conductor 5 mm

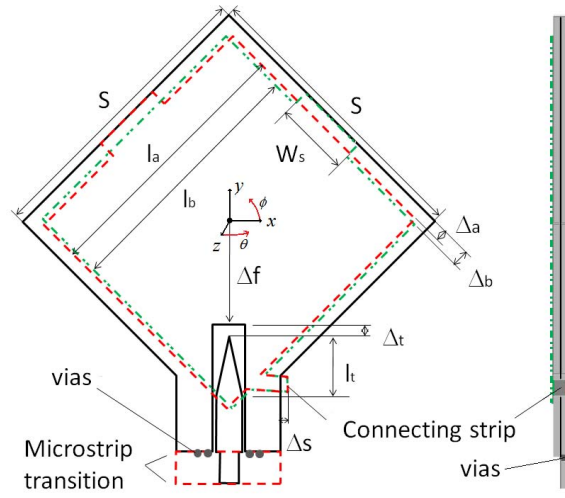


Figure 3.5. Proposed omnidirectional CP antenna. Left: frontal view, right: side view.

and slot 0.6 mm wide), sandwiched between two layers of substrate. Four vias are used to connect the groundplanes, two located on each side of the CPW-microstrip joint. The use of a short section of microstrip facilitates soldering of an SMA connector but has no significant meaning for antenna performance.

The radiators are electromagnetically coupled directly from a 50Ω CPW located along their diagonal. One end of the line (underneath the patch) is triangularly tapered to enhance this coupling, in accordance with the principles outlined in Section 3.3. Both the substrate and groundplane is significantly reduced and extends only around 5 mm above the patch footprint. This is done in order to achieve good omnidirectional CP performance. The patches are connected by a 3 mm wide copper conducting strip, going around the groundplane at the distance Δ_s . This adds additional inductance, improving the impedance match.

The antenna is shown in Fig. 3.5. The parameters are: $l_a = 51.2$ mm, $l_b = 49.6$ mm, $W_s = 14$ mm, $S = 55.8$ mm, $\Delta_a = 2.3$ mm, $\Delta_b = 3.1$ mm,

$\Delta_f = 19.5 \text{ mm}$, $\Delta_t = 2 \text{ mm}$, $l_t = 12 \text{ mm}$, $\Delta_s = 1 \text{ mm}$.

The antenna was manufactured and measured. Proper alignment across all layers was achieved by placing small holes in the substrate around antenna. The S_{11} provides good agreement between simulation and measurement, with a fractional impedance bandwidth of 2.1% (1.579–1.613 GHz). The CP parameters were measured in semi-anechoic chamber in two consecutive measurements: the first one recorded amplitudes and phases for vertical polarization, the second - amplitude and phases for horizontal one. Values of AR and CP gains were obtained in post-processing step, as described in [16]. Omnidirectional RHCP is achieved with $\text{AR} < 4 \text{ dB}$ for all angles in the xz -plane. Although this limit exceeds 3 dB commonly accepted for circular polarisation, it still provides good cross polarisation level better than 13 dB. The omnidirectional CP bandwidth (calculated with respect to 4 dB AR) is 7 MHz (0.4%), from 1.593–1.601 GHz. The measured average AR is 2.3 dB and peak gain 1.1 dBic, which is 1.5 dB higher than [51] and 1 dB higher than [62]. The gain variation was below 3 dB in the xz -plane, which is an improvement over [52]. The simulated total efficiency is 86%. Fig. 3.6 present S_{11} characteristic of the antenna. Fig. 3.7 and 3.8 depicts AR and CP gains respectively.

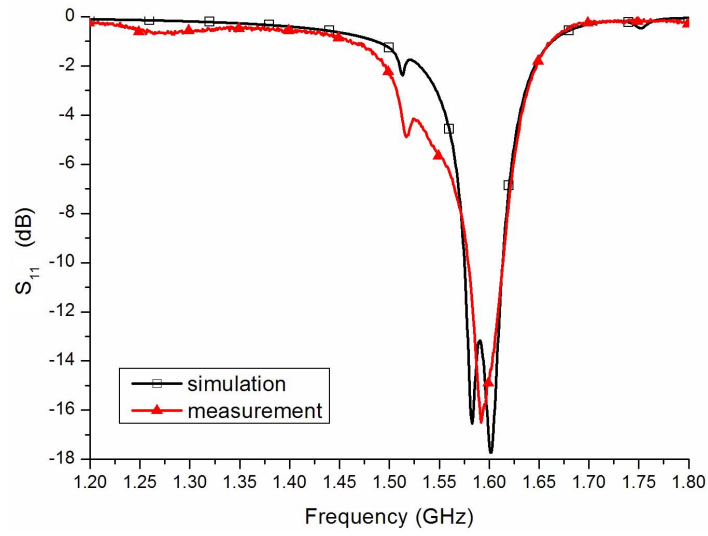


Figure 3.6. Simulated and measured S_{11} of the omnidirectional CP antenna.

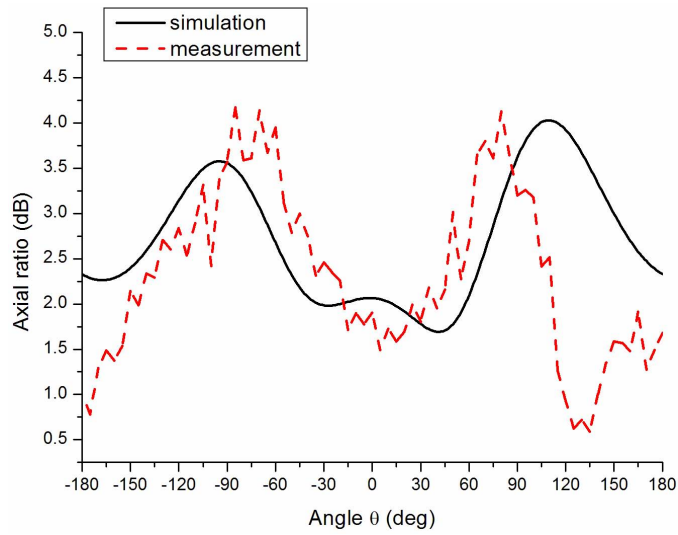


Figure 3.7. Axial ratio measured and simulated for xz -plane at 1.596 GHz.

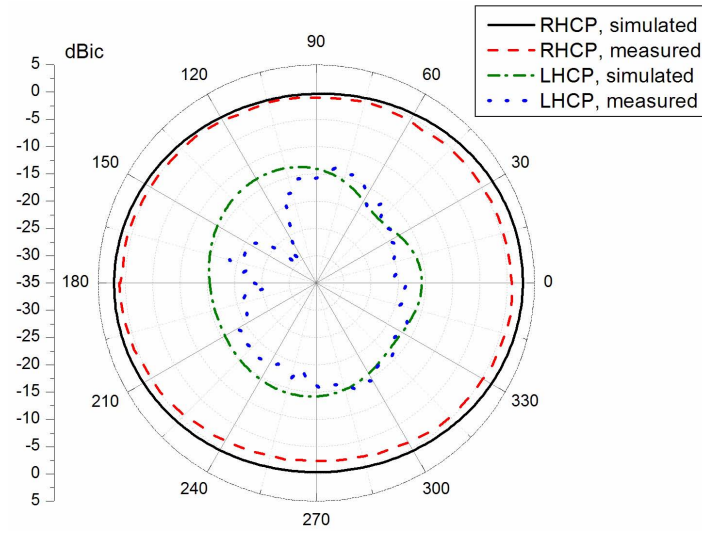


Figure 3.8. RHCP and LHCP gains measured and simulated for xz -plane at 1.596 GHz.

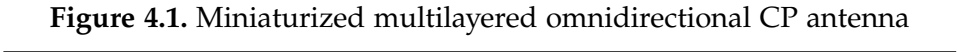
4. ADVANCED OMNIDIRECTIONAL CP ANTENNAS

4.1. Motivation

In Section 2 the basic principles of omnidirectional CP antennas were discussed. This chapter extends the basic functionality with more advanced features, allowing the use of omnidirectional CP for a wider range of applications. In Section 4.2 a method to miniaturize OCPAs is demonstrated. With the decreasing dimension of handheld devices, antennas for those applications are also expected to be smaller. In Section 4.3 a method to trim the OCPA performance is discussed. This is done to overcome manufacturing issues, which are significant for narrow band OCPAs on thin substrates. Finally, in Sections 4.4 and 4.5 the extension of OCPA into dual-band operation is discussed. This is intended for advanced satellite based navigation, which uses multiple bands to calculate the correction factor required due to ionospheric delay of the signal.

4.2. Miniaturization

Polarisation issues are not commonly investigated in electrically small antenna research, which mainly focusses on linear polarisation. Also most miniaturization techniques are efficient only in reducing a single dimension, making them not applicable for CP, where a balance between two dimensions is important. Recently a method was described in [72] on how



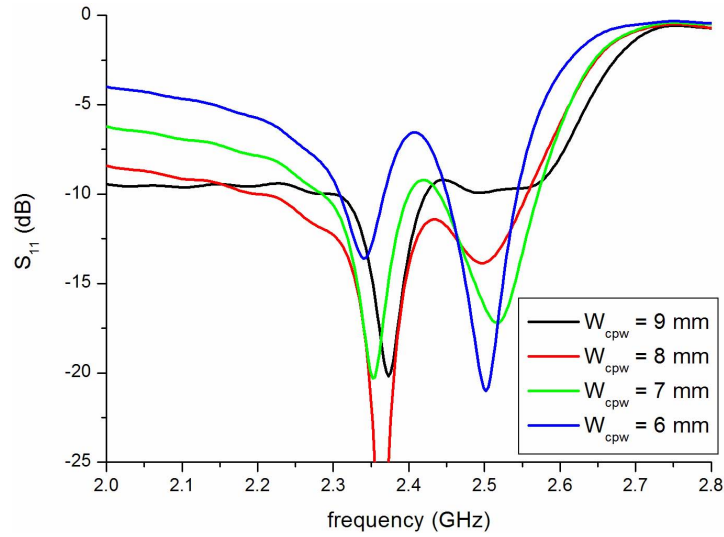


Figure 4.2. Simulated S_{11} for various W_{CPW} and S_{CPW} parameters. For all curves $S_{CPW} = 0.12W_{CPW}$.

limit. In order to compensate for this, the shape of three folded ‘corners’ was modified exhibiting pentagonal and rectangular structures, as seen on Fig. 4.1. The fourth (lower) ‘corner’ remained at its original position in order not to perturb CPW feed, and hence needed no modification.

The CPW feed consists of three sections. The first one is a $50\ \Omega$ CPW with a 3.5 mm wide middle conducting strip and 0.3 mm slots on each side. It has RF-35 substrate only on one side to facilitate soldering of an SMA connector. Next, a wider section of $50\ \Omega$ CPW was manufactured with substrate on both sides of the transmission line. In order to achieve $50\ \Omega$ impedance for this line, the ratio between the slot (S_{CPW}) and width of the middle conducting strip (W_{CPW}) should be 0.12. However, as long as the ratio is fulfilled, there is flexibility in choosing the exact CPW dimensions. Fig. 4.2 shows the simulated S_{11} for various W_{CPW} thickness (all matched to $50\ \Omega$, as the ratio is preserved). It can be seen, that the best coupling is achieved for $W_{CPW} = 8\text{ mm}$ and $S_{CPW} = 0.96$. It also preserves good match for both orthogonal modes in the patch: it can be seen on Fig. 4.2, that a

wider W_{CPW} improves the match for lower mode, but deteriorates it for higher one. Also, the antenna produces additional radiation at frequencies below 2.3 GHz, which is stronger for a wider W_{CPW} . This radiation is most likely produced by the wider slots in CPW.

The antenna was manufactured using facilities of the National University of Ireland, Maynooth. Fig. 4.3 depicts the measured and simulated reflection coefficients. Comparing simulation and measurement, both curves exhibit similar shapes. However, for the frequencies below 2.3 GHz the measured curve is significantly different than the simulated one. As the antenna employs three buried layers, it was impossible to measure its exact manufactured dimensions and use them to improve simulation. However based on the parameter study presented in Fig. 4.2 it can be assumed, that this discrepancy is due to manufacturing inaccuracy, specifically due to wider CPW slot dimension. The wider impedance bandwidth, as compared to the antenna from Section 3.5, is due to the use of thicker 3 mm substrate (two layers of 1.5 mm). The optimum CP frequency (for which the results on Fig. 4.4 and Fig. 4.5 are shown) is 2.390 GHz for simulation and

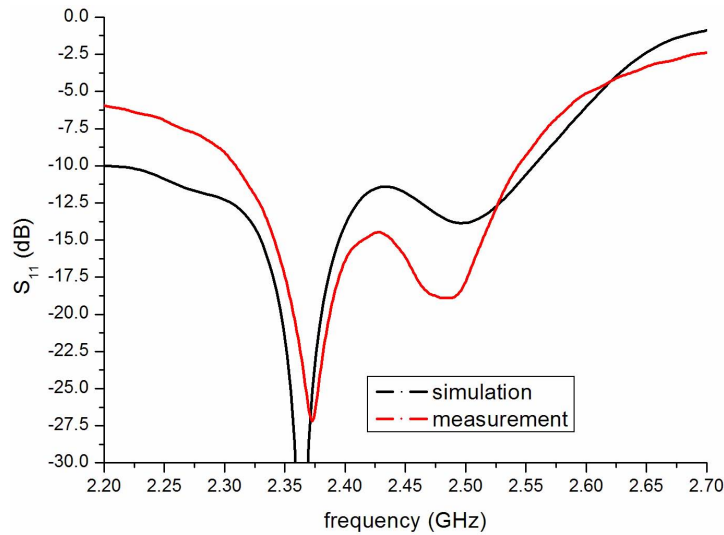


Figure 4.3. Simulated and measured S_{11} of the miniaturized antenna

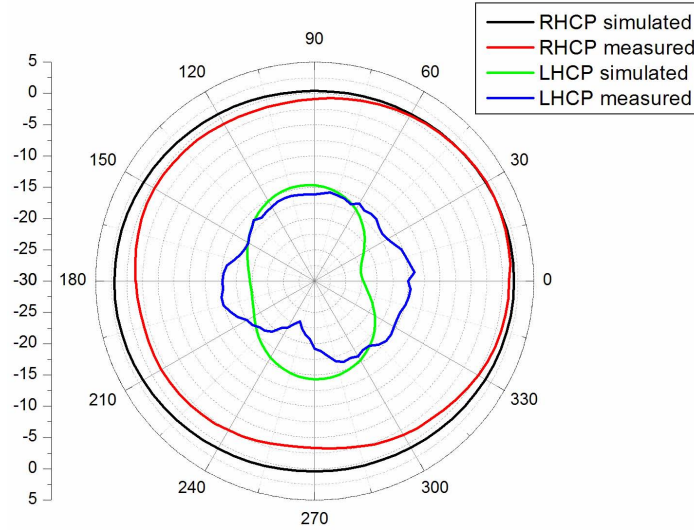


Figure 4.4. Simulated and measured realized gain (dBic) of the miniaturized antenna.

2.393 GHz for measurement. The measured AR is below 4 dB for all angles with an average value of 2.78 dB. The maximum realized gain is 2 dBic for simulation and 1.7 dBic for measurement. This discrepancy, especially visible for $\theta = 260^\circ$, is due to the small groundplane effect, which could not be fully compensated for by the use of ferrite bead. The antenna is more compact and rectangular compared to the diagonally oriented patch. The total footprint area is approximately 20% smaller than an antenna with classical non-folded patch operating within the same band.

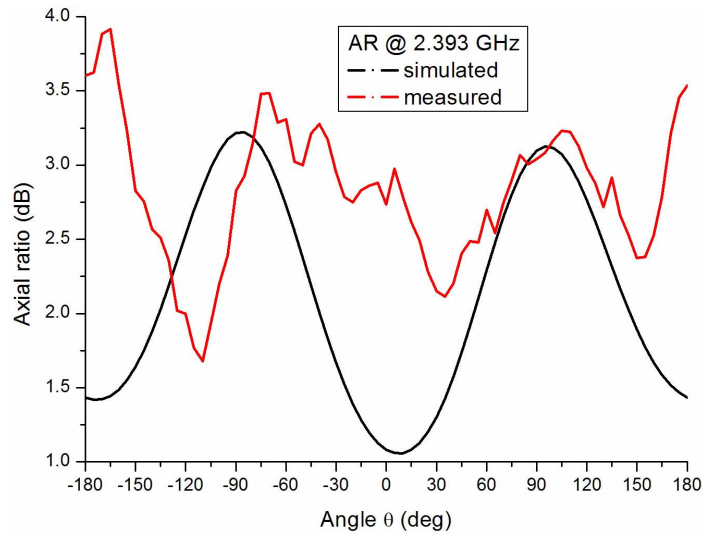


Figure 4.5. Simulated and measured axial ratio of the miniaturized antenna at 2.393 GHz.

4.3. Fine Tuning of Omnidirectional CP Antenna

The solution proposed in Section 3.5 offers an omnidirectional CP bandwidth of 7 MHz. Although this is sufficient for GPS L1 applications, it is relatively narrowband and manufacturing tolerances and alignments may cause problems: a small misalignment of one of the patches may further reduce this bandwidth. To overcome this issue, a method to adjust the resonant frequencies of all four resonant modes (two orthogonal modes on each patch) will be presented. The method can be employed in a post-manufacturing phase to compensate for potential malfunction.

The antenna is shown in Fig. 4.6 and consists of three metallisation layers. Similar to the previous antennas developed here it is a back-to-back coupled patch antenna fed by a CPW. At the top of each patch a two slots are introduced with a mechanically adjustable capacitor soldered across the middle of each slot. This forces surface current on the patch to flow around the slot and through the capacitor. As a consequence the resonant frequency of each mode of the patch is inversely proportional to that ca-

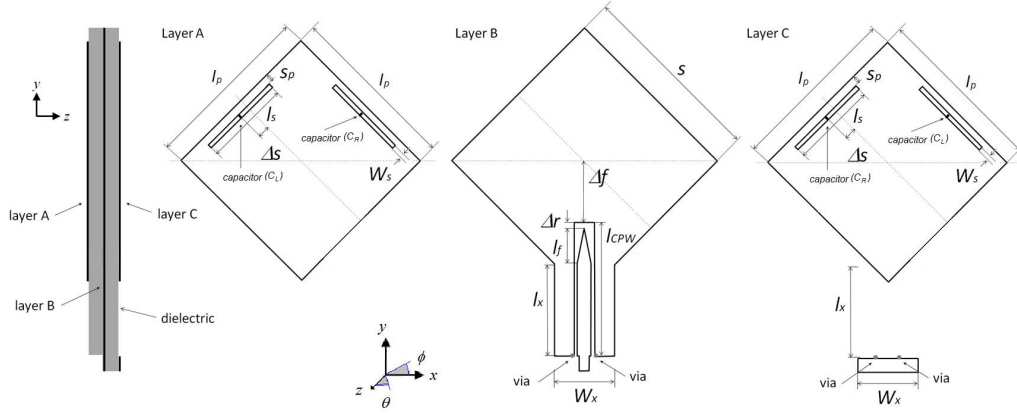


Figure 4.6. Omnidirectional CP antenna with fine tuning capability.

capacitance [75].

Proposed antenna uses square patch with both slots of same length. The phase perturbation required for CP is introduced by a small difference between the values of left (C_L) and right (C_R) capacitors. This allows to change the polarisation between RHCP, linear vertical and LHCP.

The antenna was designed for a capacitor value of around 1.5 pF. This is lower than the range of commercially available variable capacitors, therefore a serial connection of a fixed 2.2 pF capacitor and a mechanically adjustable

3 – 10 pF capacitor was implemented. For practical application, this allows very fine tuning (as required for CP generation) in the range from 1.27 pF to 1.8 pF.

The connection offers the range from 1.27 pF to 1.8 pF. To include the losses of additional solder, a serial resistance of 0.4Ω was added in simulation. The antenna dimensions are: $L_p = 48.5$ mm; $S_p = 1.9$ mm; $L_s = 25.4$ mm; $W_s = 1.4$ mm; $S = 53.7$ mm; $\Delta_s = 3$ mm; $\Delta_f = 18.6$ mm; $\Delta_r = 2$ mm; $L_{CPW} = 46.4$ mm; $L_x = 37$ mm; $W_x = 20$ mm; $L_f = 12$ mm. The results presented for this antenna are simulations obtained with CST Microwave Studio.

4.3.1. Principles of Operation

The adjusting mechanism will be demonstrated on an example of GPS L1 band at 1.575 GHz and Beidou/Galileo E2 band at 1.561 GHz. The process consists of two stages. The first will adjust impedance parameters to be roughly in the band of interest. The second stage will adjust polarisation properties with some iterative fine-tuning of the band.

The capacitors can be tuned in the range from 1.27 pF to 1.8 pF. The antenna resonates at 1.512 GHz when $C_{des} = 1.8pF$ and at 1.635 GHz when $C_{des} = 1.27pF$. It can be assumed, that the resonant frequency is inversely proportional to the capacitances. The relation can be expressed by the equation:

$$C_{des} = C_B + (C_A - C_B) \frac{f_B - f_{des}}{f_B - f_A} \quad (4.1)$$

where:

f_{des} is desired resonant frequency

C_{des} is desired capacitance

f_B is the highest tunable resonant frequency (here 1.635 GHz)

C_B is capacitance corresponding to f_B (here 1.27 pF)

f_A is the lowest tunable resonant frequency (here 1.512 GHz)

C_A is capacitance corresponding to f_A (here 1.8 pF)

In the next step, a small difference between C_L and C_R (as seen on Fig. 4.6) is introduced to achieve RHCP, so that $C_L = C_{des} - 0.5\Delta_C$ and $C_R = C_{des} + 0.5\Delta_C$. Fig. 4.7 shows the effects of such a perturbation on an example of GPS L1 band ($C_{des} = 1.529pF$). Increased C results in better AR, however also decreases impedance match. This is equivalent to introducing a small difference between the patch length and width.

Antenna reflection coefficients are shown on Fig 4.8 and realized gains on Fig. 4.10. It can be seen, that antenna configurations operating at higher fre-

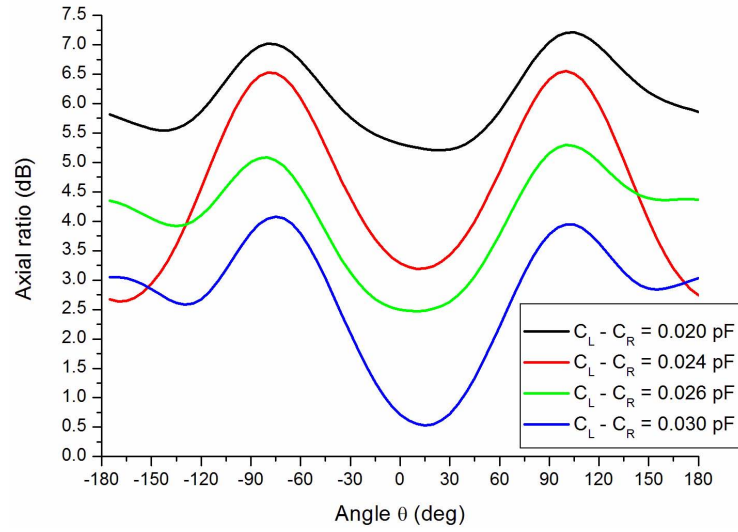


Figure 4.7. Simulated axial ratio as a function of the small difference between C_R and C_L , demonstrated for GPS L1 configuration (at 1.575 GHz).

quencies (i.e. employing lower capacitances) have larger bandwidth than the configurations operating at lower frequencies. This is due to the Q factor of the mechanically adjustable capacitors: as the resistance is kept constant, increased capacitance increases stored energy, causing higher Q and narrower bandwidth. As a consequence, the configurations operating at higher bandwidths require greater difference ΔC between right and left capacitor to achieve good CP. In the investigated antenna this difference is 0.03 pF for GPS L1 configuration (1.575 GHz) and 0.02 pF for Beidou/Galileo configuration (1.561 GHz).

Fig. 4.9 shows reflection coefficients of the antenna for two configurations on a Smith chart. It can be seen, that with changed capacitance the curve rotates along the capacitance lines on the Smith chart. This limits the range of available tuning, since if the capacitance is too large or too small, the CP will be outside of 10 dB return loss circle. However for linear polarisation this limit is greater, since the antenna operates in the minimum of the resonance.

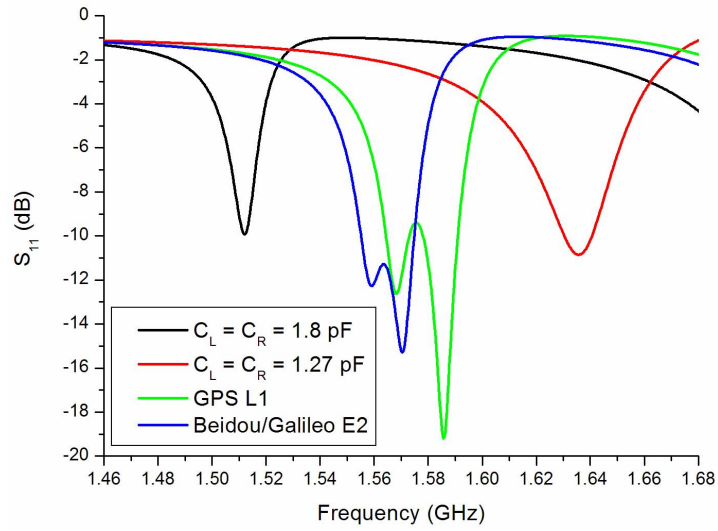


Figure 4.8. Simulated reflection coefficient of the antenna in four configurations. Please note, that the two extreme curves (black and red) represent vertically polarised mode and they establish the upper and lower limits of tuning capability.

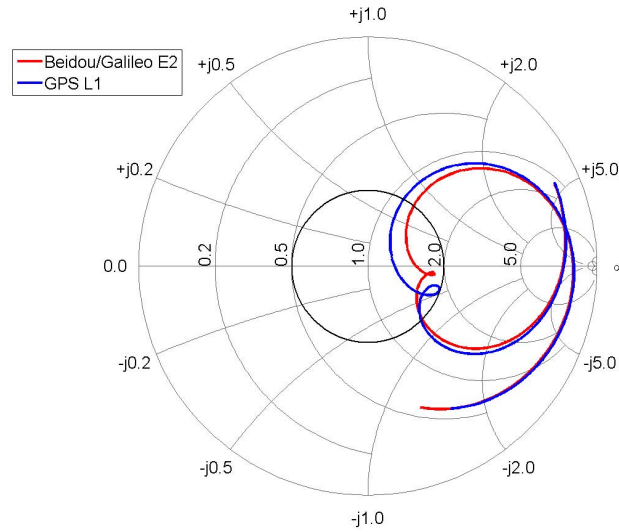


Figure 4.9. Smith chart of the antenna for two investigated configurations (simulated data). It can be seen, that the change in lumped capacitors rotates the curve on the Smith chart. This limits the achievable tuning range, as with higher or lower capacitances the CP area (seen as a small loop) is outside of the 10 dB return loss circle (marked black).

4.3.2. Results

Applying the following steps for GPS L1 band (1.575 GHz) and Galileo/Beidou E2 band (1.561 GHz) two different antenna configurations were obtained. For GPS L1 band applying Equation 4.1 yields $C_{des} = 1.529 \text{ pF}$ ($f_{des} = 1.575 \text{ GHz}$; $f_A = 1.512 \text{ GHz}$; $C_A = 1.8 \text{ pF}$; $f_B = 1.635 \text{ GHz}$; $C_B = 1.27 \text{ pF}$). To achieve RHCP a Δ_C of 0.03 pF was introduced and after some fine tuning, using CST Microwave Studio, the final capacitor values were $C_L = 1.549 \text{ pF}$ and $C_R = 1.519$. The resultant omnidirectional AR is no greater than 4.1 dB with a mean value of 2.64 dB.

For Beidou/Galileo E2 band at 1.561 GHz Equation 4.1 yields $C_{des} = 1.589 \text{ pF}$. After introducing $\Delta_C = 0.02 \text{ pF}$, in the fine-tuning phase the optimum configuration was found to require slightly higher capacitances than calculated by Equation 4.1 with $C_L = 1.623 \text{ pF}$ and $C_R = 1.603 \text{ pF}$. The axial ratio is below 5.3 dB with mean value of 3.06 dB. The radiation patterns are omnidirectional dipole-like for both configurations. Radiation gain for both antennas can be seen in Fig. 4.10.

4.4. Dual Band Enhancement Techniques

In order to improve positioning accuracy, modern GNSS systems operate in more than one band. For the GPS system, the bands used are the L1 band at 1.575 GHz, L2 at 1.227 GHz and L5 at 1.176 GHz. The forthcoming Galileo will also use several frequencies: the L1 band at 1.575 GHz and also incorporating additional bands of E2 (1.561 GHz) and E1 (1.589 GHz), thus being more broadband than a GPS signal with the same centre frequency; also the E6 band centred at 1.278 GHz and E5a/E5b bands around 1.176 GHz and 1.207 GHz. The chinese Beidou system currently uses the E2 band at 1.561 GHz and parts of E6 (1.268 GHz) and E5b (1.207 GHz) bands.

Although multiband operation allows more accurate navigation, it introduces additional challenges for antenna designers. To simplify and minia-

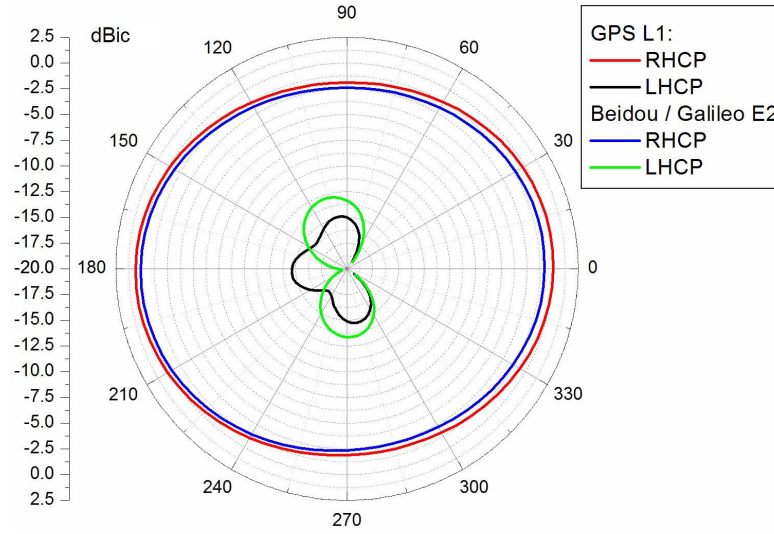


Figure 4.10. The simulated realized gains of antenna in xz -plane for two configurations. GPS L1 is shown for 1.575 GHz and Beidou/Galileo E2 for 1.561 GHz.

turize the receiver, a single antenna operating within multiple bands is the most convenient solution. The open literature offers insight into various approaches for dual-band CP patch antenna.

The oldest approach relies on stacking multiple patches on top of each other [76]. In this configuration each of the patches resonates at a different frequency, with the larger patches (i.e. operating at lower frequency) being on the bottom of the stack to prevent them from shielding the other patches. Usually, only the top layer is connected directly to the coaxial cable and the layers below are proximity-coupled. As it was recently reported in [77], this configuration allows up to quad-band operation with four patch layers. Its disadvantage however is the increased antenna thickness.

Another approach in [78] advocates the use of dual-negative metamaterial. The basic principles of such materials were already described in section 3.1.4 and hence will be not repeated here. To achieve dual-band operation in classical materials one can use the first and second resonance of

the patch (or any other resonator). However usually the ratio between these two frequencies (for a canonical patch shapes) is around 2. This makes the technique of little practical use, as there is little flexibility in adjusting the frequencies. On the contrary, in metamaterials the slope of the dispersion curve in the dual-negative region can be designed by adjusting the values of series capacitance and parallel inductance [79]. In such material, a $+1^{st}$ (first resonance of $\epsilon_r > 0$ range) and -1^{st} resonance (first resonance of $\epsilon_r < 0$ range) can be used. The frequency of the -1^{st} resonance can be changed by modifying the slope of the dispersion curve. The parallel inductance is most commonly realized as a via that connects antenna patch with the groundplane [59]. In such realisation the parallel inductance is function of via's diameter and substrate's height. However commercially available components offer only limited, discrete number of via diameters and substrate heights. This results in limited flexibility when controlling inductance and poses a problem for practical realisation of dual-band antennas based on meta-material.

Another technique requires cutting slots in the patch. This has been done in many shapes and forms. In [80] an S-shaped slot is cut in a rectangular patch in order to achieve dual-band CP operation. In [81] complex thin slots are placed along the edges of an octagonal patch. However the simplest and most understood approach was proposed by Maci et al. in [82, 83]. The proposed approach uses the 1^{st} and 3^{rd} resonant mode of a rectangular patch, since the 2^{nd} mode (and all even modes) produces a null at the boresight. In order to decrease the frequency of the 3^{rd} resonant mode two slots are cut in the patch, each along the radiating edge. The slot position is usually placed, so that it is '*invisible*' for the 1^{st} mode, and only impacts the 3^{rd} resonant mode. The current on the patch needs to flow around the slots, therefore prolonging its path and reducing the resonant frequency. For the 3^{rd} order resonance of the patch the thin strip between the slot and patch edge can be described as a $\lambda_0/4$ stub, as shown on Fig. 4.11. Its resonant frequency is therefore given by the following

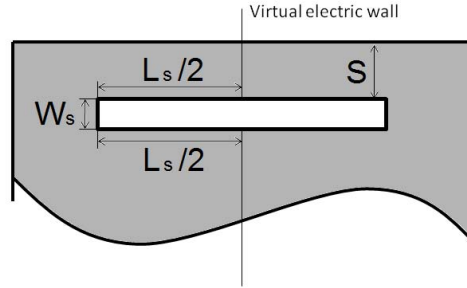


Figure 4.11. Depiction of the slot in the patch as a quarter-wavelength stub.

equation, as in [82]:

$$f_{300} = \frac{c_0}{2(L_s + W_s)\sqrt{\epsilon_{eff}}} \quad (4.2)$$

where:

c_0 is speed of light in vacuum

ϵ_{eff} is effective permittivity

L_s, W_s are slot dimensions, as described in Fig. 4.11

In [84] an extension of this method was proposed by introducing a lumped capacitor, soldered across each slot. This allowed further reduction of the Frequency Ratio (FR) between the two operating bands.

The approach advocated in this thesis employs the use of a 1st and 2nd resonance for dual-band CP operation (see Fig. 4.12). It offers three main benefits over [82–84]:

- smaller Frequency Ratio
- even if antenna is designed to use only 1st and 3rd resonance, the 2nd resonance still exist and will produce radiation when excited at proper frequency. This may cause serious problems if any intermodulation product of the radio transmitter happens to be at that frequency.

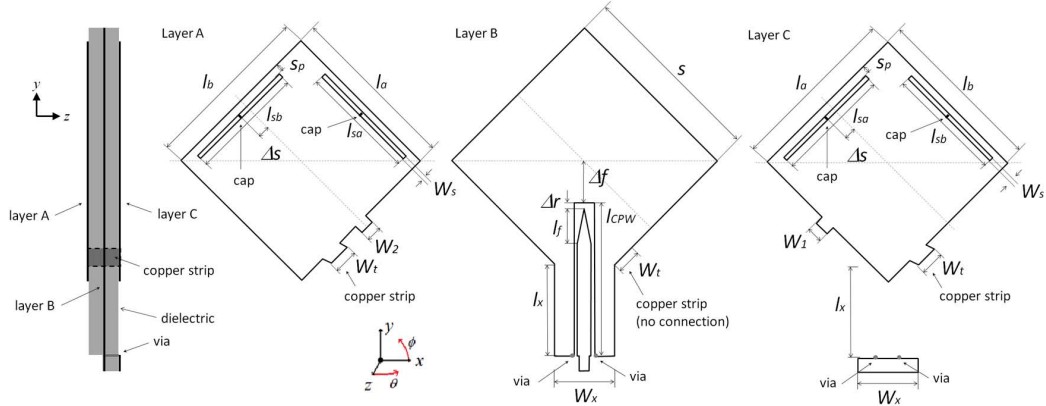


Figure 4.12. Dual-band omnidirectional CP antenna.

- The use of 2^{nd} resonant mode requires only a single slot in the patch. For the case, when the dual-band operation is enhanced with capacitors as in [84], this means that the number of required lumped components is reduced by half.

The single slot, if properly placed, can also modify the current distribution to provide maximum radiation at boresight. For this configuration, its width is comparably greater than [82]. This make the slot more influential also on the 1^{st} order resonance and hence both bands are impacted, as seen on Fig. 4.13

The FR between the bands is primarily determined by the lumped capacitance. For instance, to tune the antenna for the L1 / L2 GPS band a capacitor of approximately 1 pF is required, giving a FR of around 1.26. Table 4.1 provides some typical FRs for different capacitor values, on an example of an antenna from Section 4.5. Simulated values are compared with measured FR. All values in Table 4.1 are given for slot lengths $l_{sb} = 36.8mm$ and $l_{sa} = 35.8mm$ (slot difference introduced to provide CP). Above a certain value there is no further decrease in FR, although both operating frequencies continue to decrease. Full S_{11} for the most significant capacitor values is shown in Fig. 4.13.

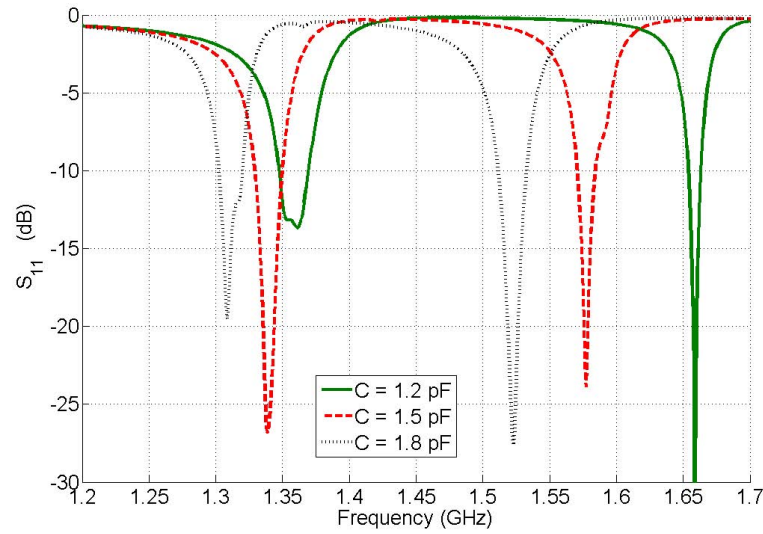


Figure 4.13. Simulated S_{11} for the investigated capacitor values in antenna presented on Fig. 4.12.

Fig. 4.14 shows S_{11} for various slot lengths. Also here, there is a difference between the two slots, which is kept constant at 1 mm throughout all configurations. It can be seen, that the resonant frequency decreases with increased slot lengths, which qualitatively agrees with the trend described in Equation 4.2. However due to the use of a capacitor and two slots, an exact prediction is no longer possible.

Table 4.1. Frequency ratios for different capacitor values, demonstrated on an exemplary antenna from Section 4.5.

Capacitor value (pF)	Lower frequency (GHz)	Upper frequency (GHz)	Simulated FR	Measured FR
1.0	1.366	1.724	1.26	1.28
1.2	1.357	1.660	1.223	1.207
1.5	1.341	1.584	1.178	1.182
1.8	1.314	1.523	1.159	1.153
2.0	1.291	1.494	1.158	1.148

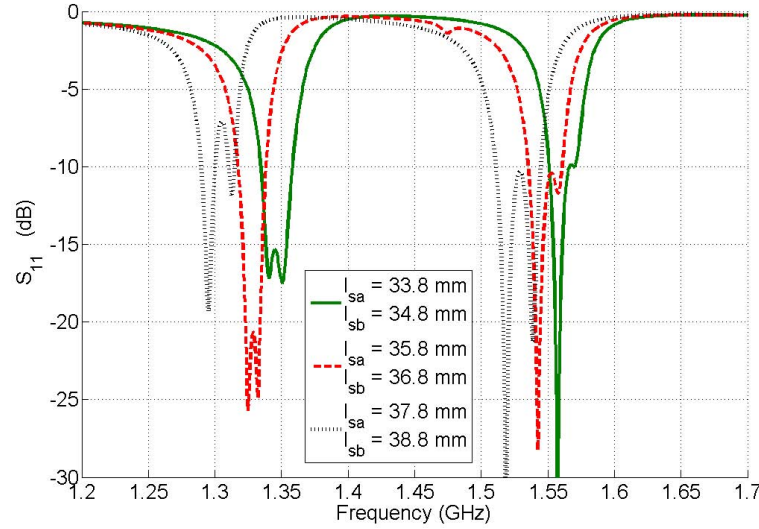


Figure 4.14. Simulated S_{11} for various slot lengths. The difference between the slots is kept constant at 1 mm through all simulations.

4.5. Dual Band Omnidirectional CP Antenna

The dual band capabilities of a patch antenna are applied here for the omnidirectional CP antenna technology. The back-to-back configuration has been extended with a slot and capacitor load [85]. The antenna is shown in Fig. 4.12. Two slots are located at the upper part of each patch with a 1.5 pF lumped capacitor soldered across the centre. The patches are connected with a narrow copper strip.

The radiators are electromagnetically-coupled to a $50\ \Omega$ CPW (with slot 1 mm wide, central strip - 4.7 mm) located along the diagonal of the patches. The end of the line is triangularly tapered to increase its impedance. The parameter l_{CPW} was optimised to realize best matching (as the input resistance of the patch decreases towards its centre). The use of the tapered transformer provides greater immunity to the slight difference in input impedance of the two resonant modes of the patch. The other end of CPW transforms into a microstrip line (ground planes are connected by vias). This is done to facilitate soldering of an SMA connector.

The structure was manufactured using a LPKF Proto Mat milling robot [10]. The ground plane (layer B) was milled on both substrates, providing better symmetry between the patches. The alignment was made by drilling rows of densely spaced holes along the outside antenna perimeter and using them to visually align the layers.

The antenna was simulated using the CST MWS Frequency Domain Solver. The parameter values are: $l_a = 57$ mm; $l_b = 57.1$ mm; $s_p = 2.25$ mm; $l_{sb} = 36.8$ mm; $l_{sa} = 35.8$ mm; $W_s = 1.5$ mm; $\Delta_s = 3$ mm; $W_t = 5.0$ mm; $\Delta_f = 14.0$ mm; $\Delta_r = 2.0$ mm; $l_f = 12.0$ mm; $l_{cpw} = 50.8$ mm; $W_X = 20.0$ mm; $l_X = 29.7$ mm; $s = 64$ mm. The width of the tuning stubs are $W_1 = 9.0$ mm for layer C side and $W_2 = 6.0$ mm for layer A.

The manufactured antenna with the above parameters radiates CP in two bands of 1.567 GHz and 1.325 GHz, which give a FR of 1.18 (significantly smaller than [84]). The measured S_{11} is in agreement with simulation and, as seen on Fig. 4.15, exhibits a good dual-band response, with no additional resonances between those bands. This is as expected by employing the 2nd resonant mode rather than the 3rd mode as in [82]. Fig. 4.17 shows the measured AR (only values below 6 dB) as a function of angle θ and frequency. It can be seen, that the dual-band omnidirectional CP performance has been achieved.

The simulated AR in xz -plane varies from 0.1 dB to 3.9 dB for the lower band and from 0.2 dB to 4.3 dB for the upper band. For the measured prototype these values are respectively from 0.4 dB to 3.8 dB and from 0.6 dB to 4.8 dB (see Fig. 4.16). This exceeds the 3 dB limit commonly accepted for unidirectional CP antennas. However for planar omnidirectional antennas this seems a reasonable trade-off, given the good level of cross polarisation. Generally, an AR level of 5.68 dB corresponds to 10 dB of cross polarisation [16], which is assumed to be sufficient for many applications. The proposed antenna offers cross polarisation better than 12 dB in the whole xz -plane.

Measurement of antenna's total efficiency was not possible with the

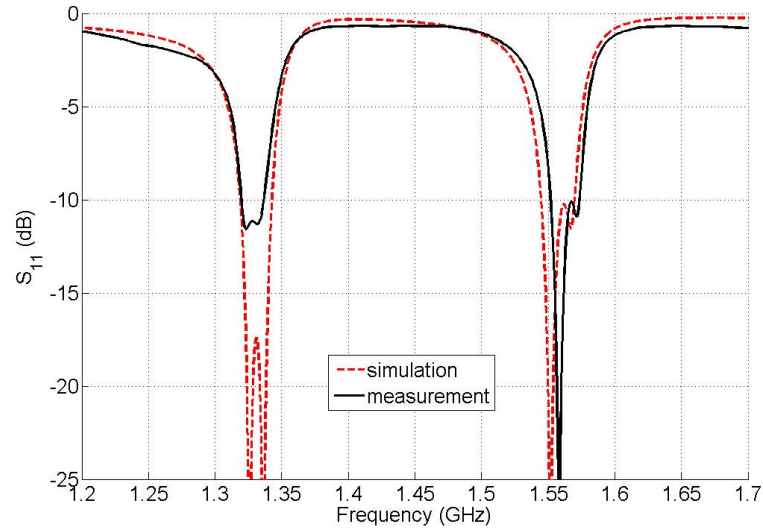


Figure 4.15. Measured and simulated S_{11} of the dual-band omnidirectional CP antenna.

available measurement facilities, however the simulated total efficiencies are 60% for the lower band and 50% for the upper. For single band omnidirectional CP antenna (as described in section 3.5) the efficiency was much higher (86%), what suggest that the losses in capacitors are mainly responsible for such low values.

Figures 4.18 to 4.21 show the radiation pattern for the lower and upper band respectively. The RHCP gain ranges from -0.7 dBic to -4.5 dBic for the upper band and from -0.7 dBic to -4 dBic for the lower band. For the lower band this is up to 2 dB less than the simulated gain. Most likely it is due to the fact, that the ferrite bead was unable to fully cancel the effect of the current on the outside of the cable. Additional simulations, which incorporated a short section of the cable as in [69], support this explanation. Manufacture of a balun which operates on two frequencies so close to each other poses a significant challenge. At the time of antenna development there was no commercially available balun, that would be suitable for the proposed antenna.

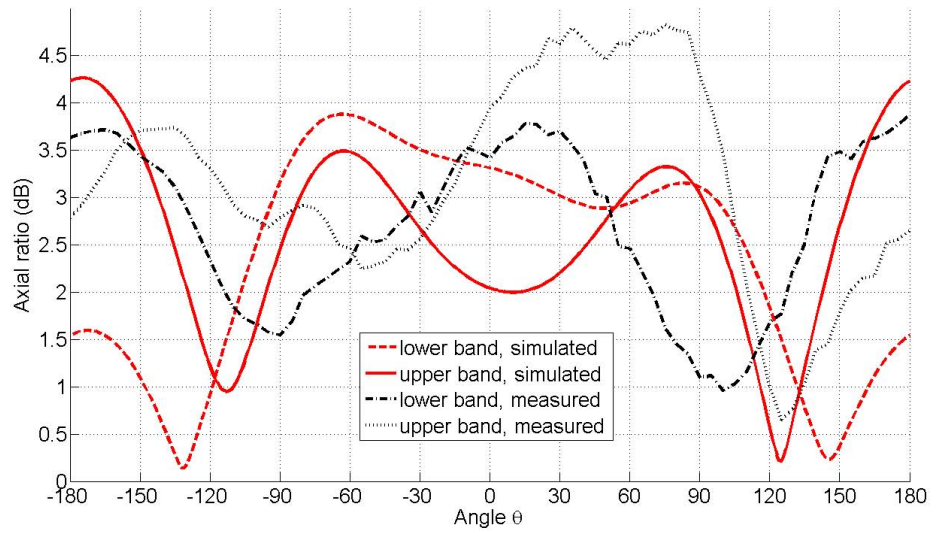


Figure 4.16. Measured and simulated AR for the upper and lower bands.

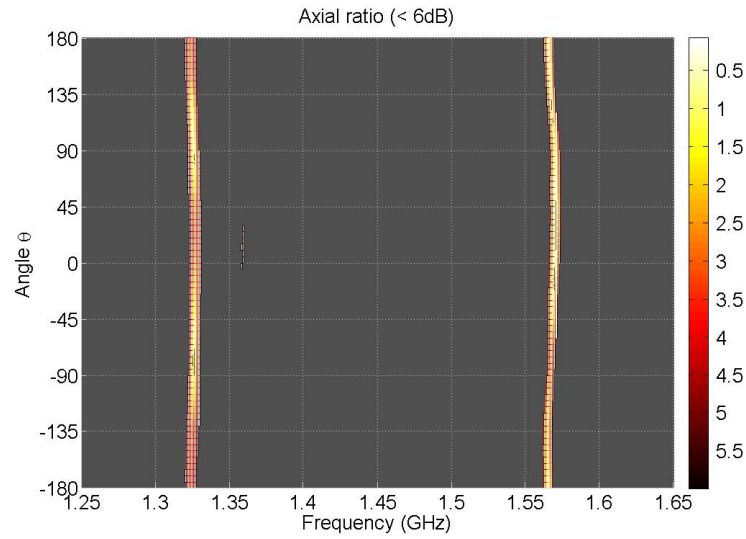


Figure 4.17. Measured AR as a function of angle θ (in xz -plane) and frequency

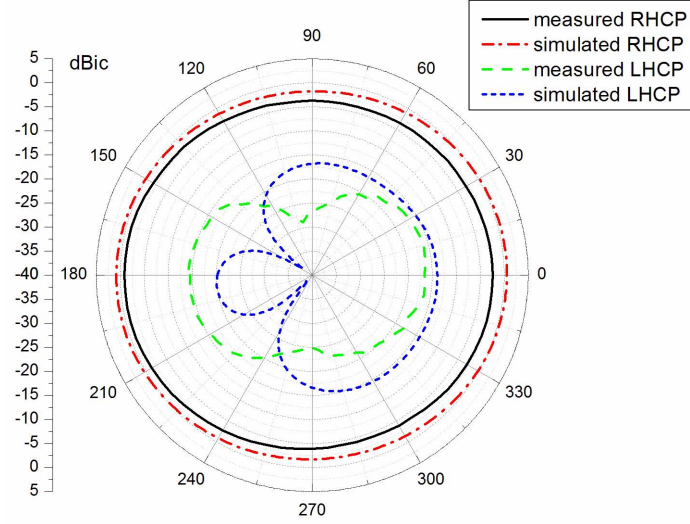


Figure 4.18. The measured and simulated CP gains at lower frequency in xz -plane ($\phi = 0^\circ$ cut). Simulated curve shown for 1.341 GHz and measured - 1.325 GHz

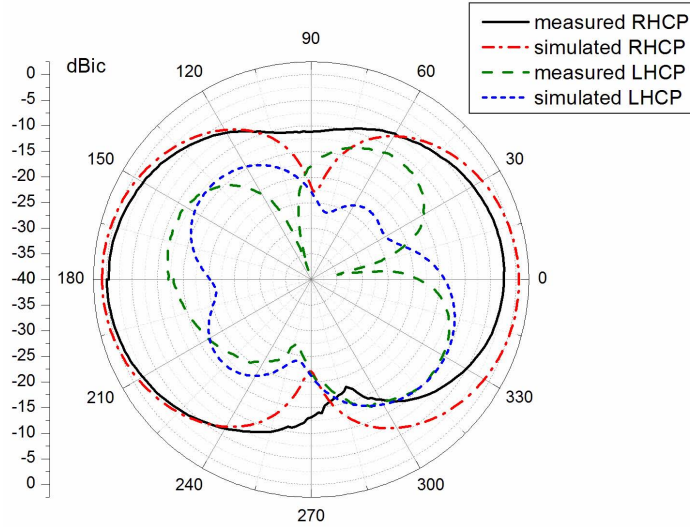


Figure 4.19. The measured and simulated CP gains at lower frequency in yz -plane ($\phi = 90^\circ$ cut). Simulated curve shown for 1.341 GHz and measured - 1.325 GHz

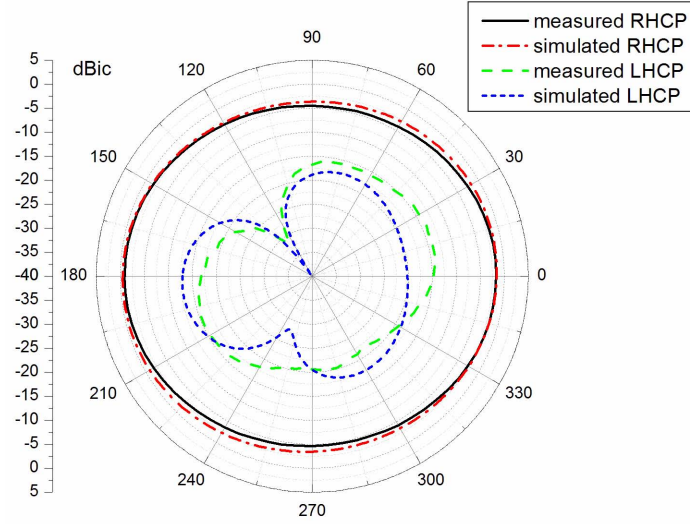


Figure 4.20. The measured and simulated CP gains at higher frequency in xz -plane ($\phi = 0^\circ$ cut). Simulated curve shown for 1.584 GHz and measured - 1.567 GHz

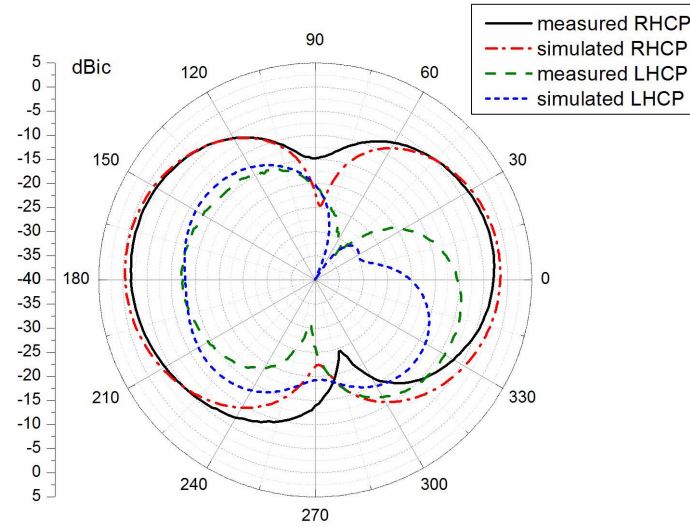


Figure 4.21. The measured and simulated CP gains at higher frequency in xz -plane ($\phi = 90^\circ$ cut).

4.5.1. Design Process

The overview of the design sequence of the dual-band omnidirectional CP antenna is as follows [85]:

1. Calculate the initial lengths of the patch (l_a and l_b , which at this stage can be equal), which should be approximately one half of an electrical wavelength at the lower resonant frequency (TM_{100} mode) for the given substrate.
2. Initially set the slot length $l_{sa} = l_{sb} = 0.63l_a$; the slot-to-edge separation $s_p = 0.04l_a$ and the slot width $W_s = 0.026l_a$. With these values, increased lumped element capacitance (within 1 - 2 pF range) reduces the FR. This property and a full-wave electromagnetic simulation was used to yield the desired FR. Note that the FR reduction factor may vary for different substrates.
3. The lumped capacitors should lower both resonant frequencies. Therefore additional adjustment is needed, by properly setting the patch size (l_a and l_b) and slot parameters (l_{sa} , l_{sb} and W_s).
4. The impedance match is adjusted by proper selection of parameters s_p and Δ_f , as well as small variations in the ground plane size S .
5. The AR at both frequencies is tuned to achieve omnidirectional CP radiation. This requires adjustment of stub widths W_1 and W_2 , as well as introducing a small difference between slot lengths l_{sa} and l_{sb} , and between the patch dimensions l_a and l_b . (Note that where the symmetry is compromised an independent adjustment might be necessary).

4.5.2. Impedance Match

The energy is coupled equally and in-phase into both patches, in a manner similar to that presented in Section 3.3. The influence of the reduced ground plane and triangular tapering of the CPW has already been explained. However, for the dual-band antenna, also the slot loading plays an important role for impedance match. If one employs the stub model presented in Fig. 4.11, the s_p parameter corresponds to the width of such defined stub, significantly changing its impedance. However by increasing s_p the unperturbed area in the middle of the patch is decreased, shifting operating frequency. For the lower band, the capacitor loaded slot increases the current path and decreases the operating frequency.

The two patches are additionally connected with a copper strip. To ensure in-phase excitation (required to achieve omnidirectional CP in xz -plane) it is positioned close to the feed point. It acts as an additional inductance, providing better match. Its position was experimentally optimised.

4.5.3. Axial ratio

The proposed design uses three independent parameters to control AR at both frequencies:

- an almost square geometry ($l_b > l_a$)
- an additional stub with variable width (W_1 and W_2)
- different slot lengths ($l_{sb} > l_{sa}$)

Hypothetically many more methods exist (i.e. truncated corners, asymmetric slits [86], or additional slots). Although only one perturbation technique is used in many dual-band antenna designs, here the use of three independent techniques allows more independent control of the AR for

each frequency band. A brief description of each of the methods and its impact with respect to dual-band performance is given below.

The almost-square patch is a classical method to achieve CP with patch antenna. However, for the dual-band configuration, it will affect the lower band more than the upper one. This can be explained by referring to the stub model again. If the patch dimension increases, but the position of the slot remaining the same, then effectively parameter S (as seen on Fig. 4.11) is also increased. This influences the impedance of the stub, however its resonant frequency remains unchanged (apart from the contribution by varied effective permittivity, which is very small).

An additional stub protruding from one side of the patch adds reactance, therefore shifting the resonance frequency of that mode downwards. Fig. 4.22 shows a parameter study of different values of W_1 and W_2 . It can be seen, that in both bands the upper of the two orthogonal modes remains at the same frequency and only the lower mode shifts downwards with increased stub width. Greater values of W_1 and W_2 could provide better AR but degrade the matching as seen in Fig. 4.22 for the case of

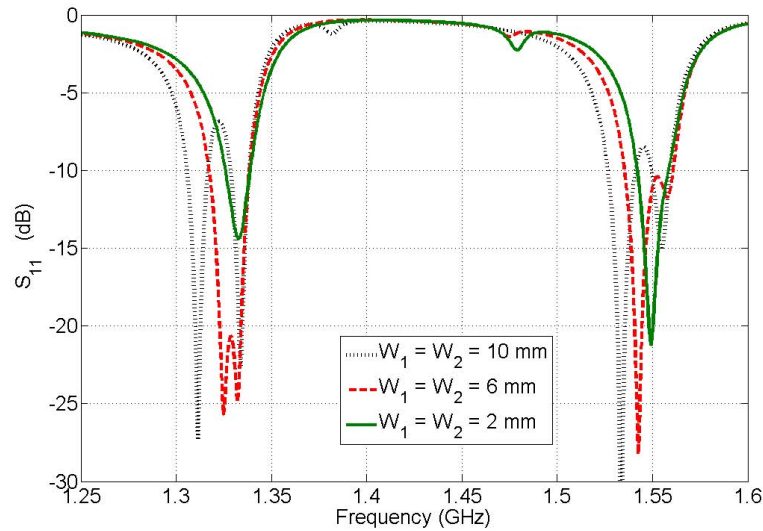


Figure 4.22. The simulated S_{11} for different stub widths W_1 and W_2 .

$W_1 = W_2 = 10$ mm.

The prototype exhibits slightly different performance between patches on layers A and C. To compensate for these effects, the stubs on layer A ($W_2 = 6$ mm) and layer C ($W_1 = 9$ mm) are slightly different, as specified in antenna parameters.

A small difference between the slot lengths has been used for CP generation in [84]. Fig. 4.23 shows the simulated S_{11} for different values of l_{sb} , while l_{sa} is kept constant. Fig. 4.24 shows AR in +z direction for the same values. Similarly to W_1 and W_2 , parameter l_{sb} steers the lower mode in each band. It can be seen, that the upper mode in the lower band is kept constant for all parameters. In the upper band some small perturbation can be seen also for the upper mode, which is most likely due to the interference between the slots: widening the slot shifts its boundary closer to the other slot. Typically the difference between slot lengths should be small, as the AR is heavily dependent on this parameter. Fig. 4.24 shows that even a small variation of 1 mm can strongly degrade the AR and shift its optimum frequency by up to 6 MHz. For $l_{sa} > l_{sb}$ LHCP is achieved (assuming no other perturbation elements).

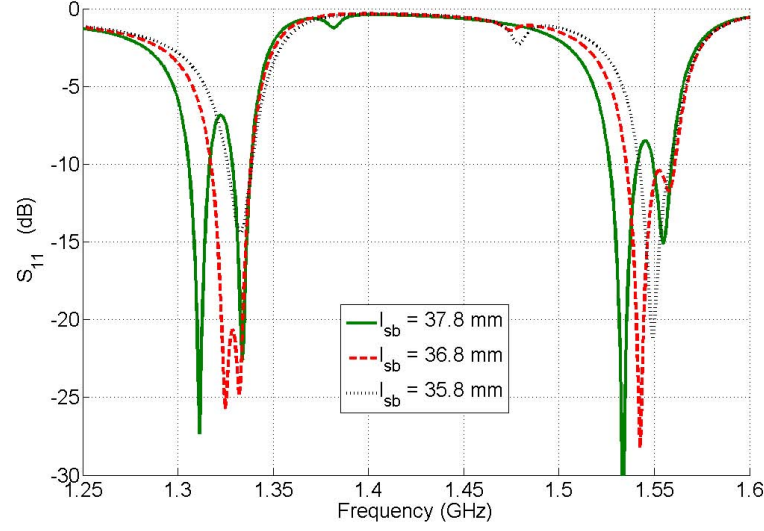


Figure 4.23. The simulated S_{11} for different values of l_{sb} . The other slot is kept constant at $l_{sa} = 38.8\text{mm}$.

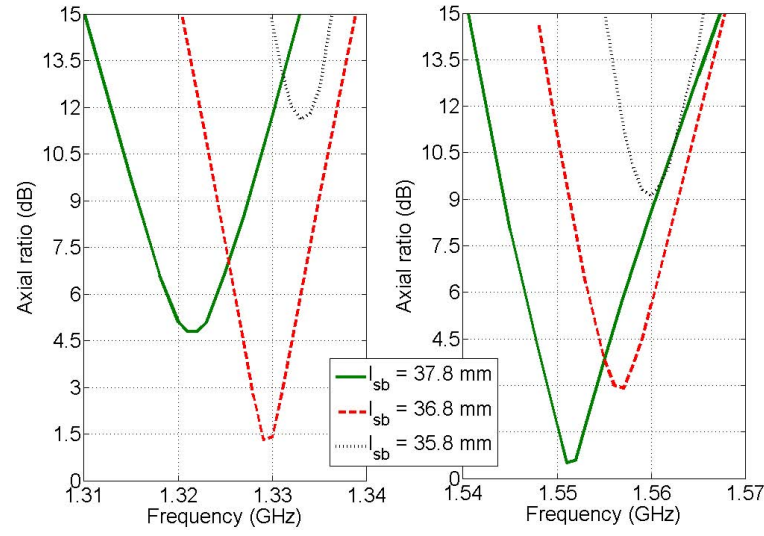


Figure 4.24. The simulated AR for different values of l_{sb} . The other slot is kept constant at $l_{sa} = 38.8\text{mm}$.

5. RECONFIGURABLE OMNIDIRECTIONAL CP ANTENNA

5.1. Reconfigurable CP Antennas

Recent advances in MIMO and diversity radio techniques stimulated increased development of reconfigurable antennas. This is a very practical feature, allowing real-time antenna adjustment to changing environments or system requirements. Most reconfigurable CP antennas deal with polarisation reconfigurability and allow switching between RHCP and LHCP (or less frequently between two circular and two linear polarisations). To name just a few circular polarisation reconfigurable designs: in [21] an L-shaped slot, with two pin diodes soldered across it, is incorporated into a rectangular microstrip patch. The pin diodes short-circuit either the horizontal or vertical part of the slot, therefore modifying the perturbation element and switching the sense of CP. Hsu and Chang in [18] proposed a truncated corner CP patch antenna, which uses a piezoelectric transducer to cover or un-cover truncation, therefore switching between RHCP and LHCP. Wu and Okoniewski in [87] presented another CP patch antenna, in which the perturbation element (metallised slug) is pneumatically moved from one edge of the patch to another, therefore covering or un-covering a slot. Since the slot acts as a mode perturbation, the sense of CP can be reversed. Centiner et al. proposed in [88] a spiral antenna, which uses multiple MEMS switches to re-route the flow of the current in the spiral. Pyo et al. in [89] introduced a microstrip antenna with a rectangular inner

conductor to generate RHCP and outer slot to generate LHCP. Two diodes switch between these two elements.

Some polarisation-reconfigurable antennas offer four modes, with two linear and two circular polarisations. This is the case in [25], where a square patch antenna is fed through a special 90° hybrid coupler. Two branches of the coupler are made with varactor diodes. When the diodes are on, a capacitance makes the circuit behave like a normal hybrid coupler and therefore provides RHCP and LHCP polarisation at its two inputs. However, when the varactor is switched to low capacitance (0.15 pF) the coupling between the two lines is very low. The circuit effectively acts as two separated lines. Applying the feed at its input ports produces linear polarisation. Another quad-polarisation reconfigurable antenna was proposed by Chen and Row in [90]. The antenna is based on a reconfigurable antenna with two linear polarisations, which are switched by a combination of two pin diodes. By adding a perturbation element, controlled by third diode, four polarisations (horizontal, vertical, LHCP and RHCP) can be produced.

However the most desired reconfigurable feature is usually the ability to change the antenna radiation pattern. The oldest solution to electronically steer the antenna beam involves antenna arrays, which consist of multiple antennas and complex feed networks which controls the amplitudes and/or phases at the antenna feeds. Implementing a steered beam with single antenna, as in [91], offers a significant reduction of antenna size and manufacturing costs. Despite many concurrent designs available for linearly polarised antennas, the CP designs are very rarely reported. In [92] Liu et al. proposed four parasitic cross elements to steer the radiation from a circular patch. Each cross can be independently switched on or off by pin diodes. Another approach introduces the elements of reconfigurability for a single-arm spiral antenna in [93]. By switching additional sections of the spiral some degree of beam reconfigurability is introduced. In this case switching elements are MEMS components.

In the following sections a pattern reconfigurability method is proposed, based on the previous findings on omnidirectional CP antennas. It will be shown, that by properly steering the phase relations between various sections of omnidirectional CP antenna the plane of omnidirectionality and consequentially the whole radiation pattern can be rotated.

5.2. Antenna Geometry

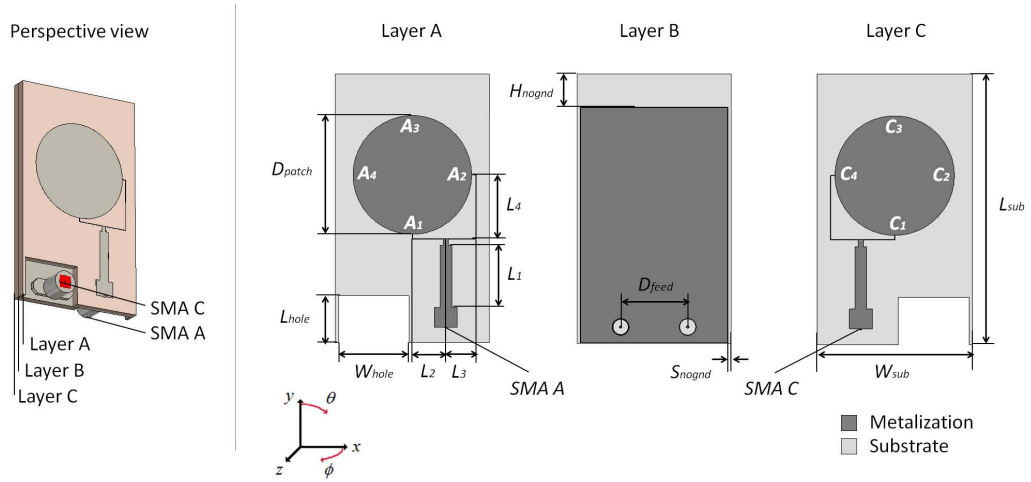


Figure 5.1. Proposed antenna design. Left: general perspective view with two SMA connectors on front and rear sides; Right: view of three metallization layers (as seen from $+z$ direction). Point marked as $A_1 - A_4$ and $C_1 - C_4$ are referred to as quadrature points on each patch.

The reconfigurable omnidirectional CP antenna is based on antenna designs presented in Sections 3 and 4. It uses two layers of Taconic RF-35 substrate. To decrease antenna Q and increase bandwidth, thicker substrate is used, which is of height $h = 3$ mm (therefore total antenna height is 6 mm). To generate RHCP each patch is fed by two feeds with 90° phase shift (see Fig. 5.1). This was done to increase axial ratio bandwidth, with respect to antennas using a perturbation element. To achieve RHCP in the front and

back direction, the feeds with 90° shifts are located on the opposite sides on layer A and C (i.e. points A_2 and point C_4).

The antenna shown in Fig. 5.1 has two inputs, each with an SMA connector (feed A and feed C) located on opposite sides of substrate. The inner SMA pins are connected through a groundplane hole to a 50Ω section of microstrip line. This line connects to a quarter wavelength transformer (68Ω impedance, 4 mm wide, $L_1 = 18.5\text{mm}$) and then to 94Ω microstrip sections (2 mm wide). A simple power splitter divides the signal into two 186Ω lines (0.2 mm wide), which are connected to the edge of the patch (one of them through 90° phase shifter). As discussed in Section 3, the groundplane is reduced and is smaller than the substrate footprint (by S_{nognd} in $\pm x$ direction and H_{nognd} in y direction).

The dimensions of the proposed structure are as follows: $D_{patch} = 35.4\text{mm}$; $L_{hole} = 14\text{mm}$; $W_{hole} = 21\text{mm}$; $L_1 = 18.5\text{mm}$; $L_2 = 10\text{mm}$; $L_3 = 9\text{mm}$; $L_4 = 19\text{mm}$; $H_{nognd} = 10\text{mm}$; $S_{nognd} = 1\text{mm}$; $D_{feed} = 20\text{mm}$; $L_{sub} = 80\text{mm}$; $W_{sub} = 46\text{mm}$.

5.3. Principles of Operation

The reconfiguration mechanism allows the rotation of the radiation pattern around the z -axis, changing the angle at which the omnidirectional CP radiation pattern is produced. It can theoretically produce an omnidirectional radiation pattern in any cut incorporating z -axis. To explain the principles, the phase difference at the SMA input connectors (feed A and feed C in Fig. 5.1) is investigated. Equal amplitude at these two ports is a necessary condition to create omnidirectional radiation pattern. However the phase shift between these two ports can be used to change the plane in which this pattern is produced (referred to as omnidirectional plane). Let γ be the angle between the omnidirectional plane and the xz -plane. It was discovered, that for an idealized antenna by introducing a phase shift Δ_{ph}

between SMA A and SMA C the angle γ will change in accordance with equation:

$$\gamma = \frac{1}{2}\Delta_{ph} \quad (5.1)$$

To explain this phenomena, we will investigate phase relationships at the quadrature points of both patches (points $A_1 - A_4$ and $C_1 - C_4$, as depicted on Fig. 5.1). The omnidirectional plane rotates around the $\pm z$ axis, therefore regardless of the antenna configuration for every phase shift Δ_{ph} there will be strong CP radiation in $\pm z$ directions, that is the directions normal to the patches.

Table 5.1 describes the phase between corresponding quadrature points (A_{1-4} and C_{1-4}) in both patches. For $\Delta_{ph} = 0^\circ$ the phase at points A_1 and C_1 is equal, say 0° . Due to the phase shifters, at points A_2 and C_4 it will be delayed by 90° with respect to A_1 and C_1 . From the properties of circular resonator, we can deduce that points A_3, C_3 will be delayed by 180° and points A_4, C_2 by 270° . The phase in each patch *rotates* in opposite directions to provide RHCP in both front and rear directions. As the patches are oriented back-to-back, two corresponding quadrature points on layers A and C (that is A_n and C_n) will create in-phase electric field if their phases differs by 180° (as seen in Fig. 5.2.a). Therefore radiation will be produced

Table 5.1. Phase between corresponding quadrature points in two patches for two most significant Δ_{ph} configurations.

Points	$\Delta_{ph} = 0^\circ$			$\Delta_{ph} = 180^\circ$		
	layer A	Layer B	Difference	Layer A	Layer B	Difference
A_1/C_1	0°	0°	0°	180°	0°	180°
A_2/C_2	90°	270°	180°	270°	270°	0°
A_3/C_3	180°	180°	0°	0°	180°	180°
A_4/C_4	270°	90°	180°	90°	90°	0°

in this direction. On the contrary, if two corresponding points have the same phase, the produced electric field will be out-of-phase. This means that (at some distance from antenna) the electric field from the patch on layer A will cancel out with electric field from the patch on layer C and hence no radiation will be produced in that direction (as seen in Fig. 5.2.b).

Following the same reasoning, if between SMA A and SMA B a phase shift of $\Delta_{ph} = 180^\circ$ is introduced, the points C_1 will be delayed by 180° with respect to point A_1 . Applying the same reasoning for $\Delta_{ph} = 0^\circ$ phase shifts between the quadrature points can be calculated as in Table 5.1. This results, that for $\Delta_{ph} = 180^\circ$ the radiation will be produced in the direction of points A_1/C_1 and A_3/C_3 (where 180° phase shift is present between the two layers) and in the direction of points A_2/C_2 and A_4/C_4 a null in radiation pattern will occur. The demonstrated reasoning can be used for any value of phase shift Δ_{ph} . To support the above explanation with simulation results, Fig. 5.2 shows the simulated (using CST Microwave Studio) electric field between the patches in points A_3/C_3 seen from y direction.

5.4. Measurements

This theory refers to an ideal case, when the antenna is fed from an ideal source (with no transmission lines to impact the radiation pattern). In practice, the proposed steering mechanism will be perturbed by a couple of factors. For measurement in an anechoic chamber the antenna is fed using cables, attached to phase shifting circuitry (a rat-race coupler and 90° hybrid coupler were used). As discussed in Section 3, the reduced ground plane causes a current to flow on the outside of the feed cables. This was mitigated by the use of ferrite bead, mounted on the feed coaxial line close to antenna SMA connectors (SMA A and SMA C).

The antenna is also positioned above an additional metallisation, formed by the the phase shifting circuitry. For $\Delta_{ph} = 0^\circ$ the impact of this extra

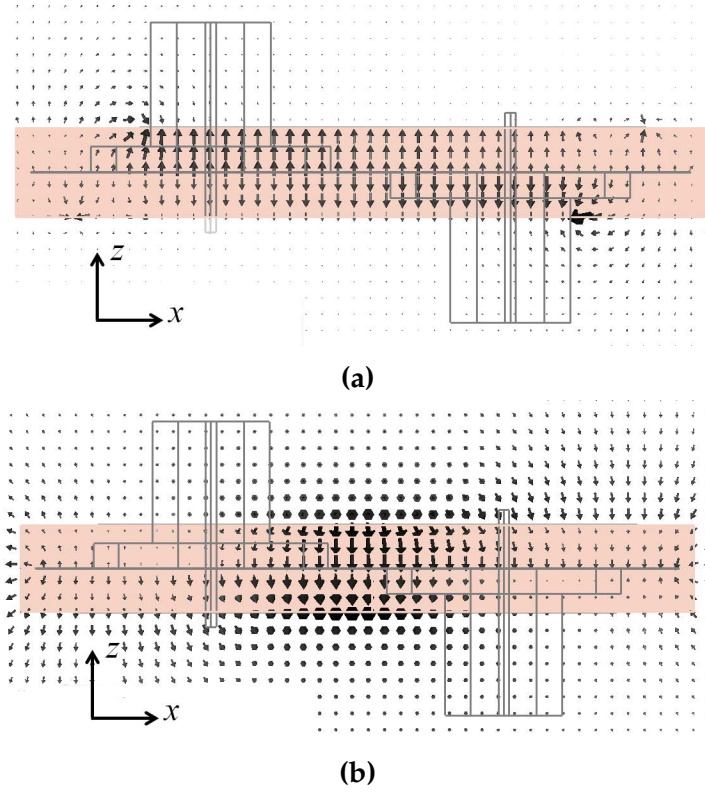


Figure 5.2. Electric field between points C_1 and C_3 for: a) $\Delta_{ph} = 180^\circ$; b) $\Delta_{ph} = 0^\circ$.

metallisation is very small, as the antenna radiates in the xz -plane. However for other configurations (especially for $\Delta_{ph} = 180^\circ$, which radiates in yz -plane) it significantly perturbs the radiation pattern. There are two principal consequences related to this. Firstly, the radiation in $-y$ direction ($\theta = 180^\circ$) where the feeds are located, has significantly lower gain due to the energy being shielded by the phase shifting circuitry (a microstrip circuit with its groundplane positioned towards the antenna). However, the reflected RHCP wave becomes LHCP. Since the AR is determined by the cross polarisation level (Eq. 1.4), for the $+y$ direction ($\theta = 0^\circ$) a drop in AR can be also seen. To minimize this effect, the phase shifting circuitry was separated from the antenna by a brick of cubic absorbing material (ECCSORB LS-26 [94]), placed on a dedicated PVC holder (30 cm long). This improved the measurement performance, however some disturbances were still present throughout the measurement results. The photo of measurement configuration is shown in Fig. 5.3.

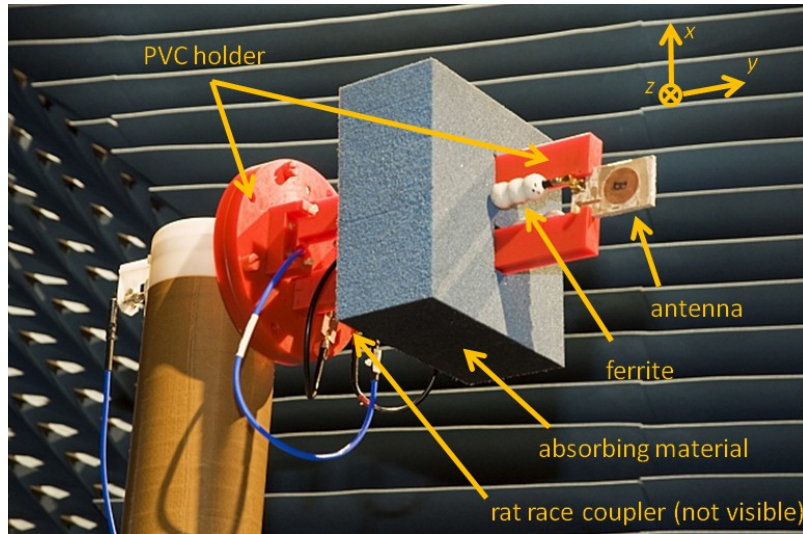


Figure 5.3. Photo of the measurement configuration for gain and radiation pattern, made in the anechoic chamber of RWTH Aachen University, Germany.

A reconfigurable omnidirectional CP antenna was designed for the WLAN band of 2.4 – 2.5 GHz. Simulated and measured S_{11} and S_{22} are shown on Fig. 5.4 and are in good agreement (as the antenna is symmetric, only one curve is shown for simulation). The isolation between the two ports is above 15 dB in the whole band of interest. The small discrepancy in reflection coefficient is due to manufacturing tolerance: the fabrication technique was constrained by a resolution of 0.2 mm [10], which corresponds to the width of the $186\ \Omega$ microstrip lines. The reflection coefficients were measured at antenna ports SMA A and SMA C with no absorber mounted around the antenna at this time.

Inputs SMA A and C were connected by phase-matched cables to a rat-race coupler to provide $\Delta_{ph} = 0^\circ$ and $\Delta_{ph} = 180^\circ$ and to 90° hybrid coupler to provide $\Delta_{ph} = +90^\circ$ and $\Delta_{ph} = -90^\circ$.

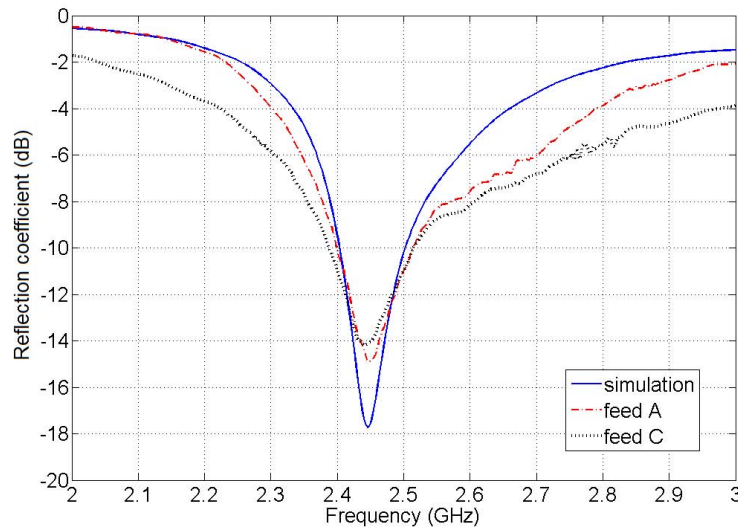


Figure 5.4. Measured and simulated reflection coefficients at SMA A and SMA C. Due to symmetry, only one curve is shown for simulation.

5.4.1. Configuration $\Delta_{ph} = 0^\circ$

Figs. 5.5 to 5.8 show the realized gains and AR for the configuration $\Delta_{ph} = 0^\circ$. Figs. 5.5 and 5.6 shows RHCP and LHCP realized gains in two orthogonal planes. In Fig. 5.5 the omnidirectional plane ($\gamma = 0^\circ$) is clearly visible, whereas Fig. 5.6 shows the figure-of-eight shape. The shouldering (visible in yz -plane around $\theta = 0^\circ$ and $\theta = 180^\circ$) is most likely due to the effects of the feed network. The average measured AR in the xz -plane is 3 dB and for all angles in the omnidirectional plane ($\gamma = 0^\circ$) it is better than 5.68 dB. Fig. 5.7 show measured AR around a full sphere (with respect to the coordinate system in Fig. 5.1. From Figures 5.5, 5.6 and 5.7 it can be seen, that the pattern is dipole-like both in terms of RHCP gain and axial ratio. This is similar performance to the antennas described in previous Sections 2-3. In fact, for those antennas (as well as for [52]) the use of a common CPW as a feed automatically imposed $\Delta_{ph} = 0^\circ$. Fig. 5.8 shows the measured AR for the omnidirectional plane ($\theta = 90^\circ$) as a function of ϕ and frequency. The AR bandwidth (as outlined in Section 1.4.3, with respect to 5.68 dB limit) is 30 MHz (1.2% from 2.464 to 2.494 GHz). The measured RHCP gain varies from +2 to -2 dBic, which is comparable to the gain of a dipole.

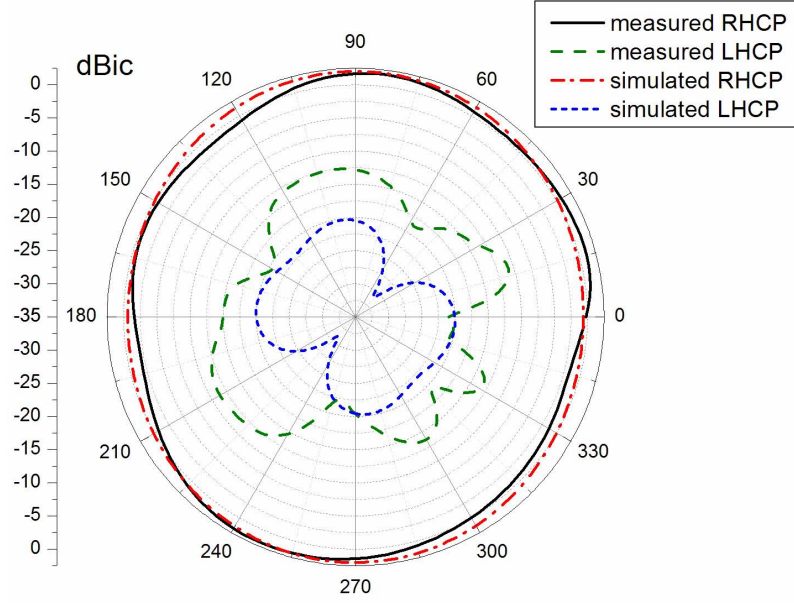


Figure 5.5. Simulated and measured gains of the proposed antenna at 2.47 GHz for $\Delta_{ph} = 0^\circ$ in xz -plane ($\theta = 90^\circ$ with varying ϕ).

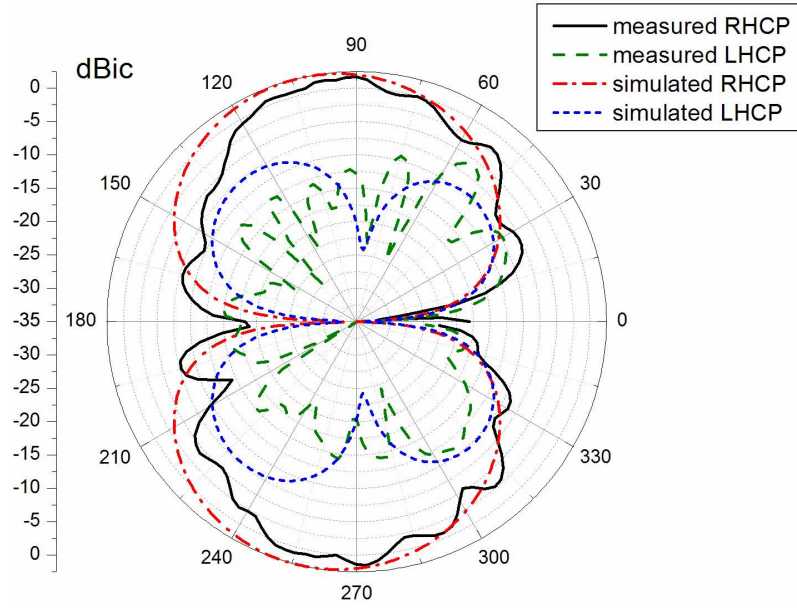


Figure 5.6. Simulated and measured gains of the proposed antenna at 2.47 GHz for $\Delta_{ph} = 0^\circ$ in yz -plane ($\phi = 90^\circ$ and $\phi = 270^\circ$ with varying θ).

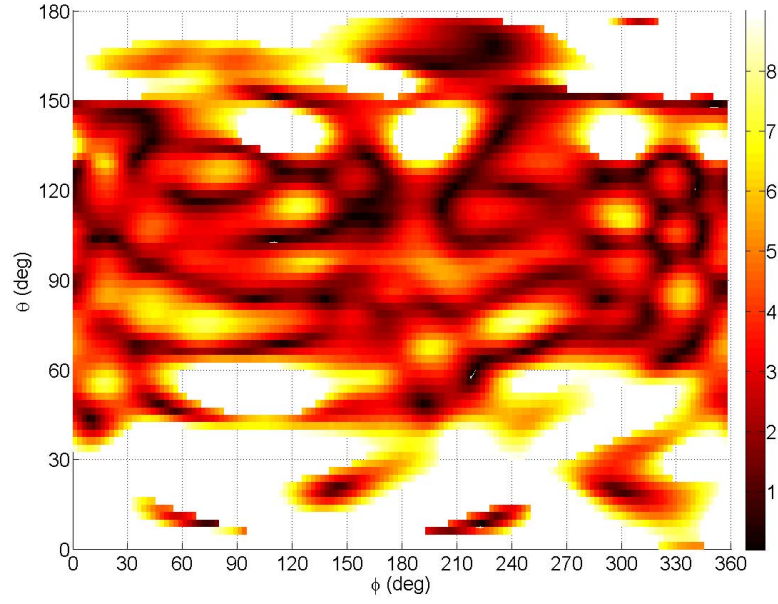


Figure 5.7. Measured AR for $\Delta_{ph} = 0^\circ$ at 2.47 GHz, as a function of (θ, ϕ) . Values above 9 dB are not shown for clarity.

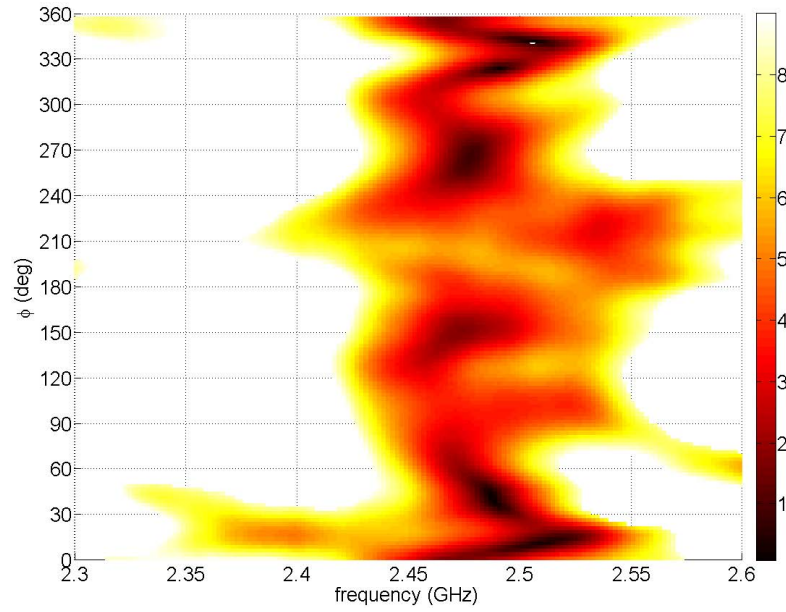


Figure 5.8. Measured AR for $\Delta_{ph} = 0^\circ$ as a function of frequency and angle ϕ in the plane of omnidirectionality. Values above 9 dB are not shown.

5.4.2. Configuration $\Delta_{ph} = 180^\circ$

Figs. 5.9 to 5.12 show the realized gains and AR for the configuration $\Delta_{ph} = 180^\circ$. Similarly to plots in Section 5.4.1, Fig. 5.9 shows the omnidirectional plane (here $\gamma = 180^\circ$), whereas Fig. 5.10 shows a perturbed figure-of-eight shape. The two consequences of the feed structure, mentioned in section 5.4, can be clearly seen in Fig. 5.9 (drop in radiated power at $\theta = 180^\circ$) and in Fig. 5.11 (decreased AR at $\theta = 0^\circ$). The figure of eight shape in Fig. 5.10 is slightly tilted both in simulated and measured data, which is most likely an impact of microstrip lines on the antenna surface. The decrease in AR is visible in the xz -plane (horizontal) at $(\theta = 90^\circ; \phi = 0^\circ)$ and $(\theta = 90^\circ; \phi = 180^\circ)$, which match with the nulls of RHCP gain.

The radiation pattern can be divided into three areas, indicated on Fig. 5.12, where different phenomena dominate the antenna performance:

- For angles $150^\circ \leq \theta \leq 235^\circ$, that is the directions obstructed by the phase shifting circuitry, the AR varies from 0.4 to 11 dB, with three noticeable peaks exceeding the 5.68 dB limit.
- For angles $10^\circ \leq \theta \leq 150^\circ$ and $235^\circ \leq \theta \leq 350^\circ$ the view is unobstructed and good CP radiation is produced, with an average AR of 2.5 dB. The maximum gain is 2.6 dBic. For this region, the AR bandwidth (5.68 dB limit) stretches from 2.434 to 2.484 GHz (50 MHz, 2%). This is more wideband than in the case of $\Delta_{ph} = 0^\circ$ and is also downshifted in frequency, with respect to that configuration. This is due to fact, that in the $-y$ direction there is extra dielectric to support $\lambda_0/4$ transformers and power dividers. The overlapping band of both $\Delta_{ph} = 0^\circ$ and $\Delta_{ph} = 180^\circ$ configurations is 2.466 - 2.484 GHz (0.8 %).
- For angles $350^\circ \leq \theta \leq 10^\circ$ there is no visible drop in RHCP gain, however the AR deteriorates up to 8.5 dB. This is due to reflection from the phase shifting circuitry. Although the reflected LHCP signal

is small (due to the use of absorber), it is sufficient to strongly degrade the AR as indicated by Eq. 1.4.

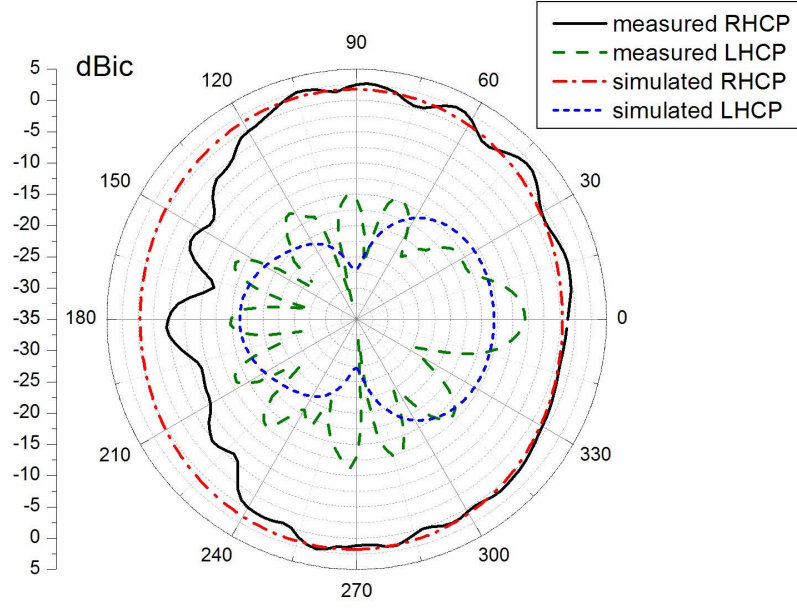


Figure 5.9. Simulated and measured gains of the proposed antenna at 2.47 GHz for $\Delta_{ph} = 180^\circ$ in yz -plane ($\phi = 90^\circ$ and $\phi = 270^\circ$ with varying θ).

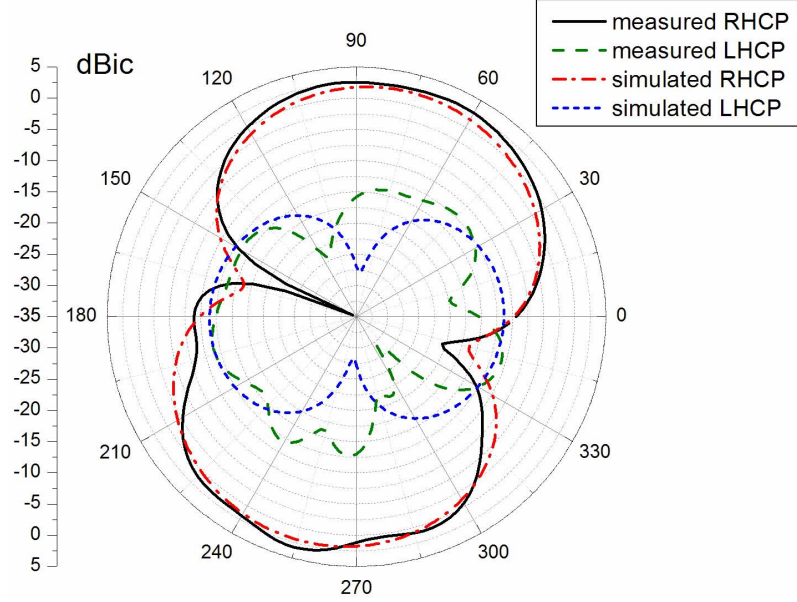


Figure 5.10. Simulated and measured gains of the proposed antenna at 2.47 GHz for $\Delta_{ph} = 180^\circ$ in xz -plane ($\theta = 90^\circ$ with varying ϕ).

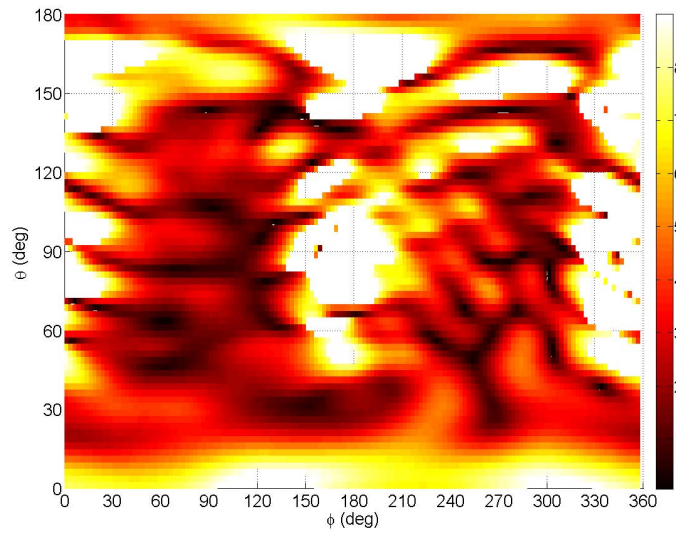


Figure 5.11. Measured AR for $\Delta_{ph} = 180^\circ$ at 2.47 GHz, as a function of (θ, ϕ) . Values above 9 dB are not shown for clarity.

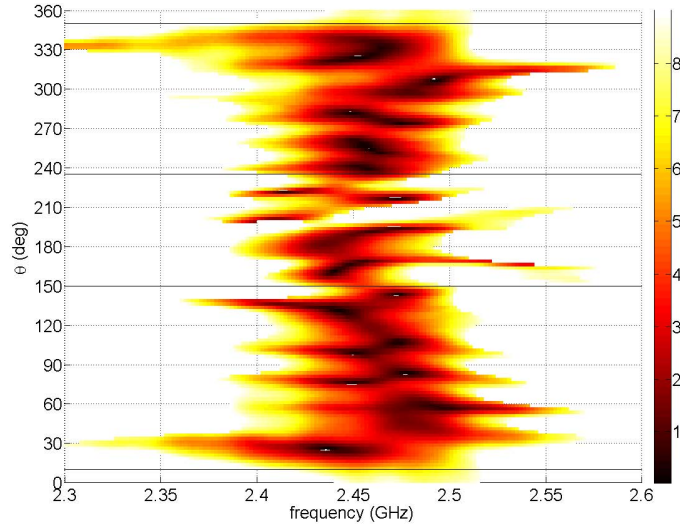


Figure 5.12. Measured AR for $\Delta_{ph} = 180^\circ$ as a function of frequency and angle θ in the plane of omnidirectionality. Values above 9 dB are not shown.

5.4.3. Configuration $\Delta_{ph} = +90^\circ$

To generate omnidirectional radiation at $\gamma = 45^\circ$ a 90° hybrid coupler was used as a phase shifting circuit. The plane, which incorporates z axis and is tilted at $\gamma = 45^\circ$ with respect to the xz -plane will be for brevity referred to as γ_{45} and is defined by the following equation:

$$\theta = \text{arctg}(\cos\phi) \quad (5.2)$$

Accordingly, an orthogonoal plane which also incorporates the z -axis but is tilted at $\gamma = 135^\circ$ with respect to the xz -plane will be referred to as γ_{135} and is defined as:

$$\theta = \text{arctg}(-\cos\phi) \quad (5.3)$$

Figs. 5.13 and 5.14 shows the measured and simulated gain in two principal cuts, as defined by Equations 5.2 and 5.3. In the omnidirectional plane γ_{45} the maximum gain is 4 dBic and for angles $220^\circ \leq \phi \leq 130^\circ$, good om-

nidirectionality is observed. For angles $130^\circ \leq \phi \leq 220^\circ$ a drop in RHCP down to -6.6 dBic can be seen. In the presented cut $\phi = 180^\circ$ is the direction located closest to the phase shifting circuitry, therefore this decrease in realized gain is considered to be caused by it. In the γ_{135} plane (Fig. 5.14), the measured figure-of-eight shape is less prominent than expected from simulation. The decrease in axial ratio is observed for angles ϕ from 180° to 360° (especially around $\phi = 270^\circ$), whereas on the other side for angles ϕ from 10° to 235° (around $\phi = 90^\circ$) good AR below 3 dB is preserved (Fig. 5.15). The average AR over the full γ_{45} plane is 3.19 dB.

Fig. 5.16 depicts the AR in the γ_{45} -plane as a function of frequency. The small discontinuities in this figure are due to the discretization of the angle, as the measurement was made in regular ϕ and θ 2.5° steps. Therefore the gathered sampling points do not always fit into γ_{45} plane. The sample, which for given ϕ was closest to the desired plane, was incorporated into the plot.

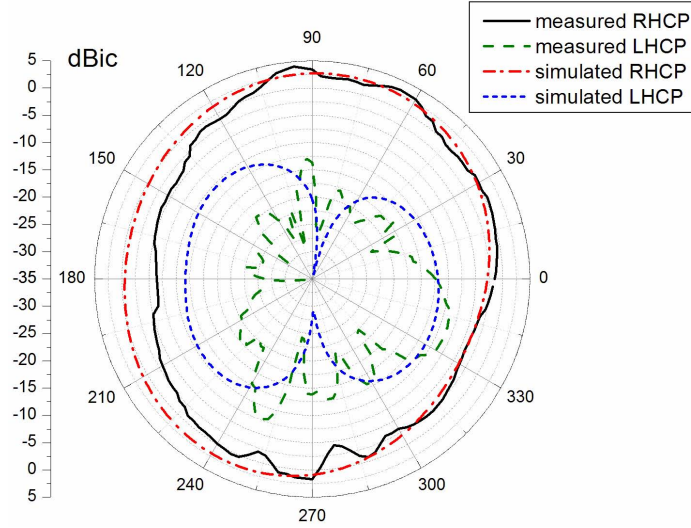


Figure 5.13. Simulated and measured gains of the proposed antenna at 2.47 GHz for $\Delta_{ph} = +90^\circ$ in γ_{45} -plane (defined by Equation 5.2).

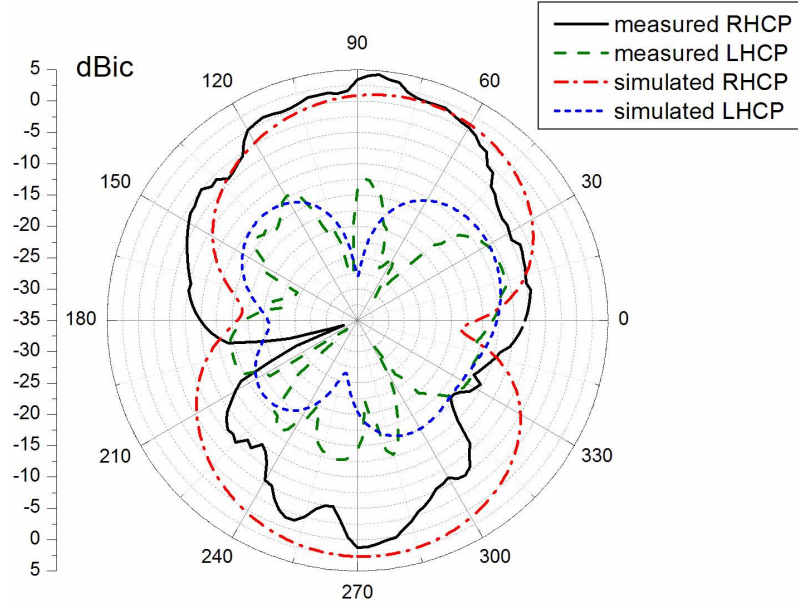


Figure 5.14. Simulated and measured gains of the proposed antenna at 2.47 GHz for $\Delta_{ph} = +90^\circ$ in γ_{135} -plane (defined by quation 5.3).

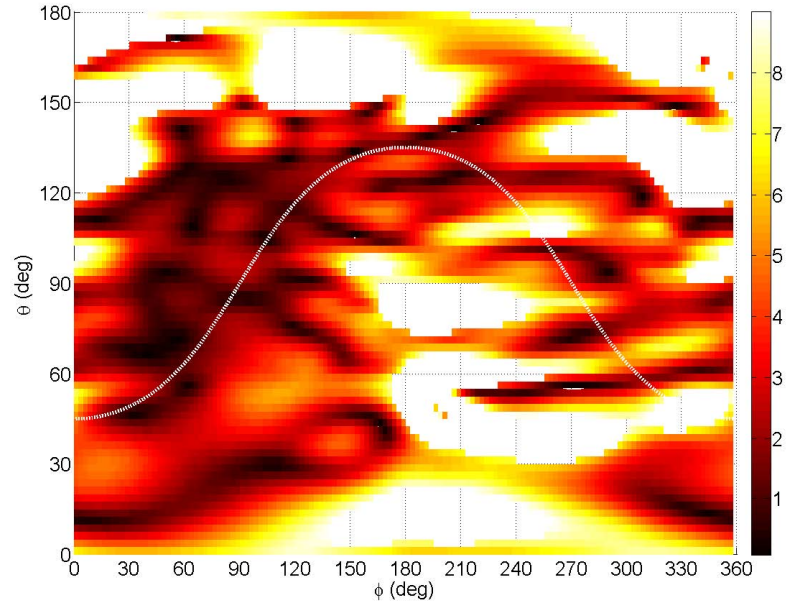


Figure 5.15. Measured AR for $\Delta_{ph} = +90^\circ$ at 2.47 GHz, as a function of (θ, ϕ) . White line shows cut for γ_{45} plane. Values above 9 dB are not shown.

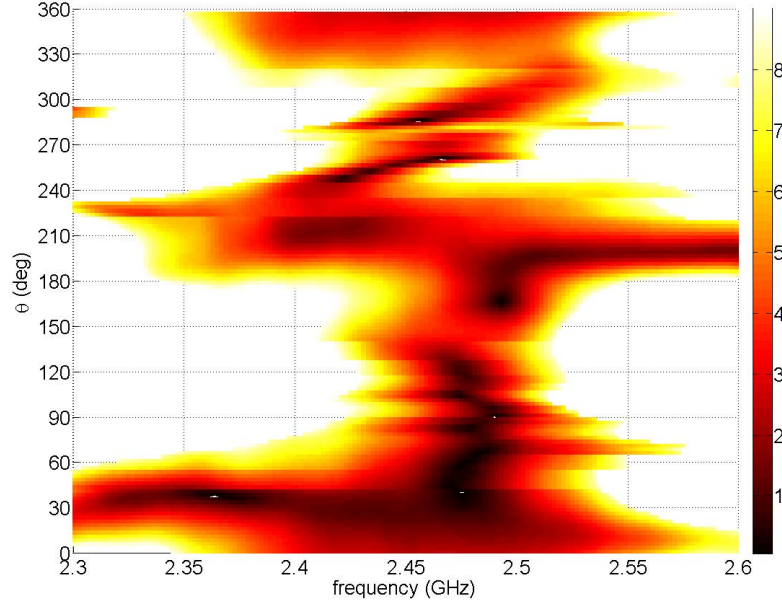


Figure 5.16. Measured AR for $\Delta_{ph} = +90^\circ$ as a function of frequency and angle θ in the plane of omnidirectionality γ_{45} .

5.4.4. Configuration $\Delta_{ph} = -90^\circ$

Similarly to the results presented in Section 5.4.3, a 90° hybrid coupler was used to achieve $\Delta_{ph} = -90^\circ$. For this configuration the omnidirectional plane is the γ_{135} -plane (seen in Fig. 5.17) and a figure of eight occurs in the γ_{45} -plane (seen in Fig. 5.18). In γ_{135} plane the angle closest to the phase shifting circuitry (located around $\theta = 180^\circ$) is $\phi = 0^\circ$, hence a drop in RHCP gain can be seen for this direction. Maximum RHCP realized gain is 3.3 dBic. Fig. 5.19 shows good AR performance for the angles $160^\circ \leq \phi \leq 310^\circ$, where it is kept below 4 dB. This exhibits a symmetry with $\Delta_{ph} = +45^\circ$ configuration, where good AR was obtained for $160^\circ \leq \phi \leq 310^\circ$. The average AR in the whole γ_{135} -plane is 3.65 dB.

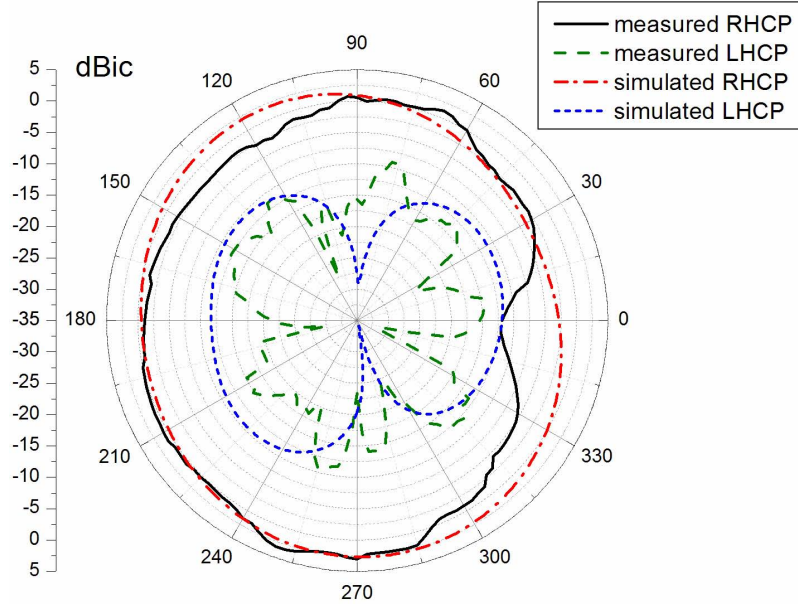


Figure 5.17. Simulated and measured gains of the proposed antenna at 2.47 GHz for $\Delta_{ph} = -90^\circ$ in γ_{135} -plane (defined by Equation 5.3).

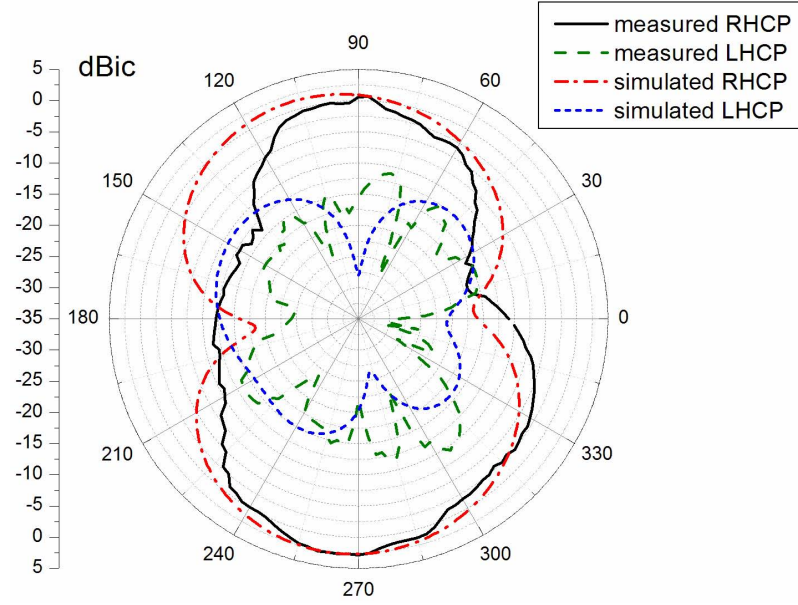


Figure 5.18. Simulated and measured gains of the proposed antenna at 2.47 GHz for $\Delta_{ph} = -90^\circ$ in γ_{45} -plane (defined by Equation 5.2).

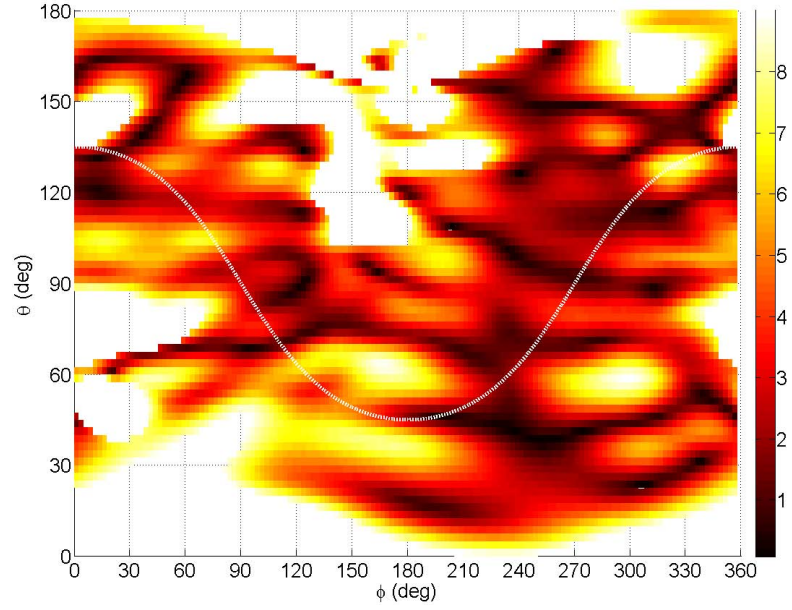


Figure 5.19. Measured AR for $\Delta_{ph} = -90^\circ$ at 2.47 GHz, as a function of (θ, ϕ) . White line shows cut for γ_{135} plane. Values above 9 dB are not shown.

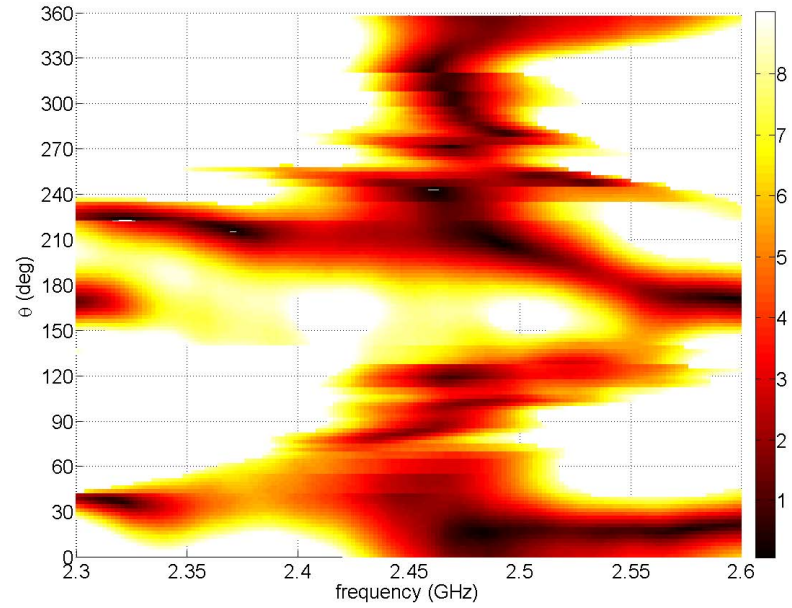


Figure 5.20. Measured AR for $\Delta_{ph} = -90^\circ$ as a function of frequency and angle θ in the plane of omnidirectionality γ_{135} .

5.5. Measurement Improvement

Measurements described and discussed in Section 5.4 confirmed the functionality of the reconfigurable OCPA, however the data suffers from many inaccuracies. As the antenna radiates in practically any direction (for various configurations), its measurement poses a significant challenge, as the antenna needs to be powered and mechanically supported. Recently Manteuffel et al. presented in [95] an antenna measurement technique, which could help overcome this problem. In the proposed method an electronic chip, which produces a signal of constant known power in a desired frequency band, is connected to the AUT and acts as a power source. The technique allows antenna measurement without feed cables. For the reconfigurable OCPA with integrated phase shifting circuitry the method could be applied to produce more accurate data. On the other hand the chip provides no phase reference, complicating CP measurement: the horizontal and vertical polarisations from two consecutive measurements can't be combined to calculate AR. However to accurately measure CP parameters with the proposed technique, one can employ either a spinning dipole or use a dual polarised horn attached to a VNA with at least three ports.

6. DUAL CIRCULARLY POLARISED PATCH ANTENNA

6.1. Background

In Section 4 the advantages of reconfigurable CP antennas were demonstrated, with respect to both polarisation and pattern reconfigurability. Also, a flexible solution to CP pattern reconfigurability was proposed. In this chapter, a dual CP antenna is presented, which is considered to be more compact than antennas using classical 90° hybrid couplers. Unlike many switched sense CP antennas discussed in Section 5.1 [18, 21, 87–89], the proposed design employs no switching components (pin diodes, MEMS switches, piezoelectric transducers, pneumatic pumps etc.) and the two channels for RHCP and LHCP can be used simultaneously [96]. Unlike the antennas described in Sections 2 to 4, the antenna presented in this section is unidirectional.

Recently Li et al. proposed a dual linearly polarised antenna, employing even and odd modes of a CPW transmission line [97–99]. The concept of even and odd modes is often used to analyse microwave circuits, especially couplers. It refers to a transmission line with three independent metallisations, like coupled microstrip lines or CPW. One of the metallisation (for coupled microstrip it is ground plane, for CPW it will be the middle conductor) is considered as a reference. If the signals in the two remaining metallisation layers are in phase, it is referred to as an even mode; if the signals are 180° out of phase, it is an odd mode [100].

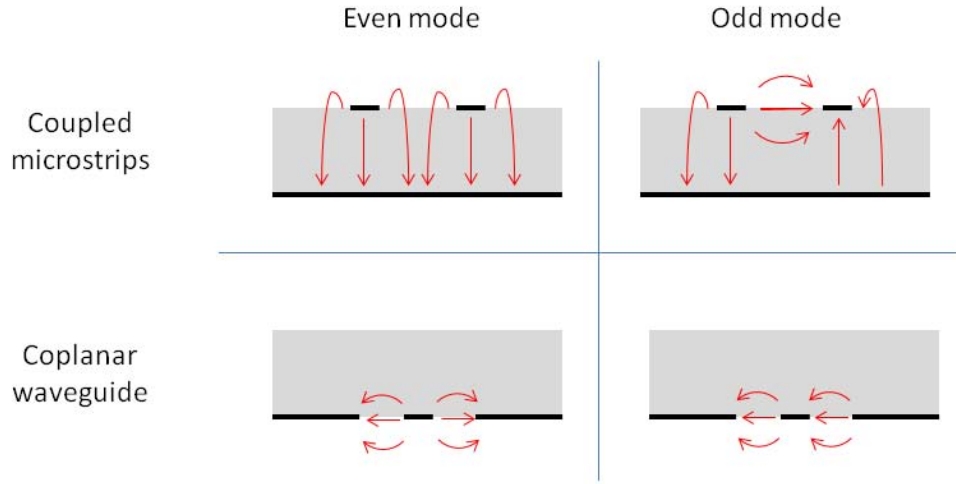


Figure 6.1. Electric field lines for even and odd modes in two most common multi-mode transmission lines.

Fig. 6.1 shows the electric field lines for both modes in two most commonly used dual mode transmission lines: coupled microstrips (top) and coupled slotlines, or coplanar waveguide (bottom). Coupled microstrips are much better understood and easier to calculate. However their main disadvantage is that the electromagnetic wave propagates at different speeds for even and odd mode. This is because in the even mode the greater part of the electric field propagates in the dielectric substrate (with $\epsilon_r > 1$) than in the odd mode. This leads to different values of effective permittivity for each mode. On the other hand, in the coplanar waveguide all the metallisations are located at the border between air and dielectric, what minimises the difference between the propagation speed of each mode. It should be noted however, that odd mode of coupled slotlines is a TE mode, what complicates analytical calculations.

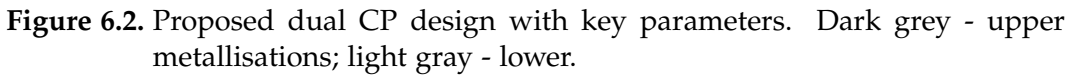
Soliman et al. proposed in [33] to use the two slots in CPW as two independent feeds for a CP aperture antenna. The CPW is excited in its basic (even) mode, with a bridge short circuiting the two outermost conductors.

Two slots comprising CPW are separated from each other and 90° phase shifter is applied in one of them. The slots are connected to an aperture, which as a result radiates a RHCP beam to the front and LHCP to the rear.

Although the solution proposed in this chapter is a microstrip patch antenna, it is based on the findings by Li and Soliman for aperture antennas [33, 97]. By extending one of the CPW slots (or, alternatively, one of coupled microstrip lines) by 90° the phase difference between the two metallisation becomes 90° for even mode and 270° for odd mode. This, when used as two orthogonal feeds for a microstrip patch, will generate opposite sense circular polarisation.

6.2. Antenna Design

The proposed design [96] is described in Fig. 6.2. The structure was prototyped on a Taconic RF-35 substrate ($h = 1.5$ mm, $\epsilon_r = 3.5$). The patch was elevated on an additional layer of substrate to decrease the Q factor and increase bandwidth. Port 1 is attached directly to the $50\ \Omega$ CPW (inner conductor: 2.4 mm wide, slots: 0.2 mm), therefore exciting the even mode (a standard mode of operation for CPW). This produces a LHCP beam. A microstrip line on the upper substrate layer couples the power into the CPW, exciting the odd mode. This produces a RHCP beam. To minimize the unwanted reactance in the odd mode, introduced by the microstrip passing over the CPW, the microstrip was tapered down to $W_m = 1.7$ mm width. This minimized disruption of the CPW without introducing reflections in the microstrip. The lengths L_{m1} and L_{m2} were initially set so that their sum $L_{m1} + L_{m2}$ is approximately a $\lambda_0/4$. This was used as a base for optimisation with the parameter sweep tool, embedded in CST Microwave Studio. The odd mode is filtered at port 1 by the SMA connector. This is because the outer flange of SMA effectively short circuits the two outermost metallisations, preventing the even mode from propagating beyond this point



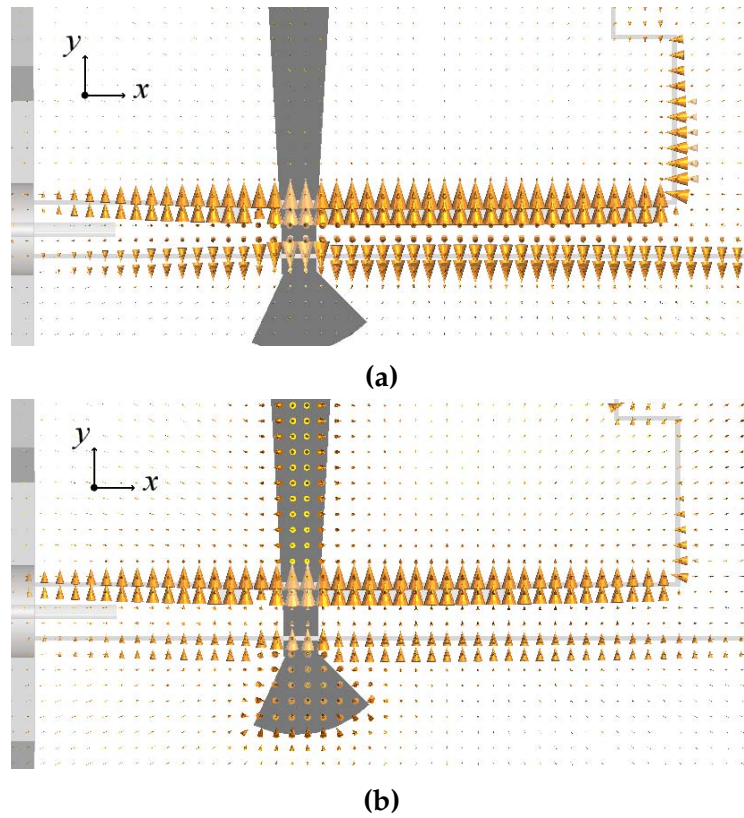


Figure 6.3. Simulated electric field in the feed line: a) even mode, excited from the SMA from the left side (port 1); b) odd mode, excited from the microstrip line from the top (port 2).

6.3. Antenna Measurements

Fig. 6.4 shows the reflection and isolation coefficients for the two input ports (both measured and simulated). The device is reciprocal ($S_{12} = S_{21}$), hence only one curve for isolation data is shown. The measured port-to-port isolation is up to 20 dB and is better than 10 dB across the band of 2.515–2.598 GHz (3.2 %). In this band both S_{11} and S_{22} are below -10 dB, therefore the isolation is the most critical parameter for antenna wideband radiation. It is important to understand, that although the bandwidths for $S_{11} < -10\text{dB}$ and $S_{22} < -10\text{dB}$ are much wider than the isolation bandwidth, it does not indicate antenna radiation, as explained in Section 1.4.1. In fact, due to the mechanism outlined in Section 6.4, the energy reflected at the patch input will propagate backwards into the other port (i.e. power fed to port 1 will mainly output at port 2 and vice versa). This mechanism

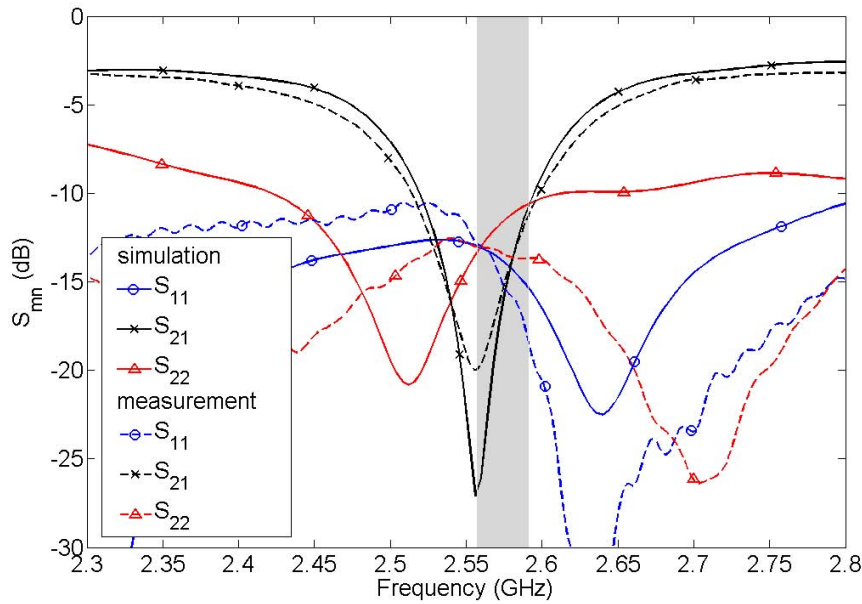


Figure 6.4. Reflection and isolation coefficients for the proposed antenna. Grey strip indicates the bandwidth, for which AR < 3 dB at boresight in both modes (i.e. 2.557 - 2.591 GHz).

keeps the reflection coefficients low in a very large band, despite the lack of any radiating mechanism.

Fig. 6.5 shows the AR at boresight for both modes. Both AR are relatively wideband, which is due to the use of the two port feed with a 90° phase shifter. The odd mode is more narrowband and shifted upwards in frequency. This is most likely due to the use of the coupling mechanism between a microstrip and CPW: the power coupled from the microstrip into the first slot is slightly greater than coupled into the second slot (this can be seen in Fig. 6.3.b), thus perturbing the equal amplitude requirement for CP generation. For the even mode, the AR bandwidth is 8%, which is generally as expected (compared to 9.9% in [33]). Despite these discrepancies, there is a good CP and impedance performance (i.e. all S-parameters below -10 dB) for both modes in the band between 2.557 - 2.591 GHz, giving a combined 3dB AR bandwidth of 34 MHz (1.3 %).

Figs. 6.6 to 6.9 depict realized gains for both modes for elevation (yz -plane, Figs. 6.6 and 6.7) and horizontal cuts (xz -plane, Figs. 6.8 and 6.9). The measured realized gains at 2.575 GHz are 7.4 dBic for LHCP in port 1

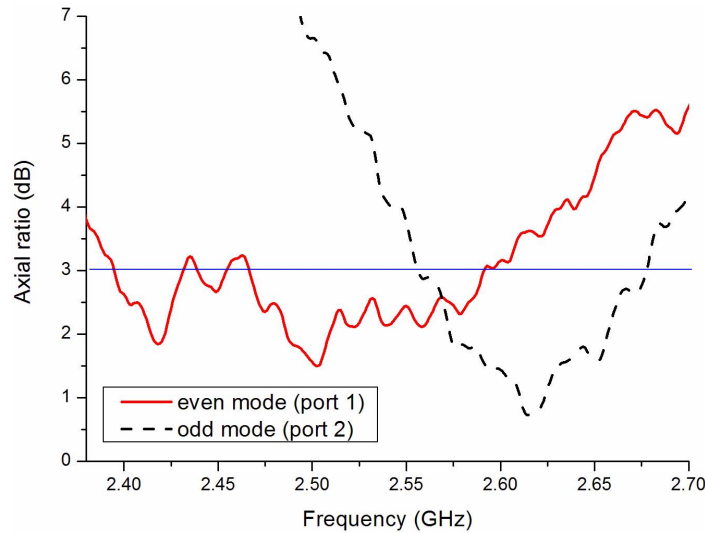


Figure 6.5. Measured AR at boresight as a function of frequency for two modes.

and 4.8 dBic for RHCP in port 2. This difference is most likely due to the coupling mechanism. The boresight ARs are 2.45 dB for port 1 and 1.82 dB for port 2.

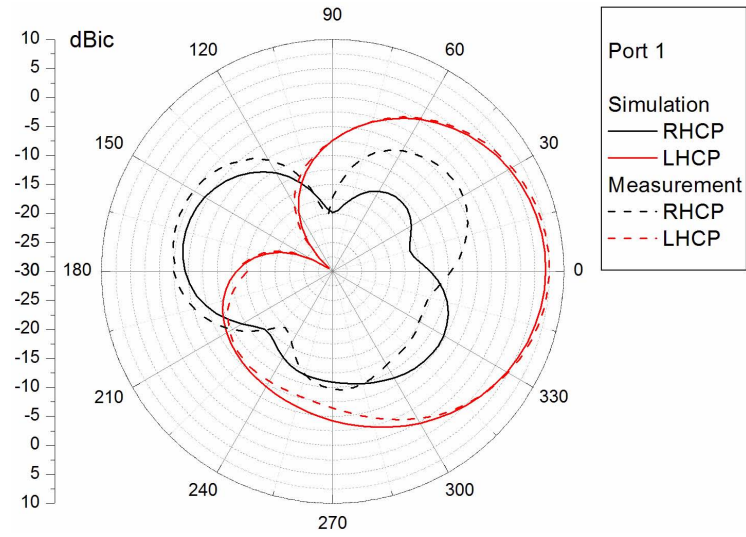


Figure 6.6. Realized gains in yz -plane for port 1 exciting even mode at 2.575 GHz.

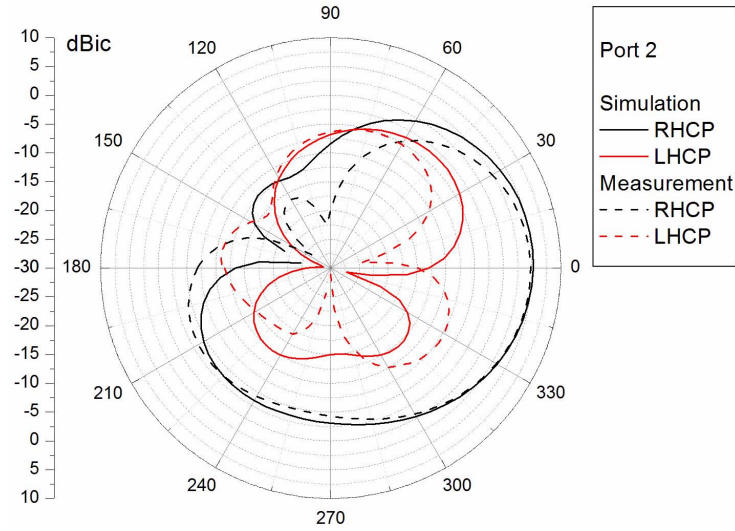


Figure 6.7. Realized gains in yz -plane for port 2 exciting odd mode at 2.575 GHz.

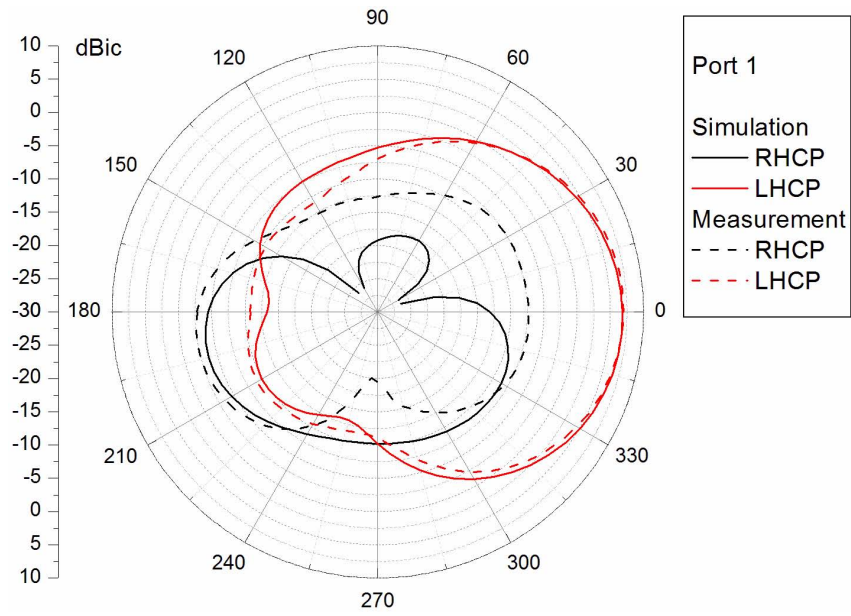


Figure 6.8. Realized gains in yz -plane for port 1 exciting even mode at 2.575 GHz.

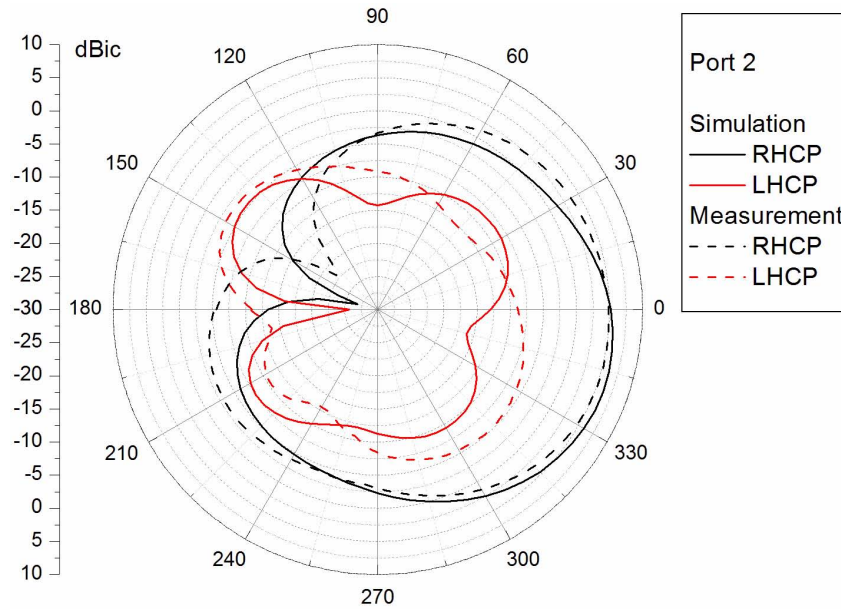


Figure 6.9. Realized gains in yz -plane for port 2 exciting odd mode at 2.575 GHz.

6.4. Port-to-Port Isolation

Although the coupling mechanism for this proposed dual CP antenna and the linearly polarised antenna proposed in [97] are similar, the port-to-port isolation between the two modes is determined by completely different mechanisms. This is because the CP antenna uses a 90° phase shifter. Fig. 6.10 depicts the relative phases of electric fields in both slots for a scenario, when the circuit is excited by odd mode (for even mode it is sufficient to reverse the direction of all arrows). At the beginning electric field in both slots have the same phase, however after separation one slot passes through a 90° phase shifter. If the signal is reflected at antenna input, it propagates backwards and in one slot passes again through the 90° phase shifter, after which the two slots join together to form CPW. Since the signal in one slot passed twice through 90° shifter the phase difference between the slots is 180° , which corresponds to even mode. Therefore all power reflected at the input of the patch will return as an opposite mode,

deteriorating the port-to-port isolation.

This reasoning is of course idealised one, which does not take into account inaccuracies in phase and amplitude (i.e. due to imperfect coupling mechanism). However its purpose is to demonstrate, that the isolation (S_{21}) is directly dependant on antenna performance. For antennas with high Q factor (i.e. on thinner substrate) a good isolation will be achieved within narrower bandwidth, whereas for low Q factor a wideband performance will be achieved at the cost of worse isolation. The design of the mode coupler plays a secondary role.

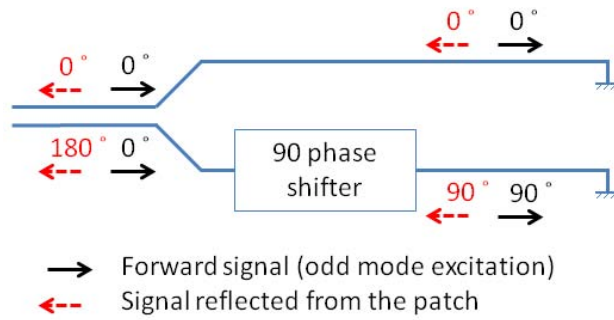


Figure 6.10. Schematic depiction of the port-to-port isolation mechanism.

7. CONCLUSIONS AND FUTURE DEVELOPMENTS

7.1. Conclusions

The thesis introduced omnidirectional CP antennas, which are realisable as low-profile planar structures. The technique was discussed and demonstrated for the simple case of single-band antenna, as well as for more advanced miniaturized and dual-band designs.

A reconfigurable CP antenna, able to receive signals from practically any direction, was proposed for the first time. The measurements, despite some difficulties, prove basic principles of the steering mechanism.

Finally it was demonstrated that odd and even transmission line modes can be implemented to achieve dual sense circularly polarized antenna.

7.2. Impact of the Proposed Solutions

Solutions for circularly polarised antennas proposed in this thesis are intended to pave the way towards more advanced radio systems, especially those embedded into small devices. The antennas are based on the microstrip patch antenna concept. This has a great manufacturing advantage, as the technology is very efficient, low cost and suitable for mass production. The resultant antennas are also low profile, which simplifies their integration with radio devices. Each of the developed antenna features allows multiple new applications:

7.2.1. Omnidirectionality

The omnidirectional CP antennas are able to cover large areas with only a single antenna, thus reducing manufacturing costs and complexity of radio systems. They are suitable for devices collecting or sending information to multiple points, like WLAN routers, wireless sensor networks etc. For RFID technologies omnidirectional CP antenna mounted on a tag would significantly decrease the probability of non-detection. This is because the dipole-like radiation pattern ensures radio coverage for most directions and the use of CP prevents polarisation losses due to misalignment.

For satellite applications, the omnidirectional CP antennas can be used for Telemetry, Tracking and Command modules onboard spin stabilized satellites. These satellites rotate along one of their axes to provide a stable orbit and to control the attitude. Due to the rotation, omnidirectional CP antennas are required. Currently available commercial solutions use an antenna surrounded by a polariser [101]. The solution proposed in Section 3 is more compact and lightweight, which is of especially significant benefit for space applications.

It was also shown in Table 3.1, that for some GNSS applications it is beneficial to use omnidirectional CP antennas. Such antennas provide better performance if the attitude of the receiver is unknown, which is mostly the case for applications involving remote tracking.

7.2.2. Reconfigurability

Arguably the biggest benefit which antenna design can offer to modern radios systems is reconfigurability. The solution proposed in Section 5 brings all the advantages offered by omnidirectional CP antenna even further. The reconfiguration method uses only a phase shift to steer the pattern, and therefore allows the combination of multiple radiation patterns. For instance, feeding the antenna through either a rat-race coupler or a 90°

hybrid coupler would result in two dipole-like patterns, with their omnidirectional performance in planes orthogonal to each other. This should be sufficient to cover a full sphere, that is 360° in ϕ and 180° in θ . However, the two signals at the coupler outputs need to be processed in two separated channels (which can be considered as MIMO or diversity systems). This is because the combination of these two signals at high frequency would naturally produce some nulls for the angles, where the two signals are out-of-phase. This is because, as demonstrated by Mathis [15], isotropic coverage can't be produced with single feed antenna.

The antenna can also be used in more classical radio systems, when switching between different modes. This gives slightly better performance in term of SNR, as the power from $\pm z$ direction won't be split into two channels. Also, for signals incoming from xy -plane (i.e. plane of the antenna substrate), scanning can be used to approximate the angle of arrival of the signal.

The antenna can benefit practically all radio systems, which use MIMO or pattern diversity. For devices communicating with multiple receivers, the antenna can prove to be even more useful than a simple omnidirectional CP antenna. For instance in multi-floor buildings it would allow a WLAN router (or a controller of a sensor network) to communicate at the same time (or switching within very short periods of time) with devices located on different floors, where placing an additional router may not be economically or technically justified.

The significance of this antenna development was also recognized by the DIT Hothouse commercialization office, which granted it the 2012 DIT Inventor Competition Award for the best postgraduate/staff invention [102].

7.2.3. Dual Polarisation

The proposed dual circularly polarised antenna is advantageous for CP polarisation diversity systems. Unlike many dual CP antennas ([18, 21, 87–

89]) it does not switch between two modes, allowing them to operate simultaneously. The feed network, which steers the dual CP performance, is compact and flexible. The use of odd and even modes allows a single transmission line to send two independent signals. This is of benefit for densely packed PCBs, where the phase steering mechanism can be located far from antenna (even on a separate layer or board) and transmitted through a single CPW (or any other dual mode transmission line).

7.3. Future Work

Despite many benefits outlined in Section 7.2, the proposed solutions can be further advanced to increase their impact on the communications market. The sections below will address some of the features, which were identified during the course of this work to be worth further study.

7.3.1. Generalization to Other Polarisation

The reconfigurable omnidirectional antenna proposed in Section 5 radiates CP, however the reconfiguration method can be generalized to suit any other polarisation. Although many publications exist on pattern reconfigurability of linearly polarised antennas, there seems to be no reports combining this with an omnidirectional pattern generated by a low-profile antenna. This would extend all the benefits highlighted in Sections 7.2.1 and 7.2.2 to other non-CP systems, regardless of their polarisation.

7.3.2. Bandwidth Enhancement

The proposed antennas are based on the concept of microstrip patch antennas. As such, they suffer from a general property of patch antennas, that of a relatively narrow bandwidth. However, it is considered that many of the state-of-the-art methods for decreasing the Q factor (hence increasing

bandwidth) are also applicable to OCPA. This was seen in 4.2, when the increase of the substrate thickness of the miniaturized antenna resulted in significantly wider impedance bandwidth.

A future study could investigate whether other band-enhancement methods would be applicable also for planar OCPAs. This would allow the use of the proposed antennas in high-speed data rate radio systems.

7.3.3. Measurement Improvement

As demonstrated in Section 5.4, the measurement of the reconfigurable OCPA poses a significant challenge. The antenna radiates energy in all possible directions, therefore the positioning structure to which it is mounted, the feed cables and the phase steering circuitry, all obstructs some parts of the antenna radiation. To overcome this difficulty, two steps are envisaged.

Firstly, the phase steering circuitry can be integrated with the antenna. This will reduce the amount of metallisation obstructing the measurement and, at the same time, make antenna more compact.

Secondly, the measurement procedure proposed by Manteuffel et al. [95] can be beneficial for the proposed antennas. It uses a chip, which is able to generate a signal of stable constant power within a given band. The chip is mounted into antenna as a signal source and a generated power density for certain (θ, ϕ) is measured in the anechoic chamber with a standard gain horn. The technique allows the measurement of the antenna without using any cables to connect AUT. This in fact gives an opportunity to measure antenna in the same environment, in which it will operate in a commercial product. For circular polarisation the measurements are more difficult, as the chip does not provide phase reference. Currently used technique for CP measurement records horizontal and vertical component in two separate measurements, but it is impossible to combine them without synchronising the phase. This problem can be however overcome by either using spinning dipole (at the cost of decreased accuracy) or dual-polarised standard gain horn.

BIBLIOGRAPHY

- [1] H. Hertz, *Untersuchungen ueber die Ausbreitung der elektrischen Kraft*. Leipzig: Johann Ambrosius Barth, 1892.
- [2] K. Davies and E. K. Smith, "Ionospheric effects on satellite land mobile systems," *IEEE Antennas and Propagation Magazine*, vol. 44, no. 6, pp. 24–31, Dec 2002.
- [3] J. L. Volakis, R. C. Johnson, and H. Jasik, *Antenna Engineering Handbook*, 4th ed. McGraw—Hill Book Company, 2007.
- [4] B. R. Elbert, *Introduction to Satellite Communication*, 2nd ed. Artech House, 1999.
- [5] J. Garcia, A. Arriola, F. Casado, X. Chen, J. I. Sancho, and D. Valderas, "Coverage and read range comparison of linearly and circularly polarised radio frequency identification ultra-high frequency tag antennas," *IET Microwaves, Antennas and Propagation*, vol. 6, no. 9, pp. 1070–1078, 2012.
- [6] A. M. Abbosh, "Ultra-wideband phase shifters," *IEEE Transactions on Microwave Theory and Techniques*, vol. 55, no. 9, pp. 1935–1941, Sep 2007.
- [7] A. Narbudowicz, M. John, X. L. Bao, and M. J. Ammann, "Vivaldi array for generation of uwb circular polarization," in *APSURSI - Antennas and Propagation Society International Symposium*, Chicago, Jul. 8–14 2012.

- [8] M. Martinez-Vazquez, "Considerations for the design of antennas embedded in mobile communications devices," in *LAPC Loughborough Antennas and Propagation Conference*, Loughborough, Nov. 8–9 2010, pp. 36–40.
- [9] *CST Microwave Studio Manual*, CST GmbH – Computer Simulation Technology, Sep. 2009.
- [10] LPKF Laser and Electronics. (2013, Jun.). [Online]. Available: <http://www.lpkfusa.com/RapidPCB/CircuitboardPlotters/c60.htm>
- [11] ——. (2013, Jun.). [Online]. Available: http://www.lpkfusa.com/rapidpcb/throughholeplating/multipress_s.htm
- [12] *Vector Network Analyzer R&S ZVA - Specifications*, Rohde & Schwarz, Sep. 2006.
- [13] *BBHA 9120 D - Calibrated Double Ridged Broadband Horn Antenna*, Schwarzbeck Mess - Elektronik.
- [14] RWTH Aachen University. (2013, Jun.). [Online]. Available: <http://www.ihf.rwth-aachen.de/index.php?id=48&lang=gb>
- [15] H. F. Mathis, "A short proof that an isotropic antenna is impossible," *Proceedings of the IRE*, vol. 39, no. 8, p. 970, Aug 1951.
- [16] B. Y. Toh, R. Cahill, and V. F. Fusco, "Understanding and measuring circular polarization," *IEEE Transactions on Education*, vol. 46, no. 3, pp. 313–318, 2003.
- [17] W. L. Langston and D. R. Jackson, "Impedance, axial-ratio, and receive-power bandwidths of microstrip antennas," *IEEE Transactions on Antennas and Propagation*, vol. 52, no. 10, pp. 2769–2774, Oct 2004.

- [18] S.-H. Hsu and K. Chang, "A novel reconfigurable microstrip antenna with switchable circular polarization," *IEEE Antennas and Wireless Propagation Letters*, vol. 6, pp. 160–162, 2007.
- [19] W.-S. Chen, K.-L. Wong, and C.-K. Wu, "Inset microstripline-fed circularly polarized microstrip antennas," *IEEE Transactions on Antennas and Propagation*, vol. 48, no. 8, pp. 1253–1254, Aug 2000.
- [20] Nasimuddin, Z. N. Chen, and X. Qing, "Asymmetric-circular shaped slotted microstrip antennas for circular polarization and RFID applications," *IEEE Transactions on Antennas and Propagation*, vol. 58, no. 12, pp. 3821–3828, Dec 2010.
- [21] F. Yang and Y. Rahmat-Samii, "A reconfigurable patch antenna using switchable slots for circular polarization diversity," *IEEE Microwave and Wireless Components Letters*, vol. 12, no. 3, pp. 96–98, 2002.
- [22] C.-Y. Huang and K.-L. Wong, "Coplanar waveguide-fed circularly polarized microstrip antenna," *IEEE Transactions on Antennas and Propagation*, vol. 48, no. 2, pp. 328–329, Feb 2000.
- [23] H. Aissat, L. Cirio, M. Grzeskowiak, J. Laheurte, and O. Picon, "Circularly polarised planar antenna excited by coplanar waveguide feed-line," *Electronics letters*, vol. 40, no. 7, pp. 402–403, 2004.
- [24] F. Ferrero, C. Luxey, R. Staraj, G. Jacquemod, M. Yedlin, and V. Fusco, "Theory and design of a tunable quasi-lumped quadrature coupler," *Microwave and Optical Technology Letters*, vol. 51, no. 9, pp. 2219–2222, Sep 2009.
- [25] —, "A novel quad-polarization agile patch antenna," *IEEE Transactions on Antennas and Propagation*, vol. 57, no. 5, pp. 1563–1567, May 2009.

- [26] L. Sun, Y. Lu, and G. Ou, "Axial ratio analysis of a multiple-feed microstrip antenna," in *APMC Asia-Pacific Microwave Conference*, Hong Kong, Dec. 16–20 2008.
- [27] J. Huang, "Circularly polarized conical patterns from circular microstrip antennas," *IEEE Transactions on Antennas and Propagation*, vol. 32, no. 9, pp. 991–994, Sep 1984.
- [28] M. F. Bolster, "A new type of circular polarizer using crossed dipoles," *IRE Transactions on Microwave Theory and Techniques*, vol. 9, no. 5, pp. 385–388, Sep 1961.
- [29] J. W. Baik, K.-J. Lee, W.-S. Yoon, T.-H. Lee, and Y.-S. Kim, "Circularly polarised printed crossed dipole antennas with broadband axial ratio," *Electronics Letters*, vol. 44, no. 13, pp. 785–786, 2008.
- [30] Y.-F. Lin, Y.-K. Wang, H.-M. Chen, and Z.-Z. Yang, "Circularly polarized crossed dipole antenna with phase delay lines for RFID handheld reader," *IEEE Transactions on Antennas and Propagation*, vol. 60, no. 3, pp. 1221–1227, Mar 2012.
- [31] Y. B. Chen, X. F. Liu, Y.-C. Jiao, and F.-S. Zhang, "CPW-fed broadband circularly polarised square slot antenna," *Electronics Letters*, vol. 42, no. 19, pp. 1074–1075, 2006.
- [32] S.-P. Pan, J.-Y. Sze, and P.-J. Tu, "Circularly polarized square slot antenna with a largely enhanced axial-ratio bandwidth," *IEEE Antennas and Wireless Propagation Letters*, vol. 11, pp. 969–972, 2012.
- [33] E. A. Soliman, S. Brebels, E. Beyne, and G. A. E. Vandenbosch, "Circularly polarised aperture antenna fed by CPW and built in MCM-D technology," *Electronics Letters*, vol. 35, no. 4, pp. 250–251, Feb 1999.

- [34] X. L. Bao and M. J. Ammann, "Printed circularly polarised antenna with ultra-wide axial-ratio bandwidth," *IET Microwaves, Antennas and Propagation*, vol. 5, no. 9, pp. 1089–1096, 2011.
- [35] V. H. Rumsey, "Frequency independent antennas," in *IRE International Convention Record*, vol. 5, New York, USA, Mar. 21–25 1957, pp. 114–118.
- [36] H. Nakano, R. Satake, and J. Yamauchi, "Extremely low-profile, single-arm, wideband spiral antenna radiating a circularly polarized wave," *IEEE Transactions on Antennas and Propagation*, vol. 58, no. 5, pp. 1511–1520, May 2010.
- [37] D. J. Muller and K. Sarabandi, "Design and analysis of a 3-arm spiral antenna," *IEEE Transactions on Antennas and Propagation*, vol. 55, no. 2, pp. 258–266, Feb 2007.
- [38] J. Huang, "A technique for an array to generate circular polarization with linearly polarized elements," *IEEE Transactions on Antennas and Propagation*, vol. 34, no. 9, pp. 1113–1124, Sep 1986.
- [39] H. K. Kan and R. B. Waterhouse, "A small CP-printed antenna using 120° sequential rotation," *IEEE Transactions on Antennas and Propagation*, vol. 50, no. 3, pp. 398–399, Mar 2002.
- [40] P. S. Hall, "Application of sequential feeding to wide bandwidth, circularly polarised microstrip patch arrays," *IEE Proceedings H: Microwaves, Antennas and Propagation*, vol. 136, no. 5, pp. 390–398, 1989.
- [41] J.-H. Bang, B. Enkhbayar, D.-H. Min, and B.-C. Ahn, "A compact GPS antenna for artillery projectile applications," *IEEE Antennas and Wireless Propagation Letters*, vol. 10, pp. 266–269, 2011.
- [42] H.-S. Tae, K.-S. Oh, W.-I. Son, W.-G. Lim, and J.-W. Yu, "Design of compact dual-band quadruple inverted-F/L antenna for GPS L1/L2

- band," *IEEE Transactions on Antennas and Propagation*, vol. 61, no. 4, pp. 2276–2279, Apr 2013.
- [43] M. Maqsood, S. Gao, T. Brown, and M. Unwin, "Effects of ground plane on the performance of multipath mitigating antennas for GNSS," in *LAPC Loughborough Antennas and Propagation Conference*, Loughborough, UK, Nov. 8–9 2010, pp. 2276–2279.
- [44] L. I. Basilio, R. L. Chen, J. T. Williams, and D. R. Jackson, "A new planar dual-band GPS antenna designed for reduced susceptibility to low-angle multipath," *IEEE Transactions on Antennas and Propagation*, vol. 55, no. 8, pp. 2358–2366, Aug 2007.
- [45] L. I. Basilio, J. T. Williams, D. R. Jackson, and R. L. Chen, "Characteristics of an inverted shorted annular-ring-reduced surface-wave antenna," *IEEE Antennas and Wireless Propagation Letters*, vol. 7, pp. 123–126, 2008.
- [46] *Standard Definitions of Terms for Antennas*, IEEE Antennas and Propagation Society Std. 145-1993, Mar. 18 1993.
- [47] K. Kelleher and C. Morrow, "Omnidirectional circularly polarized antennas," in *IRE International Convention Record*, vol. 1, Mar. 21–25 1955, pp. 28–31.
- [48] J. M. Fernandez, J. L. Masa-Campos, and M. Sierra-Perez, "Circularly polarized omnidirectional millimeter wave monopole with parasitic strip elements," *Microwave and Optical Tech. Letters*, vol. 49, no. 3, pp. 664–668, Mar 2007.
- [49] D. I. Wu, "Omnidirectional circularly-polarized conformal microstrip array for telemetry applications," in *APS Antennas and Propagation Society International Symposium*, vol. 2, Newport Beach, USA, 1995, pp. 998–1001.

- [50] F. R. Hsiao and K. L. Wong, "Low-profile omnidirectional circularly polarized antenna for WLAN access points," *Microwave and Optical Tech. Letters*, vol. 46, no. 3, pp. 227–231, Aug 2005.
- [51] B.-C. Park and J.-H. Lee, "Omnidirectional circularly polarized antenna utilizing zeroth-order resonance of epsilon negative transmission line," *IEEE Transactions on Antennas and Propagation*, vol. 59, no. 7, pp. 2717–2721, Jul 2011.
- [52] H. Iwasaki and N. Chiba, "Circularly polarised back-to-back microstrip antenna with an omnidirectional pattern," *IEE Proc. - Microwaves, Antennas and Propagation*, vol. 146, no. 4, pp. 277–281, Aug 1999.
- [53] K. Sakaguchi and N. Hasebe, "A circularly polarized omnidirectional antenna," in *Eighth International Conference on Antennas and Propagation*, vol. 1, Edinburgh, UK, Mar. 30 1993, pp. 477–480.
- [54] Y. M. Pan and K. W. Leung, "Wideband circularly polarized dielectric bird-nest antenna with conical radiation pattern," *IEEE Transactions on Antennas and Propagation*, vol. 61, no. 2, pp. 563–570, 2013.
- [55] Y. Xu and C. Ruan, "A novel design of circularly polarized omnidirectional antenna for Ka-band," in *GSMM Global Symposium on Millimeter Waves*, Nanjing, China, 2008, pp. 378–379.
- [56] X. Quan, R. Li, and M. M. Tentzeris, "A broadband omnidirectional circularly polarized antenna," *IEEE Transactions on Antennas and Propagation*, vol. 61, no. 5, pp. 2363–2370, 2013.
- [57] J. D. Morrow, "Polarization-adjustable omnidirectional dipole array," *IEEE Antenna and Wireless Propagation Letters*, vol. 2, no. 1, pp. 223–225, 2003.

- [58] V. Sipal, "Compact and efficient antennas based on transmission line metamaterial structures," Dipl-Ing Thesis, RWTH Aachen University, Germany, 2009.
- [59] D. Sievenpiper, Z. Lijun, R. F. J. Broas, N. N. G. Alexopolous, and E. Yablonovitch, "High-impedance electromagnetic surfaces with a forbidden frequency band," *IEEE Transactions on Microwave Theory and Techniques*, vol. 47, no. 11, pp. 2059–2074, Nov 1999.
- [60] A. Sanada, M. Kimura, I. Awai, C. Caloz, and T. Itoh, "A planar zeroth-order resonator antenna using a left-handed transmission line," in *34th European Microwave Conference*, Amsterdam, the Netherlands, Oct. 11–15 2004, pp. 1341–1344.
- [61] J. An, G.-M. Wang, C.-X. Zhang, and H.-Y. Zeng, "Compact circularly polarized omnidirectional microstrip antenna," *Microwave and Optical Tech. Letters*, vol. 51, no. 11, pp. 2643–2646, Nov 2009.
- [62] B.-C. Park and J.-H. Lee, "Dual-band omnidirectional circularly polarized antenna using zeroth- and first-order modes," *IEEE Antennas and Wireless Propagation Letters*, vol. 11, pp. 407–410, 2012.
- [63] X. Qing, Z. N. Chen, J. Shi, and C. K. Goh, "Zero-phase-shift line antennas," in *iWAT International Workshop on Antenna Technology*, Karlsruhe, Germany, Mar. 4–6 2013.
- [64] L. J. Chu, "Physical limitation of omni-directional antennas," *Journal of Applied Physics*, vol. 19, pp. 1163–1175, Dec 1948.
- [65] B. S. Collins, D. Iellici, S. Kingsley, and S. Raffaelli, "Balanced antennas for GPS and galileo receivers," in *LAPC Loughborough Antennas and Propagation Conference*, Loughborough, UK, Apr. 2–3 2007, pp. 321–324.

- [66] A. A. Serra, P. Nepa, G. Manara, and R. Massini, "A low-profile linearly polarized 3D PIFA for handheld GPS terminals," *IEEE Transactions on Antennas and Propagation*, vol. 58, no. 4, pp. 1060–1066, Apr 2010.
- [67] A. Narbudowicz, X. L. Bao, and M. J. Ammann, "Bidirectional circularly polarized microstrip antenna for GPS applications," in *LAPC Loughborough Antennas and Propagation Conference*, Loughborough, UK, Nov. 8–9 2010, pp. 205–208.
- [68] H. Iwasaki, "Circularly polarised back-to-back microstrip antenna with an omnidirectional pattern," *IEEE Transactions on Antennas and Propagation*, vol. 46, no. 10, pp. 1527–1530, Oct 1998.
- [69] L. Liu, Y. F. Weng, S. W. Cheung, T. I. Yuk, and L. J. Foged, "Modeling of cable for measurements of small monopole antennas," in *LAPC Loughborough Antennas and Propagation Conference*, Loughborough, UK, 2011.
- [70] C. Icheln, J. Ollikainen, and P. Vainikainen, "Reducing the influence of feed cables on small antenna measurements," *Electronics Letters*, vol. 35, no. 15, pp. 12112–1214, Jul 1999.
- [71] A. Narbudowicz, X. L. Bao, and M. Ammann, "Omnidirectional circularly polarized microstrip patch antenna," *Electronics letters*, vol. 48, no. 11, pp. 614–615, May 2012.
- [72] J. Oh and K. Sarabandi, "A topology-based miniaturization of circularly polarized patch antennas," *IEEE Transactions on Antennas and Propagation*, vol. 61, no. 3, pp. 1422–1426, Mar 2013.
- [73] H. Oraizi and S. Hedayati, "Circularly polarized multiband microstrip antenna using the square and Giuseppe Peano fractals," *IEEE*

- Transactions on Antennas and Propagation*, vol. 60, no. 7, pp. 3466–3470, Jul 2012.
- [74] H. R. Lee, H. K. Ryua, S. Lim, and J. M. Woo, “A miniaturized dualband circularly polarized microstrip antenna for installation into satellite mobile phones,” *IEEE Antennas and Wireless Propagation Letters*, vol. 8, pp. 823–825, 2009.
- [75] A. Narbudowicz, X. L. Bao, and M. J. Ammann, “Omnidirectional circularly polarized patch antenna with post manufacture characteristic refinement,” in *iWAT International Workshop on Antenna Technology*, Karlsruhe, Germany, Mar. 4–6 2013.
- [76] X. L. Bao and M. J. Ammann, “Dual-frequency dual circularly-polarised patch antenna with wide beamwidth,” *Electronics Letters*, vol. 44, no. 21, pp. 1233–1234, 2008.
- [77] O. P. Falade, X. Chen, Y. Alfadhs, and C. Parini, “Quad band circular polarized antenna,” in *LAPC Loughborough Antennas and Propagation Conference*, Loughborough, UK, 2012.
- [78] F. J. Herraiz-Martinez and V. Gonzales-Posadas, “A dual band circularly polarized antenna based on a microstrip patch filled with left-handed structures,” in *EuCAP 2nd European Conference on Antennas and Propagation*, Edinburgh, UK, 2007.
- [79] C.-J. Lee, K. M. K. H. Leong, and T. Itoh, “Composite right/left-handed transmission line based compact resonant antennas for RF module integration,” *IEEE Transactions on Antennas and Propagation*, vol. 54, no. 8, pp. 2283–2291, Aug 2006.
- [80] Nasimuddin, Z. N. Chen, and X. Qing, “Dual-band circularly polarized S-shaped slotted patch antenna with a small frequency-ratio,”

- IEEE Transactions on Antennas and Propagation*, vol. 58, no. 6, pp. 2112–2115, Jun 2010.
- [81] L. Lelarante and R. J. Langley, “Dual-band patch antenna for mobile satellite systems,” *IEE Proceedings - Microwaves, Antennas and Propagation*, vol. 147, no. 6, pp. 427–430, Dec 2000.
- [82] S. Maci, G. B. Gentili, P. Piazzesi, and C. Salvador, “Dual-band slot-loaded patch antenna,” *IEE Proceedings - Microwaves, Antennas and Propagation*, vol. 142, no. 3, pp. 225–232, Jun 1995.
- [83] S. Maci and G. B. Gentili, “Dual-frequency patch antenna,” *IEEE Antennas and Propagation Magazine*, vol. 39, no. 6, pp. 13–20, Dec 1997.
- [84] C.-Y. Huang, C.-W. Ling, and J.-S. Kuo, “Dual-band microstrip antenna using capacitive loading,” *IEE Proceedings - Microwaves, Antennas and Propagation*, vol. 150, no. 6, pp. 401–404, Dec 2003.
- [85] A. Narbudowicz, X. L. Bao, and M. J. Ammann, “Dual-band omnidirectional circularly polarized antenna,” *IEEE Transactions on Antennas and Propagation*, vol. 61, no. 1, pp. 77–83, Jan 2013.
- [86] Nasimuddin, X. Qing, and Z. N. Chen, “Compact asymmetric-slit microstrip antennas for circular polarization,” *IEEE Transactions on Antennas and Propagation*, vol. 58, no. 12, pp. 3821–3828, Jan 2011.
- [87] B. Wu and M. Okoniewski, “A novel scheme for realizing a microstrip antenna with switchable circular polarization,” in *EuCAP 6th European Conference on Antennas and Propagation*, Prague, Czech Republik, Mar. 26–30 2012, pp. 3278–3282.
- [88] B. A. Centiner, J. Y. Qian, G. P. Li, and F. D. Flaviis, “A reconfigurable spiral antenna for adaptive MIMO systems,” *EURASIP Journal on Wireless Communication and Networking*, no. 3, Aug 2005.

- [89] S. Pyo, J.-W. Baik, and Y.-S. Kim, "Slot-perturbed microstrip antenna for switchable circular polarisation," *Electronics Letters*, vol. 47, no. 10, pp. 583–585, May 2011.
- [90] R.-H. Chen and J.-S. Row, "Single-fed microstrip patch antenna with switchable polarization," *IEEE Transactions on Antennas and Propagation*, vol. 56, no. 4, pp. 922–926, Apr 2008.
- [91] S. V. S. Nair and M. J. Ammann, "Reconfigurable antenna with elevation and azimuth beam switching," *IEEE Antennas and Wireless Propagation Letters*, vol. 9, pp. 367–370, 2010.
- [92] H. Liu, S. Gao, and T. H. Loh, "Circularly polarized electronically steerable parasitic array radiator antenna for satellite," in *EuCAP 4th European Conference on Antennas and Propagation*, Barcelona, Spain, Apr. 12–15 2010, pp. 3278–3282.
- [93] C. W. Jung, M.-J. Lee, G. P. Li, and F. D. Flaviis, "Reconfigurable scan-beam single-arm spiral antenna integrated with RF-MEMS switches," *IEEE Transactions on Antennas and Propagation*, vol. 54, no. 2, pp. 455–463, Feb 2006.
- [94] Emerson & Cuming. (2013, Jun.). [Online]. Available: <http://www.eccosorb.com/products-eccosorb-ls.htm>
- [95] D. Manteuffel and R. Martens, "Improved radiation pattern measurements of MIMO handheld mobile terminals," in *EuCAP 7th European Conference on Antennas and Propagation*, Prague, Czech Republik, Mar. 26–30 2013, pp. 86–87.
- [96] A. Narbudowicz, X. L. Bao, and M. J. Ammann, "Dual circularly-polarized patch antenna using even and odd feed-line modes," *IEEE Transactions on Antennas and Propagation*, vol. 61, no. 9, pp. 4828–4831, Sep 2013.

- [97] Y. Li, Z. Zhang, W. Chen, Z. Feng, and M. F. Iskander, "A dual-polarization slot antenna using a compact CPW feeding structure," *IEEE Antennas and Wireless Propagation Letters*, vol. 9, pp. 191–194, 2010.
- [98] Y. Li, Z. Zhang, Z. Feng, and M. F. Iskander, "Dual-mode loop antenna with compact feed for polarization diversity," *IEEE Antennas and Wireless Propagation Letters*, vol. 10, pp. 95–98, 2011.
- [99] Y. Li, Z. Zhang, and Z. Feng, "Compact hybrid CPW-fed slot antenna array with pattern diversity," *Microwave and Optical Technology Letters*, vol. 53, no. 4, pp. 884–888, Apr 2011.
- [100] D. M. Pozar, *Microwave Engineering*, 2nd ed. John Wiley & Sons, 1998.
- [101] Rymsa. (2013, Jun.). [Online]. Available: http://www.rymsa.com/sp_products.html
- [102] DIT Hothouse commercialization office. (2013, Jun.). [Online]. Available: <http://www.dit.ie/news/archive2012/ministerforresearchandinnovationannounceswinnersofditinventorcomp/>

APPENDIX A.

LIST OF PUBLICATIONS

Patent Application

- [P1 1] M. J. Ammann, X. L. Bao and A. Narbudowicz, "An antenna for generating omnidirectional circularly polarized radiation," *UK Patent Application*, No. GB2486675 (A), Jun. 2012.

Journal Publications

- [JP 1] A. Narbudowicz, X. L. Bao and M. J. Ammann, "Omnidirectional Circularly Polarised Microstrip Patch Antenna," *Electronics Letters*, vol. 48, no. 11, pp. 614–615, May. 2012.
- [JP 2] A. Narbudowicz, X. L. Bao and M. J. Ammann, "Dual-band Omnidirectional Circularly Polarized Antenna," *IEEE Transactions on Antennas and Propagation*, vol. 61, no. 1, pp. 77–83, Jan. 2013.
- [JP 3] A. Narbudowicz, X. L. Bao and M. J. Ammann, "Dual Circularly-polarized Patch Antenna Using Even and Odd Feed-line Modes," *IEEE Transactions on Antennas and Propagation*, vol. 61, no. 9, pp. 4828–4831, Sep. 2013.

International Conference Publications

- [CP1] A. Narbudowicz, X. L. Bao and M. J. Ammann, "Dual Circularly-polarized Patch Antenna Using Even and Odd Feed-line Modes," in *Proc. LAPC - Loughborough Antennas & Propagation Conference*, Loughborough, UK, Nov. 8–9, 2010.
- [CP2] M. J. Ammann, X. L. Bao and A. Narbudowicz, "(Invited) Miniaturized and High Performance Circularly Polarized Terminal Antennas" in *Proc. EuCAP - European Conference on Antennas and Propagation*, Prague, Czech Republic, Mar. 26–30, 2012.
- [CP3] A. Narbudowicz, M. John, X. L. Bao and M. J. Ammann, "Vivaldi Array for Generation of UWB Circular Polarization" in *Proc. APS - IEEE International Symposium on Antennas and Propagation*, Chicago, USA, Jul. 8–13, 2012.
- [CP4] M. J. Ammann, X. L. Bao and A. Narbudowicz, "(Invited) Circularly Polarized Terminal Antennas for Emerging Wireless Systems" in *Proc. LAPC - Loughborough Antennas & Propagation Conference*, Loughborough, UK, Nov. 12–13, 2012.
- [CP5] A. Narbudowicz, X. L. Bao and M. J. Ammann, "Omnidirectional Circularly Polarized Patch Antenna with Post Manufacture Characteristic Refinement" in *Proc. iWAT - International Workshop on Antenna Technology*, Karlsruhe, Germany, Mar. 4–6, 2013.